ISBN 978-90-365-2652-4

High-frequency Operation and Miniaturization aspects of Pulse-tube Cryocoolers

Srinivas Vanapalli

High-frequency Operation and Miniaturization aspects of Pulse-tube Cryocoolers

Srinivas Vanapalli

Uitnodiging

Hierbij nodig ik u uit voor het bijwonen van de openbare verdediging van mijn proefschrift, met als titel:

"High-frequency Operation and Miniaturization aspects of Pulse-tube Cryocoolers"

Dit zal plaatsvinden op vrijdag 27 maart 2008 om 13:15 in collegezaal 2 van het Spiegel gebouw van de Universiteit Twente.

Voorafgaand aan de verdediging zal ik om 13:00 uur mijn werk kort toelichten.

Aansluitend is er een receptie. Daarna bent u vanaf 18:30 uur van harte welkom in Restaurant International, Boulevard 1945 322, Enschede, voor het feest met lopend buffet.

Graag zou ik van u vernemen of u bij het feest aanwezig zal zijn.

Srinivas Vanapalli
Meteorenstraat 6
7521 XR Enschede
tel. 06-45518363
vanapalli@ecn.nl

Paranimfen:

Dhirendra Tiwari
d.tiwari@tue.nl

Marcel Dijkstra
m.a.dijkstra@ewi.utwente.nl

HIGH-FREQUENCY OPERATION AND MINIATURIZATION ASPECTS OF PULSE-TUBE CRYOCOOLERS

Srinivas Vanapalli

Samenstelling promotiecommissie:

Prof. dr. ir. A. J. Mouthaan	Universiteit Twente, voorzitter
Prof. dr. ir. M. C. Elwenspoek	Universiteit Twente, promotor
Prof. dr. ir. H. J. M. ter Brake	Universiteit Twente, co-promotor
Prof. dr. ir. A. T. A. M. Waele	Technische Universiteit Eindhoven
Prof. dr. ir. T. H. van der Meer	Universiteit Twente
Prof. dr. ir. F. van Keulen	Technische Universiteit Delft
dr. ir. R. Radebaugh	NIST Boulder, Colorado
dr. ir. H. V. Jansen	Universiteit Twente
dr. ir. J. F. Burger	Universiteit Twente

This work was supported financially by "Technologiestichting STW", The Netherlands.

The work described in this thesis was carried out at the "Transducers Science and Technology" (TST), Faculty of Electrical engineering, Mathematics and Computer science (EWI), "Cooling and Instrumentation" group, Faculty of Science and Technology (TNW), University of Twente and National Institute of Standards and Technologies (NIST), Boulder, Colorado.

High-frequency operation and miniaturization aspects of pulse-tube cryocoolers.
S. Vanapalli,
ISBN: 978-90-365-2652-4
Thesis Universiteit Twente, Enschede.

Printed by Gildeprint, Enschede

Cover: Snow crystals (www.snowcrystals.com) embedded on a frozen window, designed by Marcel Dijkstra.

University of Twente (UT)

University of Twente
The Netherlands

HIGH-FREQUENCY OPERATION AND MINIATURIZATION ASPECTS OF PULSE-TUBE CRYOCOOLERS

PROEFSCHRIFT

ter verkrijging van
de graad van doctor aan de Universiteit Twente,
op gezag van de rector magnificus,
prof. dr. W. H. M. Zijm,
volgens besluit van het College voor promoties
in het openbaar te verdedigen
op donderdag 27 maart 2008 om 13.15 uur

door

Srinivas Vanapalli

geboren op 25 Februari 1979
te Visakhapatnam, India

Transducers Science and Technology (TST)

Dit proefschrift is goedgekeurd door:

Prof. dr. ir. M. C. Elwenspoek	promotor
Prof. dr. ir. H. J. M. ter Brake	co-promotor

Dedication

Karlsruhe, Germany 2002, I was indoctrinated by Prof. Dr. K. A. Padmanabhan, my former dean students in Indian Institute of Technology (IIT), Madras to pursue higher studies, instead of being contended with a mundane job. Prof. R. Dhamodharan (IIT-Madras) also played an important role. In that fall, I chose to move to Netherlands to charter unknown waters. Now, I am glad to say that I felt like I was cruising along. All this was possible because of the excellent foundation provided by my teachers at IIT Madras. I like to dedicate this thesis to all my teachers for imparting knowledge and preparing me for the challenges ahead. I like to also dedicate this thesis to my advisors, Marcel ter Brake and Ray Radebaugh for making me cryo-knowledgeable. I like to quote a few lines of Kabir (saint & spiritual philosopher):

गुरु गोविन्द दोऊ खड़े,काके लागूं पायं ।
बलिहारी गुरु आपणे, जिन गोविन्द दिया दिखाय ॥

Translation in English:

Guru and God both appear before me. To whom should I prostrate? I bow before Guru who introduced God to me.

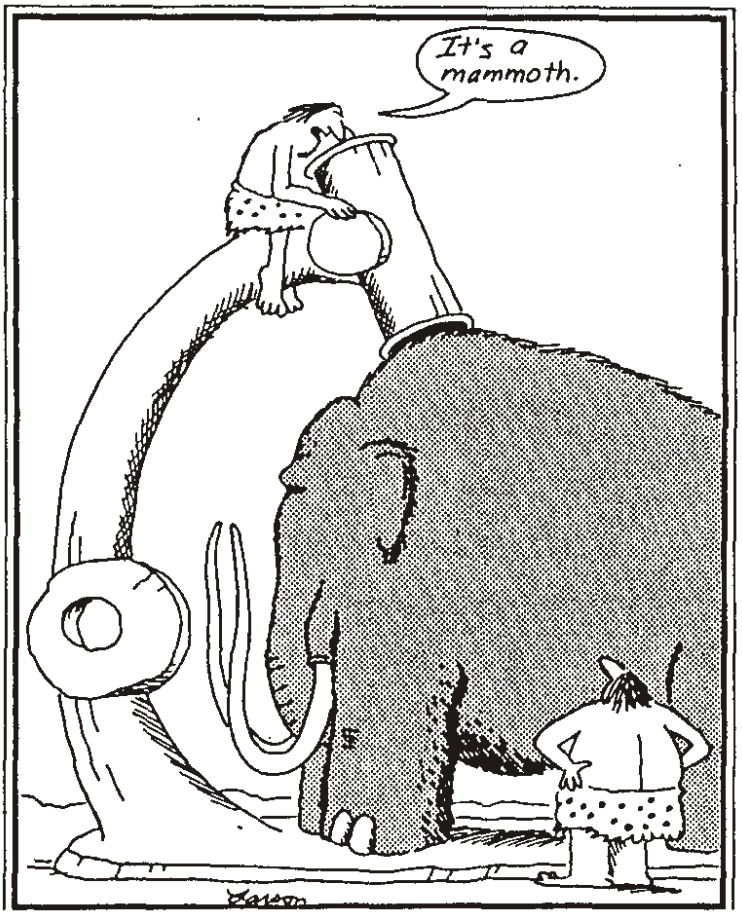

Early microscope

Cartoon by Gary Larson. Similarly, for certain applications, the present cryocoolers are very large compared to the size of the device to be cooled.

Contents

1 Introduction **1**
- 1.1 Cryocoolers . . . 2
- 1.2 Cooling principles . . . 2
  - 1.2.1 Optical . . . 3
  - 1.2.2 Thermoelectric . . . 3
  - 1.2.3 Gas cycles . . . 3
- 1.3 Scope of the thesis . . . 7
- 1.4 Regenerative cryocoolers . . . 7
  - 1.4.1 Stirling . . . 7
  - 1.4.2 Gifford-McMahon . . . 9
  - 1.4.3 Pulse-tube . . . 9
- 1.5 Objective . . . 12
- Bibliography . . . 14

2 Previous work **17**
- 2.1 Thermoelectric cooler . . . 17
- 2.2 Joule Thomson cryocooler . . . 18
- 2.3 Regenerative cryocooler . . . 19
- 2.4 What was needed? . . . 23
- Bibliography . . . 24

3 The regenerator **27**
- 3.1 Introduction . . . 27
- 3.2 Acoustic power flow . . . 31
- 3.3 Phasor Fundamentals . . . 32
- 3.4 Phasor representation of isothermal and adiabatic systems . . . 34
  - 3.4.1 Phasor representation of isothermal components . . . 35
  - 3.4.2 Phasor representation of adiabatic components . . . 35

3.5 Phasor analysis of regenerator . . . 37
3.5.1 Scaling of regenerative systems with cooling power . . . 39
3.6 Parameter Analysis . . . 41
3.6.1 Pressure drop and enthalpy flow . . . 41
3.6.2 Heat conduction . . . 45
3.6.3 Void-volume pressure loss . . . 45
3.6.4 Summary of losses . . . 46
3.6.5 Hydraulic diameter . . . 48
3.6.6 Frequency effects . . . 48
3.7 Numerical optimization of the regenerator . . . 49
3.8 Conclusions . . . 56
Bibliography . . . 57

4 Systematic design of a Pulse-tube Refrigerator 59
4.1 Introduction . . . 59
4.2 Phasor representation of PTR . . . 62
4.3 Design procedure . . . 62
4.3.1 Regenerator Optimization . . . 64
4.3.2 Regenerator sizing . . . 64
4.3.3 Pulse-tube design . . . 66
4.3.4 Inertance tube design . . . 66
4.3.5 Heat exchanger design . . . 67
4.4 Practical aspects . . . 68
4.5 Miniaturization . . . 68
4.6 Conclusions . . . 69
Bibliography . . . 69

5 120 Hz Pulse-tube Cryocooler 71
5.1 Advantages of high-frequency operation . . . 71
5.2 Design . . . 72
5.2.1 REGEN3.2 calculations . . . 73
5.2.2 Pulse-tube design . . . 76
5.2.3 Inertance tube calculations . . . 76
5.2.4 Heat exchanger calculations . . . 76
5.2.5 Phasor diagram . . . 77
5.2.6 PTR layout . . . 80
5.3 Experimental setup . . . 83
5.3.1 Pulse-tube refrigerator . . . 83
5.3.2 Instrumentation . . . 86

5.4 Experimental results . . . 87
5.4.1 Cooldown curve . . . 87
5.4.2 Load curve . . . 87
5.4.3 Background losses . . . 87
5.4.4 Variation of pressure ratio and frequency . . . 93
5.4.5 Performance comparison with REGEN3.2 calculations . . . 93
5.5 Conclusions . . . 96
Bibliography . . . 97

6 Fast cooldown modeling and experiments 99
6.1 Introduction . . . 100
6.2 Refrigeration power density . . . 100
6.3 120 Hz Pulse-tube cryocooler . . . 101
6.4 Experimental results . . . 101
6.5 Analysis . . . 104
6.5.1 Analytical Model . . . 104
6.5.2 Numerical Analysis . . . 106
6.6 Comparison of experimental and calculated results . . . 108
6.7 Conclusion . . . 110
Bibliography . . . 113

7 Investigations on microregenerators 115
7.1 Introduction . . . 116
7.2 Definitions and design . . . 117
7.3 Experimental details . . . 119
7.4 Results . . . 123
7.5 Conclusions . . . 128
Bibliography . . . 133

8 High-frequency pressure oscillator 135
8.1 Introduction . . . 135
8.2 Design . . . 137
8.3 Experiments . . . 143
8.4 Discussion and Conclusion . . . 148

9 Conclusions and recommendations 151

Summary 157

Samenvatting 159

Appendix A **163**

Acknowledgements **167**

Chapter 1

Introduction

Snow and ice, cool streams, springs, caves and cellars were long ago used to refrigerate food. Inventions in mechanical refrigerators pioneered by Dr. William Cullen, Micheal Faraday and many others have revolutionized the production of cold which is a desired product for many. Today, the refrigerator is the most used appliance, found in more than 95.0 % of homes in the developed world. In the 1980's high temperature T_c superconductors were invented which lead to a hectic activity in the superconducting science and technology leading to several applications. However, most of these applications could not be realized in practise due to non-availability of reliable, small and cheap cryocoolers. Recent developments in the cryocoolers, in particular, pulse-tube cryocoolers has rejuvenated the interest in high T_c superconducting applications. For applications such as cooling of non-dissipating superconducting circuits, the cryocooler should be further miniaturized and in a sense be "invisible". In the future, miniature cryocoolers may even find uses in desktop computers where they could cool superconducting circuits, allowing the circuits to operate at speeds hundreds of times faster than today's conventional electronics without overheating. This thesis deals with the investigation of scaling down aspects of pulse-tube refrigerators. In this chapter, a general introduction of cryocoolers is given. A short description of the pulse-tube cryocooler and the operating principle is summarized.

1.1 Cryocoolers

Cryogenics is the area of science and research, at temperatures below 120 K. At these temperatures some materials exhibit superconducting properties enabling the development of novel devices. Semi-conductor materials would also gain from the decrease in thermal noise at low temperatures often increasing the speed of such devices and systems [1]. Cryocoolers are small refrigerators capable of achieving useful refrigeration at cryogenic temperatures. The working principle of these cryocoolers are based on thermodynamic cycles. The efficiencies of these cryocoolers are of great importance due to the large power inputs required for the amount of useful refrigeration achieved which is thermodynamically limited by the Carnot $COP\ T_c/(T_w - T_c)$ (T is temperature and the subscripts c and w refer to cold and warm, respectively). Ideally, at 80 K, 2.75 W of power is required for each watt of cooling and at 4 K, 74 W is required for 1 W of cooling. A heat sink temperature of 300 K is assumed in these calculations. Power inputs in practical refrigerators are usually at least ten times these values because of various inefficiencies.

The applications of cryocoolers are varied which depend on the cryogenic temperature and cooling power. A good overview of various applications of cryocoolers was given by Radebaugh [2] and a survey of the commercial cryocoolers was done by ter Brake et al. [3]. One of the major applications of cryocoolers is cooling of various detectors for space, military and commercial purposes (night vision cameras, infrared detectors etc.). There are many applications in which cryocoolers are part of the system such as cooling of super conducting circuits and magnets. A good example of a system containing a superconducting magnet is a magnetic resonance imaging (MRI) system. This thesis focuses on the development of miniaturized cryocoolers. The requirements of the cryocooler are given in section 1.3. These micro-miniature cryocoolers can be used to cool terahertz sensors [4–6] used for detecting explosives and/or diagnosing cancer, microwave filters in wireless applications, cryosurgery [7–18] and many more applications.

1.2 Cooling principles

This section presents a short introduction to several cooling principles. Gas cycles and in particular regenerative cycle are presented in greater detail because they are essential in the cooling cycle under study in this thesis. Walker [19, 20] gives a comprehensive study of the gas cycles. The pulse-tube cryocooler, a particular type of regenerative cycle is of great interest because of several advantages. Radebaugh [21] has reviewed the progress made in pulse-tube cryocooler development. A short introduction to alternate cooling cycles is also presented. A comprehensive study of these alternative cycles is given by Radebaugh [22] and are also described by Burger [23].

1.2.1 Optical

Laser, or optical, cooling is based on anti-Stokes fluorescence principle and occurs when the amount of energy emitted by a solid, when exposed to an energy source, is more than the energy it absorbs. A laser aimed at certain materials will excite the material's atoms to a higher energy state. These excited atoms absorb a little extra energy from the heat of the surrounding material. When they produce photons, the photons are of a higher energy than the initial laser energy and this radiation of energy cools the material. Scientists at Los Alamos developed a refrigerator based on laser cooling called LASSOR – the Los Alamos Solid-State Optical Refrigerator. LASSOR uses a 1.6-watt laser to cool fluoride glass doped with ytterbium (Yb). The glass cooled from 298 to 282 K [24, 25]. For over a decade of research with several materials the temperature difference improved to 65 K from room temperature [26].

1.2.2 Thermoelectric

Thermoelectric cooling uses the Peltier effect [19] to create a heat flux between the junction of two different types of materials when an electrical voltage is applied. Thermoelectric coolers have no moving parts, they operate without noise, small lightweight package, operation in any orientation and have solid state reliability. These attractive features of the thermoelectric coolers are however undermined by maximum temperature difference achievable even with developments. The maximum temperature difference that can be achieved with a multi-stage thermoelectric cooler is less than 160 K [27]. Thus from ambient temperatures of 300 K the minimum temperature achievable is about 140 K. At these temperatures the coefficient of performance is very low. Hence, thermoelectric coolers are not suitable in their present form for cryogenic cooling.

1.2.3 Gas cycles

Refrigerators that work on gas cycles have thermodynamic processes as intermediatory steps. One of the steps would be the cooling step in which heat is absorbed from the object to be cooled into the working fluid which is later rejected at the warm part of the refrigerator in a subsequent step. Till today, gas cycles are the only principles by which cryogenic temperatures are obtained and hence are interesting candidates for miniaturization studies. Figure 1.1 shows the general classification of cryocoolers that utilize a thermodynamic cycle. Gas cycles can be primarily divided into recuperative (steady flow) and regenerative (oscillating flow) types.

Recuperative (Steady flow)

The Joule-Thomson (JT) and Brayton cryocoolers are of the recuperative type in which the working fluid flows steadily in one direction, with steady low and

***Figure* 1.1:** *Classification of dynamic cryocoolers*

***Figure* 1.2:** *Commonly used cryocoolers. $\dot{Q}_w$ represents the heat rejected to the environment at temperature T_w and $\dot{Q}_{r,net}$ represents the net refrigeration power at temperature T_c.*

high pressure lines analogous to DC electrical systems. A schematic of the Joule-Thomson cryocooler is shown in figure 1.2 (a). The compressor operates with a fixed inlet pressure and a fixed outlet pressure. If the compressor is a reciprocating type, it must have inlet and outlet valves to provide the steady flow. The recuperative heat exchangers which are mostly counter flow type for maximum effectiveness, transfer heat from the high pressure stream to the low pressure stream through a pressure partition. The high effectiveness required for recuperative heat exchangers can be expensive to realize.

In the recuperative cycles, heating of the gas occurs in the compressor during compression and cooling occurs at a particular location where the gas is expanded from the high to the low pressure. An expansion valve, orifice, capillary or porous plug is used in the Joule-Thomson (JT) cryocooler, whereas an expansion engine such as an expansion turbine is used in the Brayton cycle. However, the expansion engine is a moving element that leads to increased cost and potential reliability problems.

The main advantage of a JT cooler is the lack of cold moving parts which allows the cold end to be miniaturized, providing a rapid cool-down. Since it uses steady flow, cold can be transported across long distances for example in cryogenic catheters for cryosurgery applications [7]. Typically, nitrogen or argon is used in JT coolers, requiring pressures of 20 MPa (200 bar) or more on the high pressure side to achieve reasonable cooling. A disadvantage is the low efficiency when used in a closed cycle mode because the compressor efficiencies are very low when compressing to such high pressures. Another disadvantage of the JT cryocooler is the susceptibility of plugging or clogging the very small restriction by frozen moisture [28]. Brayton cryocoolers have cold moving parts and hence are difficult to miniaturize.

Regenerative (Oscillating flow)

The regenerative cryocoolers use atleast one regenerative heat exchanger, or regenerator, and operate with oscillating flow and pressure. They are analogous to AC electrical systems. In this analogy, pressure is analogous to voltage, and mass flow or volume flow is analogous to current. Further comparisons with electrical systems will be discussed later. In a regenerator, incoming hot gas transfers heat to the matrix of the regenerator, where the heat is stored for a half cycle in the heat capacity of the matrix. In the second half of the cycle the returning cold gas flowing in the opposite direction through the same channel, picks up heat from the matrix and returns the matrix to its original temperature before the cycle is repeated. At equilibrium, one end of the regenerator is at room temperature while the other end is at the cold temperature. Very high surface areas for enhanced heat transfer are easily achieved in regenerators through the use of stacked fine-mesh screen or packed spheres.

1.3 Scope of the thesis

Research on miniaturization of cryocoolers started at the University of Twente in the late 90s. The research, primarily funded by STW (Dutch Technology Foundation) is carried out at the Cooling and Instrumentation group headed by Prof. H.J.M ter Brake. J.F. Burger was the first research student on the project and he has investigated miniaturization aspects of various cooling principles [23], including recuperative and regenerative gas cycles. He chose to investigate JT cooler in detail and his efforts lead to the design of a sorption compressor powered closed cycle JT cooler that cooled to about 165 K [29–31]. In his conclusions he suggested investigating further both recuperative and regenerative cycles.

As a follow-up, two new projects took shape. The first was on the continuation of the work of Burger on the recuperative coolers. Lerou worked as a research student on the project and has developed JT cold tips fabricated with microsystems technologies [32]. The second project is devoted to understanding the scaling aspects of regenerative cycles and is the subject of this thesis. For both these projects the specifications of the microcooler was to provide 10 mW net refrigeration power at a cold temperature of 80 K.

1.4 Regenerative cryocoolers

1.4.1 Stirling

Because of its long history, the Stirling cryocooler may be considered the 'parent' of the other forms of regenerative cryocoolers shown in figure 1.2 (b). The Gifford-McMahon and pulse-tube refrigerators are variations of the Stirling refrigerator. Operation of the pulse-tube refrigerator is best understood by first considering the operating principles of the Stirling refrigerator.

The Stirling cryocooler shown in figure 1.2 (b) consists of a compressor, regenerator, displacer and heat exchangers. The compressor in the Stirling refrigerator is a valve less type and is also called a pressure oscillator. It is simply an oscillating piston or it could be an oscillating diaphragm. It creates an oscillating pressure in the system where the amplitude of oscillation is typically about 10 to 30 % of the average pressure. In order to provide high power densities and keep the system small, the average pressure is typically in the range of 1 to 3 MPa and frequencies are in the range of 20 to 60 Hz. Helium is almost always used as the working fluid in the regenerative cycles because of its ideal gas properties, its high thermal conductivity, and its high ratio of specific heats.

A pressure oscillation by itself in a system would simply cause the temperature to oscillate and produce no refrigeration. The second moving component, the displacer, is required to separate the heating and cooling effects by introducing motion of the gas in the proper phase relationship with the pressure oscillation.

Classical explanation of Stirling cryocooler is done with an ideal Stirling cycle [19]. Figure 1.3 shows the position of compressor and expansion pistons during intermediatory steps in a cycle. Let us assume that initially the compressor piston is away and the expansion piston is close to the face of the regenerator. All the working fluid is then in the compression space at ambient temperature T_W, the volume is a maximum, and the pressure and temperature are at the state (1) on the P-V diagram, shown in figure 1.4. During compression, process *a*, the compression piston moves towards the regenerator and the expansion piston remains stationary. The working fluid is compressed in the compression space, and the heat of compression is removed by heat exchange with the ambient.

In the process *b*, both pistons move simultaneously, the compression piston towards, and the expansion piston away from, the regenerator. The working fluid is transferred through the regenerator to the expansion space. In passing through the regenerator, the working fluid is cooled by transferring heat to the matrix, and emerges from the regenerator into the expansion space at temperature T_C.

In the expansion process *c*, the expansion piston moves away from the regenerator; the compression piston remains stationary, adjacent to the regenerator. As the expansion proceeds, the pressure decreases as the volume increases. During this process the cooled gas absorbs heat from the device it is cooling. This is the useful refrigeration of the cycle.

Finally both pistons move simultaneously to transfer the working fluid back through the regenerative matrix from the expansion space to the compression space. In passing through the matrix, heat is transferred from the matrix so the working fluid increases in temperature (process *d*).

The ideal Stirling cycle described above has two pistons: compressor and expansion piston. However, practical Stirling coolers have just one piston which is the compressor piston and the second a displacer. The displacer is different from a piston in the sense that it has to be strong enough only to overcome the pressure drop along the regenerator to shift the gas from one location to another. The cyclic process in a practical Stirling cooler can be best described as follows: When the displacer in figure 1.2 *b* is moved downward, the helium gas is displaced to the warm end of the system through the regenerator. The piston in the compressor then compresses the gas, and the heat of compression is removed by heat exchange with the ambient. Next the displacer is moved up to displace the gas through the regenerator to the cold end of the system. The piston then expands the gas, now located at the cold end, and the cooled gas absorbs heat from the system it is cooling before the displacer forces the gas back to the warm end through the regenerator. There is little pressure difference across the displacer (only enough to overcome the pressure drop in the regenerator) but there is a large temperature difference. Stirling cryocoolers usually have the regenerator inside the displacer as shown in figure 1.2 *c*.

In practice, motion of the piston and the displacer are almost always sinusoidal. The correct phasing occurs when the volume variation in the cold expansion space

leads the volume variation in warm compression space by about 90^0 (see figure 1.3). With this condition, the mass flow or the volume flow through the regenerator is approximately in phase with pressure. In analogy with AC electrical systems, real power flows only with current and voltage in phase with each other. Without the displacer in the Stirling cycle the mass flow leads the pressure by 90^0 and no refrigeration occurs. Though the moving piston causes both compression and expansion of the gas, a net power input is required to drive the system since the pressure is higher during the compression process. Likewise, the moving displacer reversibly extracts net work from the gas at the cold end and transmits it to the warm end where it contributes some to the compression work. In an ideal system, with isothermal compression and expansion and a perfect regenerator, the process is reversible. Thus, the coefficient of performance COP for the Stirling refrigerator is the same as the Carnot COP.

1.4.2 Gifford-McMahon

The Gifford-McMahon (GM) cryocooler is similar to that of the Stirling crycooler in operation except that the compressor has valves. In the mid-1960s Gifford and McMahon [33, 34] showed that the pressure oscillation for cryocoolers could be generated by the use of a rotary valve that switches between high- and low-pressure sources. This way the cold head could be placed far away from the compressor thereby reducing the noise levels. The Gifford-McMahon refrigerator has the same low-temperature parts as the Stirling refrigerator. Use of rotary valves also allowed the early GM cryocoolers to use compressors designed for air conditioning equipment which required oil removal equipment for longer lifetime. The irreversible expansion through the valves significantly reduces the efficiency of the process, but the advantage of this approach is that it allows for an oil-lubricated compressor to supply the high- and low pressure sources with oil-removal equipment on the high pressure side. The cold head could be placed quite some distance from the compressor and connected by flexible lines for the high and low pressure gas.

1.4.3 Pulse-tube

Pulse-tube cryocooler development started as a laboratory curiosity in the 1960s to become today, the most efficient and reliable cryocoolers for temperatures between about 60 and 120 K. In 1963 Gifford and Longsworth discovered a refrigeration technique which eliminates the displacer from the Stirling refrigerator which these days is known as the Basic pulse-tube Regrigerator (BPTR) [35]. It is interesting to note that the BPTR has not much in common with modern PTR's which work on a completely different principle. Efficiencies of this arrangement were very poor, and, as a result, little work was done with the basic pulse-tube refrigerator. The

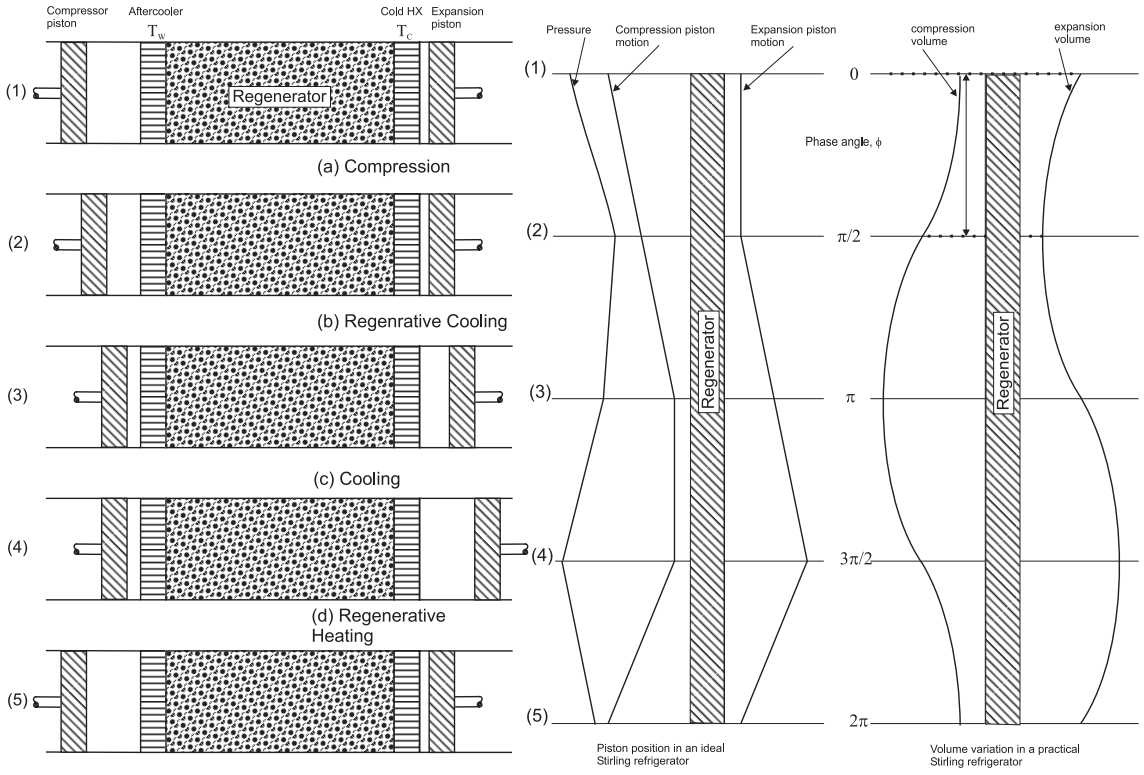

Figure* 1.3: Schematic of intermediate steps in an ideal Stirling cooler cycle. The piston position in an ideal cycle and volume variation in a practical cycle is also shown.*

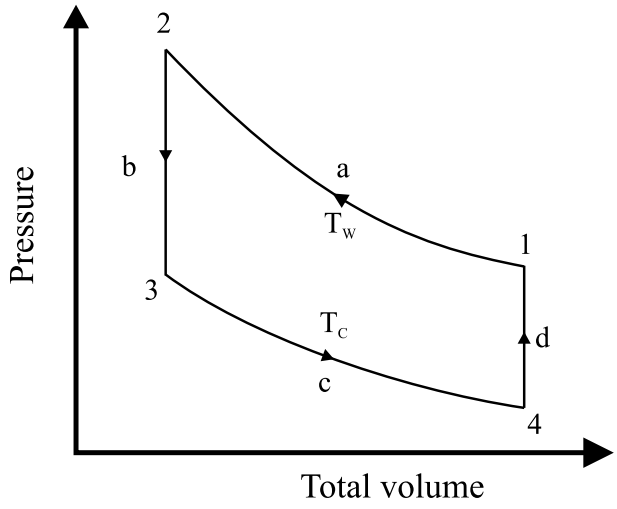

***Figure* 1.4:** *PV diagram of the Stirling cooler cycle.*

lowest temperature reached with BPTR was 124 K with a single stage PTR and 79 K with a two stage PTR [36].

In 1984 Mikulin et al. [37] inserted an orifice at the warm end of the pulse-tube to allow some gas to pass through to a large reservoir volume and achieved a low temperature of 105 K using air as the working gas. Soon afterwards Radebaugh et al. [38] reached 60 K with a similar device using Helium gas as shown in figure 1.2 (d). The proper gas motion in phase with the pressure is achieved by the use of an orifice and a reservoir volume to store the gas during a half cycle. The reservoir volume is large enough that negligible pressure oscillation occurs in it during the oscillating flow. The oscillating flow through the orifice separates the heating and cooling effects just as the displacer does for the Stirling and Gifford-McMahon refrigerators. The orifice pulse-tube refrigerator (OPTR) operates ideally with adiabatic compression and expansion in the pulse-tube. The four steps in the cycle are as follows. (1) The piston moves down to compress the gas in the pulse tube. (2) Because this heated compressed gas is at a higher pressure than the average in the reservoir, it flows through the orifice into the reservoir and exchanges heat with the ambient through the heat exchanger at the warm end of the pulse-tube. The flow stops when the pressure in the pulse-tube is reduced to the average pressure. (3) The piston moves up and expands the gas adiabatically in the pulse tube. (4) This cold low-pressure gas in the pulse-tube is forced past the cold end heat exchanger by the gas flow from the reservoir into the pulse-tube through the orifice. The flow stops when the pressure in the pulse-tube reaches to the average

pressure. The cycle then repeats.

The function of the pulse-tube is to insulate the processes at its two ends. That is, it must be large enough that gas flowing from the warm end traverses only part way through the pulse-tube before the flow is reversed. Likewise, flow in from the cold end never reaches the warm end. Gas in the middle portion of the pulse-tube never leaves the pulse-tube and forms a temperature gradient that insulates the the two ends. Roughly speaking, the gas in the pulse tube is divided into three segments, with the middle segment acting like a displacer but consisting of gas rather than a solid material.

The absence of the moving displacer in pulse-tube cryocoolers gives them many potential advantages over Stirling cryocoolers. These advantages include higher reliability, lower cost, lower vibration, less EMI (Electro Magnetic Interference). Earlier pulse-tube cryocoolers were not nearly as efficient as Stirling cryocoolers, but advances in the last ten years have brought pulse-tube refrigerators to the point of being the most efficient of all cryocoolers. The improved efficiency is because of the better understanding and the introduction of passive elements such as secondary orifice and inertance tube. Radebaugh [21] has comprehensively discussed the advances made in the pulse-tube refrigerators. In chapter 3 and 4, the importance of inertance tube is discussed.

There are three different geometries that have been used with pulse tube cryocoolers as shown in figure 1.5. The inline arrangement is the most efficient because it requires no void space at the cold end to reverse the flow direction nor does it introduce turbulence into the pulse-tube from the flow reversal. The disadvantage is the possible awkwardness associated with having the cold plate located between the to warm ends. The most compact arrangement and the one most like the geometry of the Stirling cryocooler is the coaxial arrangement. That geometry has the potential problem of a mismatch of temperature profiles in the regenerator and in the pulse-tube that would lead to steady heat flow between the two components and a reduced efficiency.

1.5 Objective

The main objective of this research was to investigate miniaturization of regenerative cryocoolers. This work will aid in designing a micro pulse-tube refrigerator for on-chip cryogenic applications. Furthermore, the understanding of high frequency operation of the regenerator will allow increasing the power density of existing commercial cryocoolers leading to reduced dimensions (size), mass and overall cost of such cryocoolers.

In summary, this thesis outlines what has previously been done, what was needed, how to do it, results (experimental), implications of the results, and future work needed.

Chapter 2 starts by discussing previous studies and why this investigation was

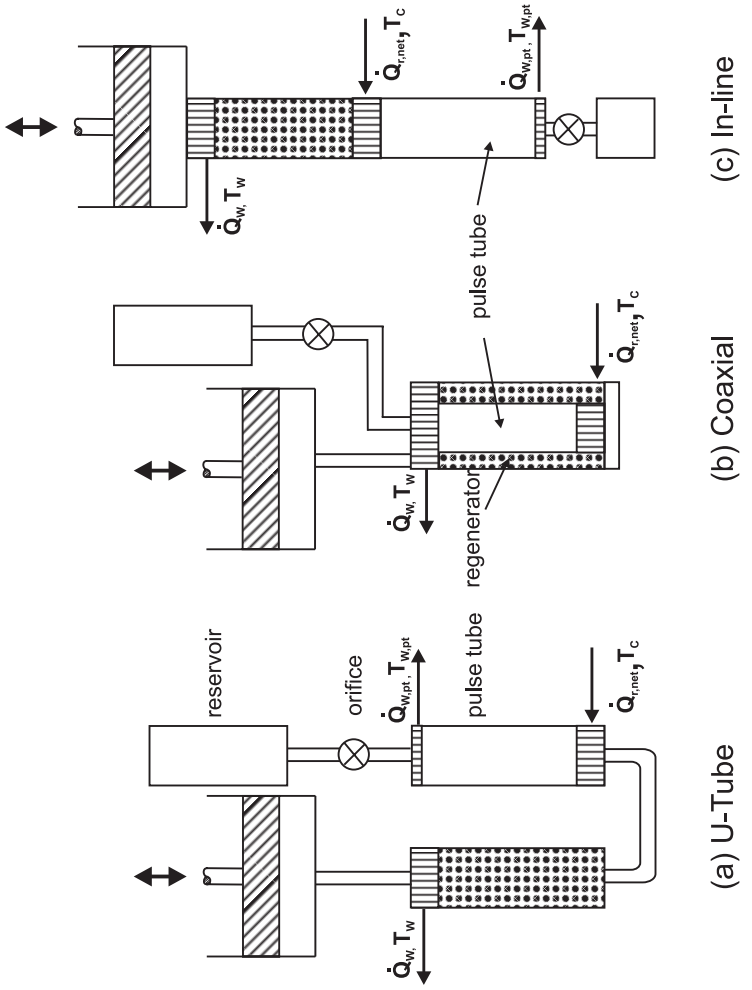

***Figure* 1.5:** *Several different geometries of pulse-tube cryocoolers.*

needed. Chapter 3 introduces the phasor representation of oscillating systems and applies this analysis for studying the influence of various parameters on the regenerator performance. Expressions for various losses in the regenerator were derived as a function of regenerator operation and geometry parameters. High frequency operation of the regenerator was also discussed in greater detail. The design rules derived for the regenerator are used in chapter 4 for a systematic design of a pulse-tube refrigerator. The scaling down limitations of a pulse tube refrigerator operating at a certain frequency are also described. For efficient operation of small pulse-tube refrigerators the operating frequency must be increased. To experimentally verify the theoretical model of high frequency regenerator operation, a 120 Hz pulse-tube refrigerator is constructed. Experimental results of the 120 Hz pulse-tube refrigerator and comparison with theoretical model are discussed in chapter 5. The 120 Hz pulse-tube refrigerator with regenerator dimensions of 30 mm length and diameter of about 10 mm, cooled to 80 K in about 5.5 minutes with a cooling power of about 3.5 W. This very fast cooldown prompted us to model the cooldown process, which is described in chapter 6. In order to operate the regenerator at frequencies of the order of 1 kHz, a step towards micro pulse-tube development, small hydraulic diameter regenerator materials are necessary. In this respect, micro pillar matrices embedded in a micro fluidic channel fabricated with microsystem technologies are investigated in chapter 7. High frequency operation of pulse-tube refrigerators would need an accompanying efficient high frequency compressor. Piezoelectric actuators were chosen as a driver for this high frequency compressor due to many advantages. Design and experiments of this compressor are discussed in chapter 8. The last chapter in this thesis summarizes accomplishments of this research and proposes future work as an extension of this investigation.

Bibliography

[1] R. K. Kirschman. Low-Temperature Electronics. *IEEE Circuits and Devices Magazine*, 6(2), 1990.

[2] R. Radebaugh. Refrigeration for superconductors. *Proc. IEEE*, 92:1719-1734, 2004.

[3] H. J. M. ter Brake, and G. F. M. Wiegerinck Low-power cryocooler survey *Cryogenics*, 42:705-718, 2002.

[4] E. Pickwell, B. E. Cole, A. J. Fitzgerald, M. Pepper, and V. P. Wallace. In vivo study of human skin using pulsed terahertz radiation. *Phys. Med. Biol.*, 49:1595-1607, 2004.

[5] E. Pickwell, B. E. Cole, A. J. Fitzgerald, V. P. Wallace, and M. Pepper. Simulation of terahertz pulse propogation in biological systems. *Appl. Phy. Lett.*, 84:2190, 2004.

[6] L. Ozyuzer, A. E. Koshelev, C. Kurter, N. Gopalsami, Q. Li, M. Tachiki, K. Kadowaki, T. Yamamoto, H. Minami, H. Yamaguchi, T. Tachiki, K. E.

Gray, W. K. Kwok and U. Welp Emission of coherent THz radiation from super conductors. *Science 23*, 318:1291-1293, 2007.

[7] E. D. Marquadt, R. Radebaugh, and J. Dobak. A Cryogenic Catheter for Treating Heart Arrhythmia. *Advances in Cryogenic Engineering*, 43, 1998.

[8] J. Dobak. A review of cryobiology and cryosurgery. *Advances in Cryogenic Engineering*, 43:889–896, 1998.

[9] R. C. Longsworth. Cryo-Probe. US patent 5,452,582, Sept. 1995.

[10] J. Fraser. Cryogenic techniques in surgery. *Cryogenics*, 19:375–381, 1979.

[11] P. Le Pivert. Cryosurgery: Current Issues and Future Trends. In *Proc. 10th International Cryogenic Engineering Conf., Butterworth, Surrey*, pages 551–557, 1984.

[12] T. Fay. Early experiences with local and generalized refrigeration of the human brain. *J. Neurosurg.*, 16:239–259, 1959.

[13] I. S. Cooper and A. S. Lee. Cryostatic congelation: A system for producing a limited controlled region of cooling or freezing of biological tissues. *J. Nerv. Ment. Dis.*, 133:259–269, 1961.

[14] M. Gonder, W. Soannes, and V. Smith. Experimental prostate cryosurgery. *Invest. Urol.*, 1:610–619, 1964.

[15] A. A. Gage. What temperature is lethal for cells. *J, Derm. Surg. Oncol.*, 464:459–460, 1979.

[16] A. A. Gage. Cryosurgery in the treatment of cancer. *Surgery, Gynecology, and Obstetrics*, 174:73–92, 1992.

[17] B. Rubinsky. Cryosurgery. *Annual Review of Biomedical Engineering*, 2:157–187, 2000.

[18] D. Theodorescu. Cancer cryotherapy: Evolution and biology. *Reviews in Urology*, 6:s9–s19, 2004.

[19] G. Walker. *Cryocoolers, Part 1: Fundamentals.* Plenum Press, New York, 1983.

[20] G. Walker and E. R. Bingham. *Low-capacity cryogenic refrigeration.* 1994.

[21] R. Radebaugh. *Pulse tube cryocoolers*, pages 415–434. 2003. edited by S. Kakac, H. Smirnov, and M.R. Avelino, Kluwer academic publishers, Dordrecht, The Netherlands.

[22] R. Radebaugh. Fundamentals of alternate cooling. *G. Walker, Cryocoolers part 2:Applications*, pages 129–175, 1983. Plenum Press, New York.

[23] J. F. Burger. *Cryogenic Microcooling - A micromachined cold stage operating with a sorption compressor in a vapor compression cycle.* PhD thesis, Universiteit Twente, 2001.

[24] R. I. Epstein, M. I. Buchwald, B. C. Edwards, T. R. Gosnell, and C. E. Mungan. Observations of laser induced flourescent cooling of a solid *Nature*, 377:500-503, 1995.

[25] C. E. Mungan, M. I. Buchwald, B. C. Edwards, R. I. Epstein, and T. R. Gosnell. Laser cooling of a solid by 16 K starting from rooom temperature *Phys. Rev. Letters*, 78:1030, 1997.

[26] T. R. Gosnell. Laser cooling of a solid by 65K starting from room temperature *Optics Letters*, 24:1041, 1999.

[27] R. J. Buist, J. Fenton, G. Lichniak, and P. Norton. Low temperature thermoelectric cooler for 145 k detector array package. *Report ADB008934*, 1976.

[28] P. P. P. M. Lerou, H. J. M. ter Brake, H. J. Holland, J. F. Burger, and H. Rogalla. Insight into clogging of micromachined cryogenic coolers. *Appl. Phys. Lett.*, 064102, 2007.

[29] J. F. Burger, M. C. van der Wekker, E. Berenschot, H. J. Holland, H. J. M. ter Brake, H. Rogalla, H. Gardeniers, and M. Elwenspoek. High pressure check valve for application in a miniature cryogenic sorption cooler. In *In Proceedings of IEEE MEMS*, 1999.

[30] J. F. Burger, H. J. Holland, E. Berenschot, J. H. Seppenwoolde, H. J. M. ter Brake, H. Gardeniers, and M. Elwenspoek. 169 kelvin cryogenic microcooler employing a condenser, evaporator, flow restriction and counterflow heat exchangers. In *In Proceedings of IEEE MEMS*, 2001.

[31] J. F. Burger, H. J. Holland, H. J. M. ter Brake, M. Elwenspoek, and H. Rogalla. Construction and operation of a 165 k microcooler with a sorption compressor and a micromachined cold stage. *Cryocoolers*, 12:643–649, 2002.

[32] P. P. P. M. Lerou, G. C. F. Venhorst, C. F. Berends, T. T. Veenstra, M. Blom, J. F. Burger, H. J. M. ter Brake, and H. Rogalla. Fabrication of a micro cryogenic cold stage using MEMS-technology. *Journal of Micromechanics and Microengineering*, 16(10):1919–1925, 2006.

[33] W. E. Gifford and H. O. McMahon. A new refrigeration process. In *Proc. Tenth International Congress of Refrigeration*, vol 1, 1959.

[34] H. O. McMahon and W. E. Gifford. A new low temperature gas expansion cycle. *Advances in Cryogenic Engineering*, 5:354–372, 1960.

[35] W. E. Gifford and R. C. Longsworth. Pulse tube refrigeration. In *Trans. ASME*, 1964.

[36] R. C. Longsworth. An experimental investigation of pulse tube regrigeration heat pumping rates. *Advances in Cryogenic Engineering*, 12:608–618, 1967.

[37] E. I. Mikulin, A. A Tarasov, and M. P. Shkrebyonock. Low-temperature expansion pulse tubes. *Advances in Cryogenic Engineering*, 29:629–637, 1984.

[38] R. Radebaugh, J. Zimmerman, D. R. Smith, and B. Louie. Comparison of three types of pulse tube refrigerators: New methods for reaching 60 K. *Advances in Cryogenic Engineering*, 31:779–789, 1986.

Chapter 2

Previous work

This chapter presents a brief overview of the past and existing efforts towards the development of miniature cryocoolers. Currently, gas cycles are the only techniques by which cryogenic temperatures are attainable. Hence, these techniques are discussed in greater detail.

2.1 Thermoelectric cooler

Figure 2.1 shows an illustration of a micro cryogenic (below -150^{0}C) thermoelectric (TE) cooler under development at Heat Transfer Physics group of Prof. Massoud Kaviany at the University of Michigan, Ann Arbor [1]. The micro machined thermoelectric cooler is supported on a substrate and is encapsulated from the external environment using a package cap that provides vacuum encapsulation and radiation shielding to minimize thermal losses. A MEMS or IC chip is mounted in the middle of the cooler and the signals are transferred out using sealed feed throughs. A major advantage of this design is its small size and potential low cost due to the use of wafer-level packaging and fabrication technologies. The thermoelectric materials used are telluride compound films.

Although the TE cooler is very interesting for microcryocooler applications, the success of the design will depend on many factors. First, is the materials that will be used to make the thermoelectric junction. As was mentioned in the previous chapter TE coolers have very low efficiency at lower temperatures (below 200 K). Till date there has been no published literature on TE coolers reaching cryogenic temperatures. The second challenge is the vacuum packaging with interconnections in the micro scale. It is rather difficult to maintain high vacuum in the microstructures. Research is being carried out at the TST group at the University of Twente to investigate vacuum packaging and interconnections.

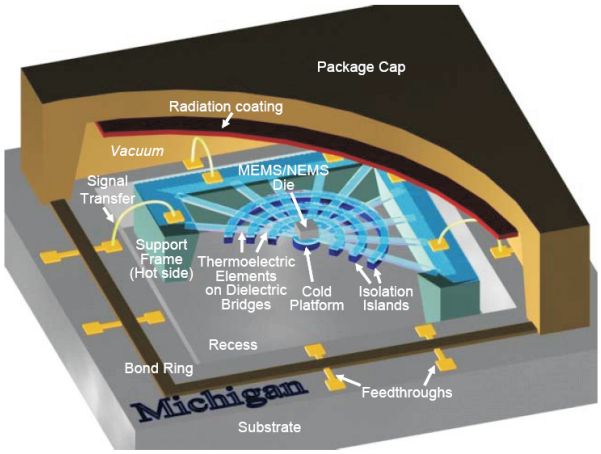

Figure* 2.1: Concept of MEMS cryogenic thermoelectric cooler under development at the University of Michigan [1].*

2.2 Joule Thomson cryocooler

During the 1980's, Little et al. pioneered the work on recuperative micro coolers. Using an abrasive etching process also called powder blasting in microsystems literature, they made a range of miniature cold stages [2, 3]. The cold stage shown in figure 2.2 *a*, used an open-loop recuperative cycle with nitrogen gas supplied from a gas bottle at a pressure of 165 bar and a flow rate of 3 mg/s. These coolers were made commercially available by MMR Technologies [4]. The smallest size is about 60 x 14 x 2 mm (1.68 cc). It can cool down to 35 K with a cooling power of 50 mW using a two stage nitrogen / neon Linde-Hampson[1] configuration.

In early 2000, Burger et al. developed a Joule-Thomson (JT) cold stage with a total volume of 0.76 cc (77 x 9 x 1.1 mm, see figure 2.2 *b*). They combined the cold stage with a sorption compressor, thus realizing a closed-cycle micro cooler [5]. This miniature cooler had a cooling power of 200 mW @ 170 K. Burger used Micro Electro Mechanical System (MEMS) technology to construct the components of the cold stage. Wet KOH etching and wafer bonding techniques were used for the fabrication of a condenser, restriction and evaporator in silicon. Counter-flow heat exchangers were made out of tiny glass capillaries. After fabrication, the different cold stage parts were glued together.

Lerou et al. followed up Burgers work on JT coolers to develop a cold-stage that would be reproducible with a simple production process. In comparison to Little's

1. This cycle is quite similar to the Joule-Thomson cycle with a difference in the compression step.

abrasive etching process, a reliable and relatively accurate wet chemical etching processes typically used in MEMS technology was used by Lerou. The prototypes of the manufactured cold tips are shown in figure 2.2 *c*. Another important difference with Little's work was the optimization of cold stages for maximum cooling power. The coefficients of performance (COP) of the micro cold stages were approximately double compared to Little's design. Similar to Little the cold stage was supplied with a high pressure nitrogen gas at 80 bar. The temperature reached by the cold stages was about 96 K [6]. However, the cold stages clogged after about 3 hour of continuous operation. Lerou et al. [7] attributes the clogging to the presence of water in the cooler that deposits in the counter-flow heat exchanger and obstructs the flow through the JT restriction. One of the recommendations of Lerou [8] to make a closed cycle JT cooler is to use a sorption compressor. At the time of writing this thesis there is a follow up project of Lerou on the micro JT stage to integrate the cold tips with a sorption compressor.

2.3 Regenerative cryocooler

Regenerative cryocoolers work with modest pressure ratios compared to recuperative cycles which make them attractive cycles for miniaturization of the entire cooler including the compressor. Several papers address the scaling issues of regenerative cryocoolers with emphasis only on the conduction loss and heat transfer effectiveness of the regenerator [9].

Nakajima et al [10] studied miniaturization of Stirling engines, which are essentially Stirling coolers operating in the reverse mode. They realized a Stirling engine with a piston swept-volume of about 0.05 cc that produces a power of 10 mW at 10 Hz.

Peterson proposed a Stirling cooler with resonantly coupled expansion piston [11] as shown in figure 2.3 (a). This cooler contains a membrane with bellows instead of cylindrical pistons. The resonance frequency of such a membrane is of the order of several kHz [16]. The aspect of regenerator operation at such frequencies was not studied by the author.

Peterson et al. [9, 12] and others [13] tried to establish a theoretical lower size limit to the regenerative cryocooler, by comparing the conduction heat losses of the regenerator as a function of length scale. Their studies suggest that, given the thermal and mechanical properties of the materials available today for manufacturing regenerators, the regenerator could be shortened to 5 - 10 mm when operating at 1 kHz.

Bowman et al. [17] patented a microminiature Stirling cooler concept as shown in figure 2.3 (b). The cold-stage temperature is placed normal to the wafer plane. The top side is the cold end where the electronics are located. The bottom side contains the compressor actuator. In between, regenerative displacers are located, suspended on thin diaphragms. There has been no work reported on the realization

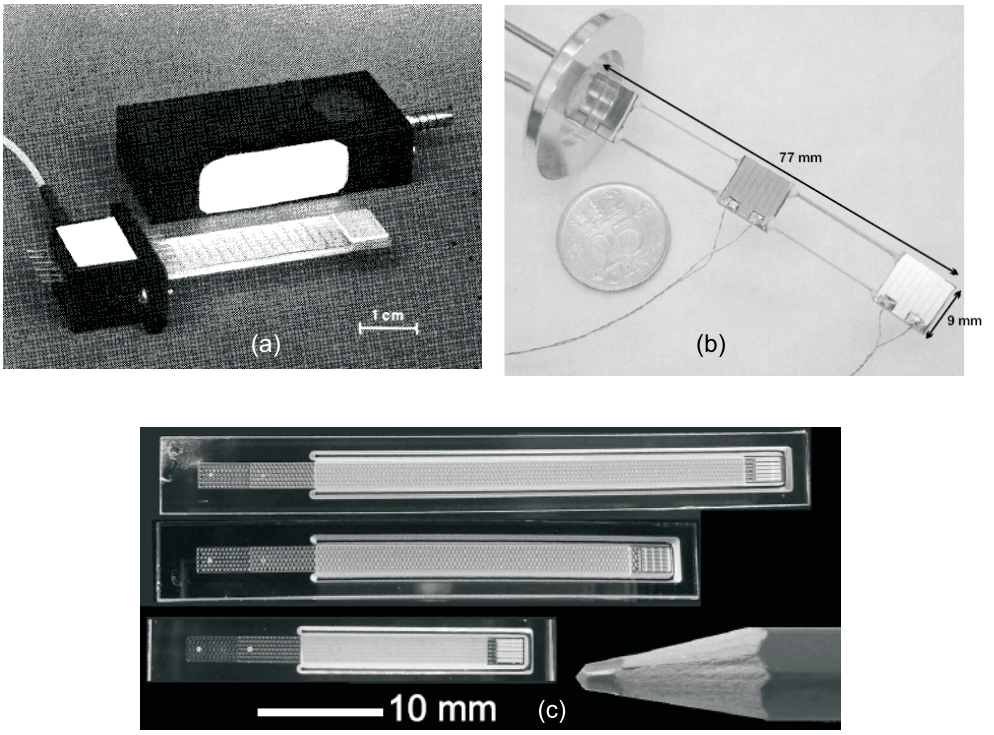

Figure* 2.2*: *Micro Joule Thomson cooler developments. (a) Realization of the first micro JT cooler by Little et al. [3] which is commercialized by MMR technologies. (b) 165 K closed cycle JT cooler with a sorption compressor (not shown in figure), described by Burger [5]. (c) Micro JT tips as presented by Lerou [8].*

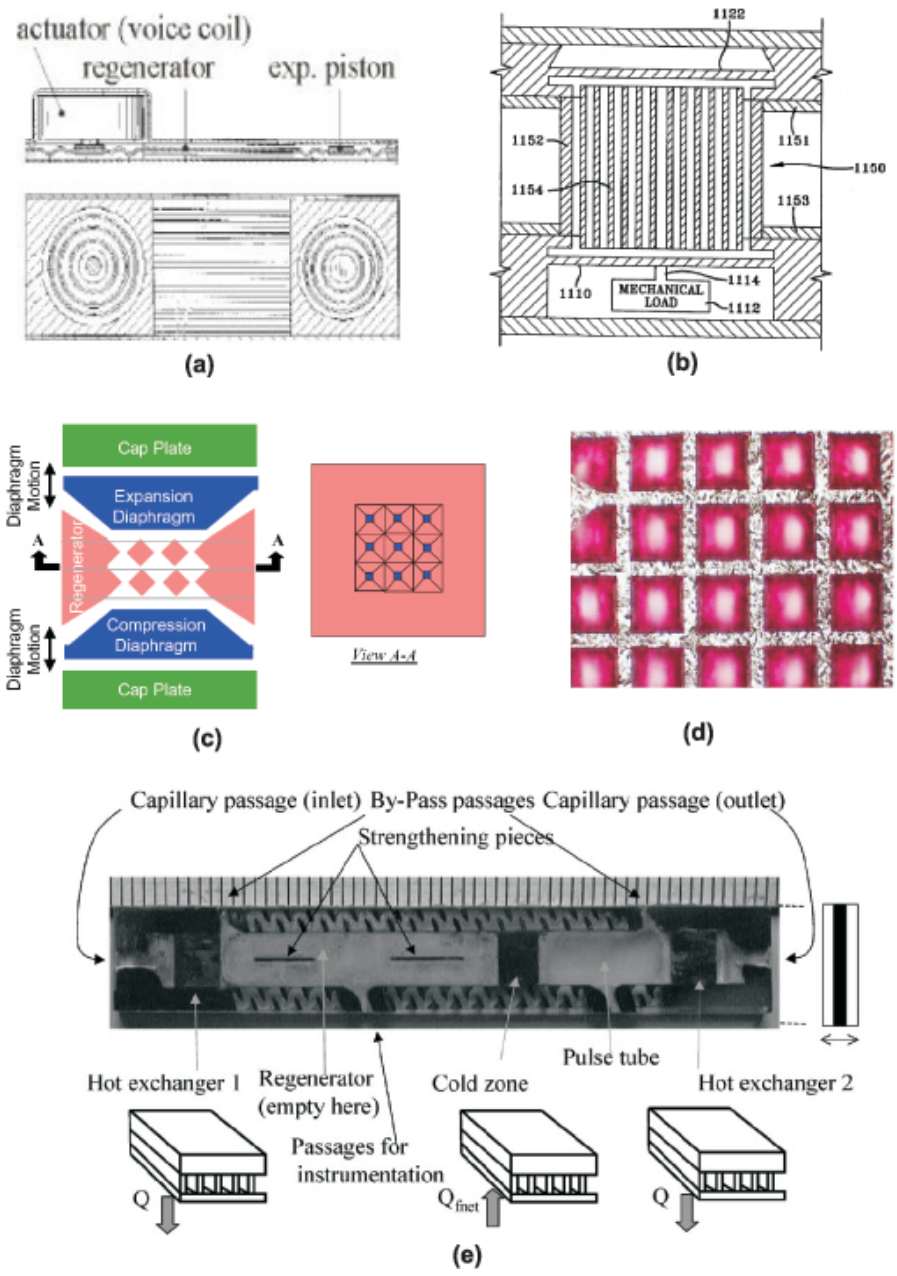

Figure* 2.3: Development of miniature cryocoolers based on Stirling cycle. (a) Concept of resonantly coupled expansion piston by Peterson [11].(b) Concept of Stirling cooler patented by Bowman et al. [17]. (c) Schematic of Stirling cooler with active diaphragms as described by Maron et al. [19] (d) Fabricated regenerator material. (e) Cross-section of double inlet pulse-tube refrigerator as described by Nikka et al. [21].*

of this cooler. As discussed by Burger [16] it is unlikely that a large temperature gradient can be sustained on a small length scale without much conduction losses. Hence, the patent of Bowman is only a concept which cannot be realized in practice.

A similar patent by Maron [14], published shortly after, basically follows the same concepts put forward by Bowman with some modifications as relating to cycle control. Some experimental work followed Moran's patent at the NASA Glenn Research Center [18]. The illustration of the proposed system is shown in figure 2.3 (c). The 1- by 1-cm regenerator will be fabricated using MEMS processes. Commercial (non-MEMS) piezoelectric actuators were proposed to drive the compression and expansion diaphragms, which are the only moving parts of the device. The diaphragms are deflected toward and away from the regenerator region in phase-shifted sinusoidal fashion to produce the Stirling cycle. Expansion of the working gas directly beneath the expansion diaphragm in each cycle creates a cold end for extracting heat, whereas compression at the other end creates a hot region for rejecting heat. Heat is transferred to and from the working gas as it is forced through the regenerator region by the moving diaphragms. The development of a regenerative heat exchanger for the proposed Stirling system was reported by Maron et al. [19]. The fabricated prototype comprised of ten separate assembled layers of alternating metal (nickel)-dielectric (photoresist) composite. Each layer is offset to minimize conduction losses and maximize heat transfer. A grating pattern of 100 μm square non-contiguous flow passages were formed as shown in figure 2.3 (d), with a nominal 20 μm wall thickness, and an overall assembled ten-layer thickness of 900 μm. Experimental results were not available and further developments on the system were not reported.

In chapter 1 we have discussed several advantages of the pulse tube refrigerator (PTR) over Stirling cryocoolers. The most distinctive feature of the PTR is that that it has no moving parts at the cold end. Hence, similar to JT cold tips, micro pulse-tube cold tips can be manufactured with less manufacturing complexity. However, the operation of a PTR is more complex than that of the JT cold tip. For efficient operation of the PTR, the processes in the pulse-tube must be nearly adiabatic which means the gas must be well insulated from the tube walls (tube radius must be an order larger than the thermal diffusion depth of the working gas). In a large system, adiabatic conditions can be easily achieved where as it gets critical when the system is miniaturized. The diffusion depth varies with frequency of operation as $1/\sqrt{f}$. Hence, increasing the frequency of operation will allow efficient operation of the pulse-tube and hence miniaturization of the PTR. Until recently, efficient operation of regenerative cryocoolers at frequencies above about 60 Hz has not been possible because of poor heat transfer in the regenerative heat exchanger. A no-load temperature of only 147 K was achieved at 350 Hz [15]. Radebaugh has shown that, with the right combination of operating parameters and regenerator geometry, efficient operation at frequencies even up to 1 kHz may be possible [20].

A double inlet orifice pulse-tube refrigerator fabricated with MEMS technologies was reported by Nikka et al. [21]. The cross-section of the fabricated orifice-PTR

is shown in figure 2.3 (e). It is made of three wafers, the top and bottom were glass wafers and the middle one is made of silicon. The silicon wafer was chemically etched to form various components of pulse-tube refrigerator. Glass beads were used as regenerator material. A commercially available linear motor compressor (not shown in figure) was used in the experiments. Experimental results show that the temperature reduction was only 10 to 12 degrees when operated at a filling pressure of 1.2 MPa and 50 Hz. As mentioned above the poor performance is because of the inefficient operation of pulse-tube at small scale at a frequency of 50 Hz.

2.4 What was needed?

As described in the previous chapter, the objective of this thesis was to investigate miniaturization of pulse-tube cryocoolers. However as mentioned above, miniaturization of pulse-tube cryocoolers is not straightforward. So the questions that need to be addressed are:

(a) What are the limitations of scaling down of pulse-tube cryocoolers?

The answer to this question depends on the scaling down constraints of various components of pulse-tube cryocooler, most important of them are, the regenerator, the pulse-tube and the phase shifting components such as the inertance tube and the reservoir. The thermodynamic behavior of these components are significantly different from each other. Regenerator has porous, densely packed material for heat storage during part of the cycle. The heat transfer process and the pressure drop are significantly affected by the geometry and the operating parameters of the regenerator. Hence, a detailed understanding of the influence of these parameters on the performance of the regenerator is necessary. Processes in the pulse tube must be nearly adiabatic for efficient operation of the cryocooler. The limitations in scaling down of the pulse-tube should be studied. The scaling down analysis should be verified experimentally to give us confidence for further scaling down the system.

(b) Can microsystems technology be used to fabricate micro pulse-tube cryocoolers?

One of the goals of the project is to investigate the use of microsystems technologies to batch produce cryocoolers. Since, this process is inherently a 2 and 1/2 D process the geometry is significantly different from the conventionally used regenerator materials. To use these new materials in the numerical programs for optimizing the regenerator, we need to obtain friction factor (pressure drop) and heat transfer correlations. Numerical simulation of the micro-structures were previously reported by several authors but there has been no systematic comparison of various structures. Hence, experimental characterization of these new materials would enable the use of new regenerative materials for micro-cryocoolers.

(c) Micro pulse-tube cryocooler would need an accompanying compressor, can

conventional compressors be scaled down?

Conventional compressors for driving pulse-tube cryocoolers are of moving coil or moving magnet type of electromagnetic actuators. Down scaling electromagnetic actuators result in issues relating to Joule heating of the coil. An alternative suitable actuation mechanism is a piezoelectric actuator. Piezoelectric actuators produce large force but very low stroke. Since micro pulse-tube cryocooler will have low gas volume, small stroke of piezoelectric actuators is not a major drawback. Micro compressors driven by piezoelectric actuators should be studied to evaluate their use to power a micro pulse-tube cryocooler.

Bibliography

[1] Prof. Massoud kaviany. http://www-personal.umich.edu/ kaviany/index.html.

[2] Logan S. Rowe R. Garvey, S. and W. A. Little. Performance characteristics of a low-flow rate 25 mW, LN2 Joule-Thomson refrigerator fabricated by photolithographic means. *Appl. Phys. Letters*, 42:1983, 1048-1050.

[3] W.A. Little. Microminature refrigeration. *Rev. Sci. Instrum.*, 55:661–680, 1984.

[4] MMR Technologies Inc., http://www.mmr.com.

[5] J. F. Burger, H. J. Holland, E. Berenschot, J. H. Seppenwoolde, H. J. M. ter Brake, H. Gardeniers, and M. Elwenspoek. 169 kelvin cryogenic microcooler employing a condenser, evaporator, flow restriction and counterflow heat exchangers. In *In Proceedings of IEEE MEMS*, 2001.

[6] P. P. P. M. Lerou, G. C. F. Venhorst, C. F. Berends, T. T. Veenstra, M. Blom, J. F. Burger, H. J. M. ter Brake, and H. Rogalla. Fabrication of a micro cryogenic cold stage using MEMS-technology. *J. Micromech. Microeng.*, 10:1956–1960, 2006.

[7] P. P. P. M. Lerou, H. J. M. ter Brake, H. J. Holland, J. F. Burger, and H. Rogalla. Insight into clogging of micromachined cryogenic coolers. *Appl. Phys. Lett.*, 064102, 2007.

[8] P. P. P. M. Lerou. *Micromachined Joule-Thomson cryocooler*. PhD thesis, University of Twente, 2007.

[9] R. B. Peterson. Size limits for regenerative heat engines. *Microscale Thermalphysical Engineering*, 2:121–131, 1998.

[10] N. Nakajima, K. Ogawa, and I. Fujimasa. Study on microengines: Miniaturizing stirling engines for actuators. *Sensors and Actuators*, 20:75–82, 1989.

[11] R. B. Peterson. Resonantly coupled alpha-stirling cooler. *US Patent 5813235*, 1998.

[12] R. B. Peterson, and M. Al-Hazmy. Size limits for Stirling cycle refrigerators. *Advances in Cryogenic Engineering*, 1997, 997-1002.

[13] J. M. Shire, A. Mujezinovic, and P. E. Phelan. Investigation of Microscale Cryocoolers. *Cryocoolers*, 10:1999, 663.

[14] M. E. Maron. Micro-scalable thermal control device. *USPTO*, 2002.

[15] K. M. Godshalk, C. Jin, Y. K. Kwong, E. L. Hershberg, G. W. Swift, and R. Radebaugh. Characterization of 350 Hz thermoacoustic driven orifice pulse tube refrigerator with measurements of the phase of the mass flow and pressure *Advances in cryogenic engineering*, 41:1411, 1996.

[16] J. F. Burger. *Cryogenic Microcooling - A micromachined cold stage operating with a sorption compressor in a vapor compression cycle.* PhD thesis, Universiteit Twente, 2001.

[17] L. Bowman and J. McEntee. Microminiature stirling cycle cryocoolers and engines. *US Patent 5749226*, 1998.

[18] M.E. Maron. Micro-scale avionics thermal management. NASA TM-2001-211095, http://gltrs.grc.nasa.gov/GLTRS, 2001. 34th International symposium on microelectronics, Maryland.

[19] M.E. Maron. Micro-scale regenerative heat exchanger. In *Conference on Micro-Nano-Technologies for Aerospace Applications*, AIAA-2004-6730, 2004.

[20] R. Radebaugh and A. O´ Gallagher. Regenerator operation at very high frequencies for microcryocoolers. *Advances in cryogenic engineering*, 51:1919, 2006.

[21] P. Nika, Y. Bailly, J. C. Jeannot, and M. De Labachelerie. An integratged pulse tube regrigeration device with micro exchangers: design and experiments. *Internation Journal of Thermal Sciences*, 42:1029–1045, 2003.

Chapter 3

The regenerator

The regenerator is the most important component of a regenerative cryocooler. The purpose of the regenerator is to transmit acoustic or PV power from the compressor to the cold end of the regenerator with a minimum of losses. These losses include thermal ineffectiveness (enthalpy flow), lost power associated with pressure drop and axial thermal conduction. These losses are complex functions of the dimensions and operation parameters of the regenerator. Phasor analysis was used in this chapter, to gain powerful insights into the influence of various parameters on the operation of the regenerator. The optimum phase relationship between the pressure and flow in the regenerator is to have them in phase at the midpoint of the regenerator, so as to minimize the amplitude of mass flow at each end of the regenerator for a given power flow through the regenerator. Parameter analysis indicates that the optimum specific area (ratio of gas cross-sectional area to mass flow) depends on the pressure drop, inefficient heat transfer, conduction and void volume losses. The conduction and void volume losses impose a limit on the length of the regenerator for a set of operating parameters. Numerical analysis of the regenerator is often the final tool used to optimize the regenerator. The convergence criteria and guesses for subsequent runs are described in this chapter.

3.1 Introduction

A regenerator is a heat exchanger which acts as a heat storage device. The difference between a regenerative and recuperative heat exchanger is that the latter has two fluids exchanging heat with each other through a separating wall. The fluids do not mix, nor do they come in direct contact with each other. A regenerative heat exchanger consists of a high heat capacity material with high surface area with which the fluid periodically exchanges energy. In Stirling type of refrigerators, the gas oscillates periodically through a single fixed matrix. The gas is heated by compression, then passed through the regenerative matrix, where the heat is absorbed by the matrix from the warm gas. Next, the fluid is cooled by expansion

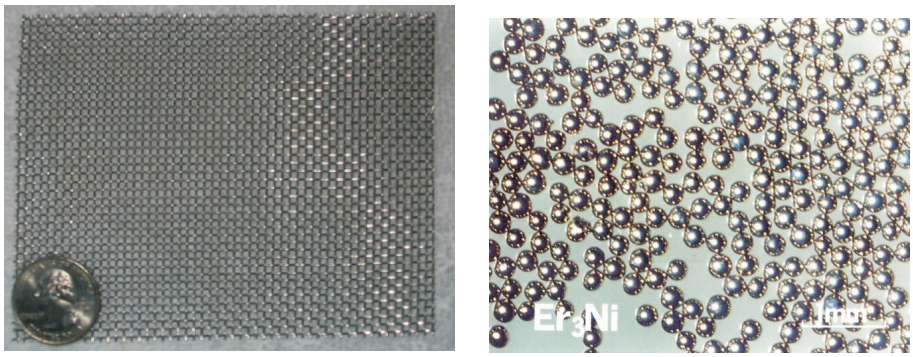

(a) Wire mesh screen (b) Spheres

Figure* 3.1: Commonly used regenerator materials.*

and passed through the matrix in the opposite direction where heat is absorbed by the gas from the matrix.

Figure 3.1 shows wire mesh screen and spheres which are typically used regenerator materials. Stirling cryocoolers use oscillating flows and pressures with frequencies of about 60 Hz. Heat flow at such frequencies can penetrate a medium only short distances, known as the thermal penetration depth δ_{th}. Figure 3.2 shows how the temperature amplitude of a thermal wave decays as it travels within a medium. The distance at which the amplitude is $1/e$ of that at the surface is the thermal penetration depth, which is given by,

$$\delta_{th} = \sqrt{\frac{\lambda}{\pi f \rho c_p}} \tag{3.1}$$

where λ is the thermal conductivity, f is the frequency, ρ is the density, c_p is the specific heat capacity of the medium. Higher frequencies lead to smaller penetration depths. For good heat transfer the lateral dimensions in the fluid or the solid must be much less than δ_{th}. Figure 3.3 shows the temperature dependence of the thermal penetration depth in helium, copper and stainless steel for a frequency of 60 Hz and 1 kHz. For copper, oscillating heat flow can penetrate large distances because of its higher thermal conductivity. However, for helium gas the thermal penetration depth is quite small, especially at low temperatures. Thus, the hydraulic diameter in the regenerator which characterizes the lateral dimension, must be much smaller.

The schematic of the regenerator with time averaged heat flows and oscillating pressure at the warm end T_w and cold end T_c is shown in figure 3.4. The amplitude

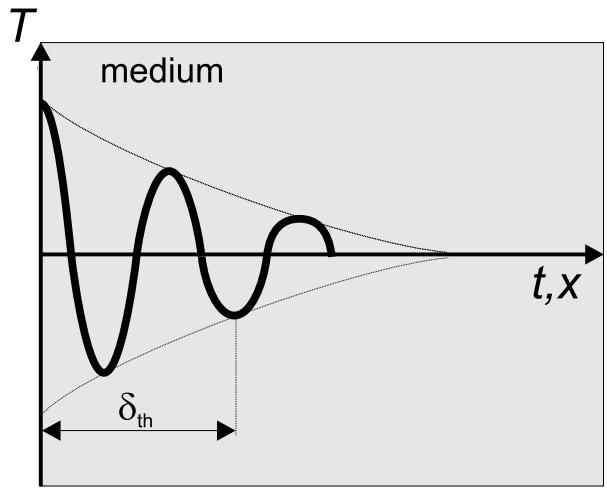

***Figure* 3.2:** *Schematic showing the decay of temperature amplitude inside a medium and the definition of thermal penetration depth.*

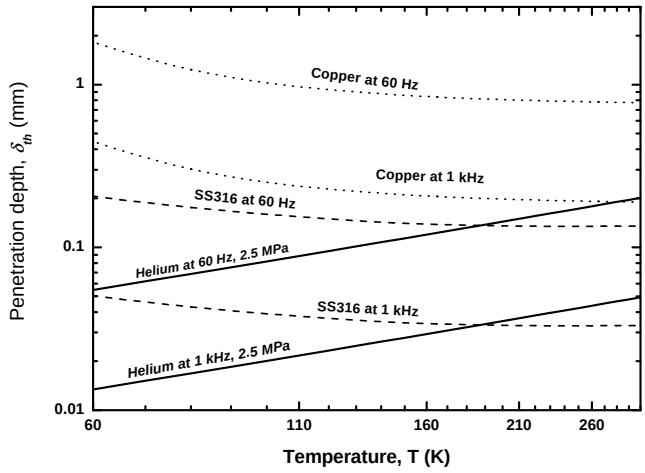

***Figure* 3.3:** *Thermal penetration depth in stainless steel (316), copper and helium (at 2.5 MPa) at a frequency of 60 Hz and 1 kHz.*

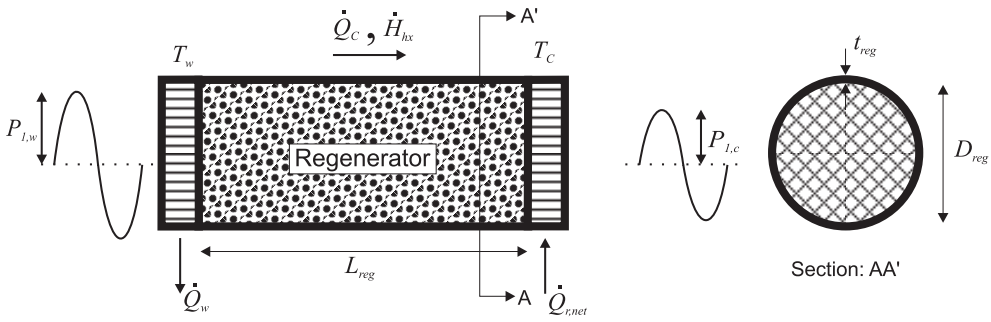

***Figure* 3.4:** *Schematic of the regenerator. The pressure oscillations at the two ends of the regenerator are shown. The pressure drop along the length of the regenerator cause the pressure amplitude at the cold end lower than the pressure amplitude at the warm end. The steady compression heat $\dot{Q}_w$ at the regenerator warm end, the net cooling power at the cold end $\dot{Q}_{r,net}$, the conduction loss from the warm to the cold end $\dot{Q}_c$ and the enthalpy flow loss $\dot{H}_{hx}$ are also shown in the figure.*

of the pressure at the cold end $P_{1,c}$ is lower than the warm end $P_{1,w}$ due to pressure drop along the length of the regenerator. $\dot{Q}_c$ and $\dot{H}_{hx}$ represent conduction and enthalpy flow losses (inefficient heat transfer between gas and the material) respectively whereas $\dot{Q}_w$ represents the heat rejected at the aftercooler and $\dot{Q}_{r,net}$ represents the net cooling power at the cold heat exchanger.

An ideal regenerator should satisfy the following conditions:

1. Zero pressure drop along the length of the regenerator ($\Delta P = 0$).
2. Enthalpy flow (the heat which is transferred to the cold end of the regenerator due to imperfect heat transfer between the gas and the solid) should be zero. ($\dot{H}_{hx} = 0$).
3. Infinite heat capacity ratio between the solid material and gas.
4. Zero void volume (gas volume).
5. Zero conduction loss from the warm to the cold end of the regenerator ($\dot{Q}_c = 0$).
6. The gas obeys ideal gas law.

The above requirements are rather conflicting because, as we will see in section 3.6, there is a trade off between pressure drop and heat transfer loss. Similarly, the gas volume in the regenerator cannot be zero and the conduction losses from the warm to the cold end cannot be avoided. Moreover, all the losses described above, vary with operating parameters and the dimensions of the regenerator. In order to gain powerful insight into the influence of various parameters on the performance of the regenerator, phasor analysis (graphical representation of oscillating parameter)

has been introduced and used in this chapter. Parameter analysis has been carried out to relate various regenerator losses as a function of operating parameters and the geometry of the regenerator. Numerical simulation is often the final step in the design of the regenerator to take into account the temperature dependence of fluid properties. An example numerical simulation of the regenerator with REGEN3.2[2] (a numerical tool that solves the conservation equations for the regenerator) was carried out and the results are qualitatively evaluated with the predictions from the parameter analysis.

3.2 Acoustic power flow

The time averaged acoustic or PV power flow[1] $\dot{W}_{PV}$ is given by,

$$\dot{W}_{PV} = \frac{1}{\tau_t} \int_0^{\tau_t} (P - P_0)\, \dot{V} dt, \tag{3.2}$$

where P is the pressure oscillation, P_0 the average or mean pressure, $\dot{V}$ is the volume flow rate evaluated at mean temperature and τ_t is the time period of oscillation. Assuming sinusoidal variations, the pressure and volume flow are given by,

$$P = P_0 + P_1 \cos\omega t \tag{3.3}$$

and

$$\dot{V} = \dot{V}_1 \cos(\omega t + \phi) \tag{3.4}$$

The terms P_1 and $\dot{V}_1$ are the amplitudes of sinusoidal pressure and volume flow, respectively, ω is the angular frequency, and ϕ is the phase by which the volume flow leads the pressure. The PV power flow for sinusoidally varying pressure and volume flow becomes,

$$\dot{W}_{PV} = \frac{1}{2} P_1 \dot{V}_1 \cos\phi \tag{3.5}$$

Expressing volume flow in terms of mass flow $\dot{m}$ using ideal gas law, the PV power becomes,

$$\dot{W}_{PV} = \frac{1}{2} P_1 \dot{m} \frac{RT}{P_0} \cos\phi \tag{3.6}$$

where R is the specific gas constant and T is the mean temperature at that location. In an ideal Stirling type of refrigerator the enthalpy flow $\dot{H}_{hx} = 0$. Applying the first law of thermodynamics across the cold heat exchanger, the gross refrigeration power $\dot{Q}_r$ is equal to the acoustic or PV power at the cold end of the regenerator $\dot{W}_{PV,c}$,

$$\dot{Q}_r = \dot{W}_{PV,c} = \frac{1}{2} P_1 \dot{V}_{1,c} \cos\phi = \frac{1}{2} P_1 \dot{m} \frac{RT_c}{P_0} \cos\phi \tag{3.7}$$

1. The power flow is equivalent to the power calculated from the PV diagram that a fictitious isothermal piston follows at that location [1]

where T_c is the cold temperature and $V_{1,c}$ is the amplitude of the swept volume at the cold end of the regenerator. The losses in the expansion process (such as expanding piston in a Stirling displacer or in a pulse-tube) and in the regenerator (both pressure drop and inefficient heat transfer) would decrease the gross refrigeration power.

In an ideal regenerator, the pressure drop along the length of the regenerator is zero and also the void volume is zero. Hence, the PV power flow at the warm end $\dot{W}_{PV,w}$ is related to the cold end PV power $\dot{W}_{PV,c}$ as,

$$\dot{W}_{PV,w} = \frac{T_w}{T_c}\dot{W}_{PV,c} \tag{3.8}$$

where T_w and T_c are the warm and cold end temperatures of the regenerator, respectively.

The coefficient of performance of the refrigerator (referred to the regenerator warm end) is defined as the the ratio of the net cooling power $\dot{Q}_{net}$ to the PV power flow at the warm end as,

$$COP = \frac{\dot{Q}_{net}}{\dot{W}_{PV,w}} \tag{3.9}$$

For an ideal refrigerator the maximum COP is given by Carnot value which, is given by,

$$COP_{Carnot} = \frac{T_c}{T_w - T_c} \tag{3.10}$$

The efficiency of the refrigerator is usually expressed in relation to the Carnot COP as

$$\eta = \frac{COP}{COP_{Carnot}} \tag{3.11}$$

Pulse-tube refrigerators operating with warm and cold end temperatures of about 300 K and 80 K respectively have efficiencies (when referred to acoustic power at the regenerator warm end) in the range of 15 to 25 % of Carnot [3].

3.3 Phasor Fundamentals

In engineering systems such as electrical and mechanical systems, sinusoidal driving functions are very common. A number of tools were developed to analyze these oscillating systems. One of the most useful and easy to understand techniques is that of phasor analysis. In case of Stirling cycle systems, the volume variations of compression and expansion spaces are usually assumed to be sinusoidal for pressure ratios lower than about 1.5. Within these limits of lower pressure ratios Stirling systems can be considered linear systems. The phasor analysis techniques provide

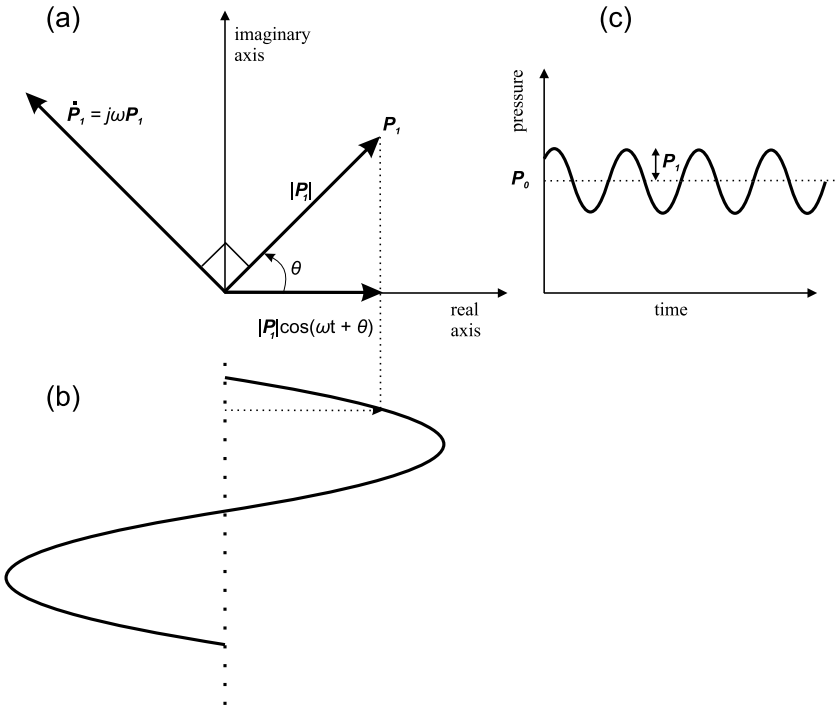

***Figure* 3.5:** *(a) Phasor representation of an oscillating sinusoidal function. The length of the arrow is equal to the amplitude of the oscillating quantity and the angle θ is the phase of quantity at $t = 0$. The derivative of phasor $\dot{\boldsymbol{P}}_1$ leads the phasor $\boldsymbol{P}_1$ by 90^0 degrees. (b) The illustration of sinusoidal function represented by the phasor. (c) Definition of average pressure P_0 and the amplitude of dynamic pressure P_1*

powerful insights into the relationship between the various parameters and into their physical significance.

A sinusoidal function $f(t) = P_1 \cdot \cos(\omega t + \theta)$ is represented by an arrow as shown in figure 3.5. This function can be generated by rotating the arrow in the counter clockwise direction. The projection of the arrow $\boldsymbol{P_1}$ on to the horizontal axis is $P_1 \cdot \cos(\omega t + \theta)$ where, the length of the arrow is P_1, the angular velocity of rotation is ω rad/s in the counterclockwise direction, the position of the arrow at $t = 0$ is θ radians from the horizontal axis. The arrow is termed as the phasor. The phasor is normally shown in the $t = 0$ position. The horizontal axis is referred to as the real axis and the vertical axis is the imaginary axis. We represent phasors in this chapter with bold variables. The phasor in figure 3.5 can be represented by the complex variable $P_1 \cdot e^{j(\omega \cdot t + \theta)}$. All the complex arithmetic can then be applied to the phasor. It must be noted that the phasor should not be confused with vectors, as an example oscillating pressure can be represented by a phasor but fundamentally pressure is a scalar quantity. The time derivative of a phasor is given as,

$$\frac{d}{dt} P_1 \cdot e^{j(\omega \cdot t + \theta)} = j\omega P_1 \cdot e^{j(\omega \cdot t + \theta)} \tag{3.12}$$

Since $j = e^{j\pi/2}$, we can write the derivative as,

$$\dot{\boldsymbol{P_1}} = \omega P_1 e^{j(\omega t + \theta)} e^{j\pi/2} = \omega P_1 e^{j(\omega t + \theta + \pi/2)} \tag{3.13}$$

Equation 3.13 shows that the time derivative of a sinusoid leads the original sinusoid by $\pi/2$ radians or 90^0. The time derivative $\dot{\boldsymbol{P_1}}$ is shown in figure 3.5.

PV power

The time averaged PV power given by equation 3.5 is represented in phasors as the dot product of the pressure and the volume flow phasor,

$$\dot{W_{PV}} = \frac{1}{2} \boldsymbol{P_1} \cdot \dot{\boldsymbol{V_1}} = \frac{1}{2} P_1 \dot{V_1} \cos s\phi \tag{3.14}$$

where the dot product treats the phasors as vectors and ϕ is the phase angle between $\boldsymbol{P_1}$ and $\dot{\boldsymbol{V_1}}$.

3.4 Phasor representation of isothermal and adiabatic systems

The first and second laws of thermodynamics describe the overall performance of the thermodynamic system. To understand the detailed behavior of the regenerative refrigerator, instantaneous operation of the components is necessary.

In a pulse-tube refrigerator the aftercooler, cold heat exchanger, warm heat exchanger and the regenerator can be considered as isothermal components. In a pulse-tube the process must be adiabatic and should have minimum heat exchange between the gas and the surrounding walls. We will first look at representing isothermal systems followed by adiabatic systems.

3.4.1 Phasor representation of isothermal components

The differential equation for conservation of mass is given by,

$$\frac{\partial}{\partial x}\left[\frac{\dot{m}}{A_g}\right] = -\frac{\partial \rho}{\partial t} \tag{3.15}$$

where ρ is the density of gas, A_g is the gas cross-sectional area. Integrating equation 3.15 over the entire length of the isothermal component would relate the mass flows at the two ends of the components. The mass flow at the two ends is given by,

$$\boldsymbol{\dot{m}_1} = \boldsymbol{\dot{m}_2} + \frac{\dot{\boldsymbol{P}} V}{R T_a} \tag{3.16}$$

where the bold variables represent time varying or phasor quantities, $\boldsymbol{\dot{m}_1}$, $\boldsymbol{\dot{m}_2}$ are the flow rate at the two ends, V is the gas volume in the component, R is the gas constant per unit mass, T_a is the mean temperature of the component. Figure 3.6 (a) shows the phasor representation of equation 3.16. The pressure phasor P is arbitrarily taken as the reference. The vertical phasor represents the mass flow of gas buffered into the volume V which is similar to the capacitive component in an electrical system. In figure 3.6 (a), the pressure drop in the component was taken to be zero, but in a real system there will be pressure drop which can be represented as shown in figure 3.6 (b). In this case the phasor representing the capacitive term is perpendicular to the average oscillating pressure P. In order to have a very basic phasor representation of a component, the pressure drop is neglected in the subsequent phasor representations.

3.4.2 Phasor representation of adiabatic components

In an adiabatic component such as the pulse-tube equation 3.16, cannot be used because the gas temperature and pressure vary in a cycle. The entropy change dS in a volume of gas V at a pressure P can be expressed as,

$$dS = \frac{c_p}{V} dV + \frac{c_v}{P} dP \tag{3.17}$$

where c_p and c_v are the specific heat of gas at constant pressure and volume respectively. In an ideal adiabatic process the entropy produced is zero, so equation 3.17 can be written as,

$$\left(\frac{\partial V}{\partial P}\right)_S = -\frac{1}{\gamma}\frac{V}{P} \tag{3.18}$$

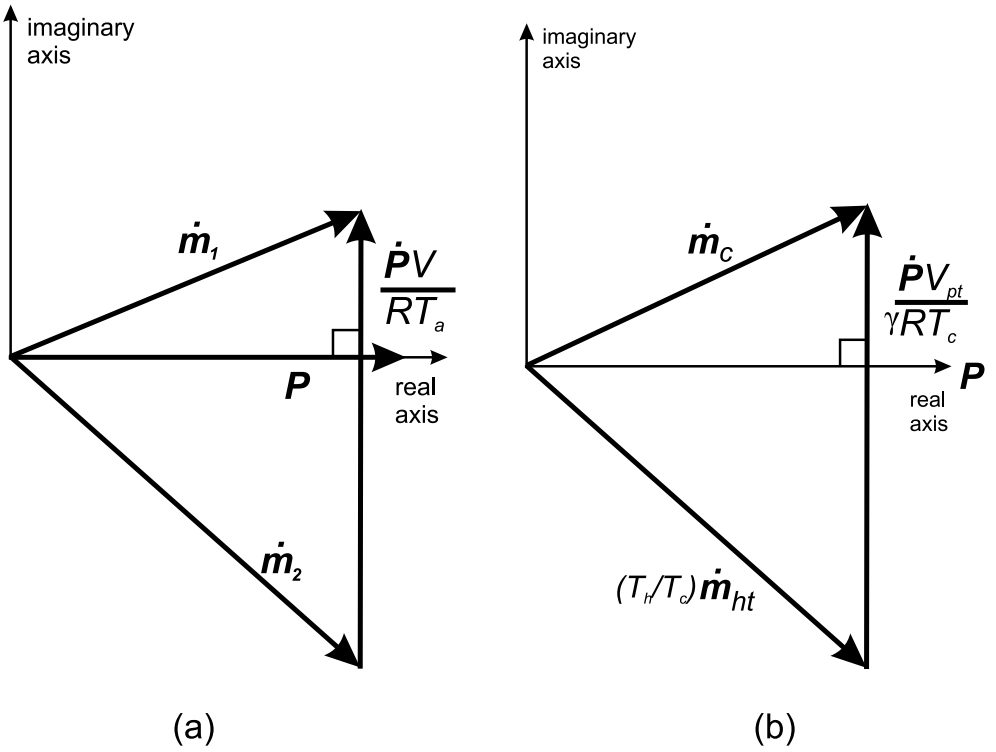

Figure* 3.6: Phasor representation of thermodynamical components. (a) The relationship between the mass flows at the two ends of the isothermal component. The vertical phasor is perpendicular to pressure phasor P and represents the flow buffered (compliance) in the gas volume V in the component. (b) The phasor diagram representing an adiabatic component such as a pulse-tube in a pulse tube cryocooler. The mass flow at the two ends of the component are related similar to that of an isothermal component but using conservation of energy instead of conservation of mass for isothermal components.*

where γ is the ratio of c_p over c_v. Equation 3.18 can be further written as

$$\frac{dV}{dt} = -\frac{1}{\gamma}\frac{V}{P}\frac{dP}{dt} \tag{3.19}$$

For an adiabatic component with volume V_{pt} equation 3.19 becomes

$$\dot{V_c} = \dot{V_h} + \frac{1}{\gamma}\frac{V_{pt}}{P}\dot{P} \tag{3.20}$$

where $\dot{V_c}$, $\dot{V_h}$ are the volume flow at the cold and hot end respectively. The relationship between the hot and cold end mass flow in a pulse-tube can be written as

$$\dot{\boldsymbol{m}}_{\boldsymbol{c}} = \left(\frac{T_h}{T_c}\right)\dot{\boldsymbol{m}}_{\boldsymbol{ht}} + \frac{\dot{\boldsymbol{P}}V_{pt}}{\gamma R T_c} \tag{3.21}$$

where T_h is the temperature at the pulse-tube warm end, T_c is the temperature at the cold end, $\dot{\boldsymbol{m}}_{\boldsymbol{ht}}$ is the mass flow at the pulse-tube warm end, V_{pt} is the volume of the pulse-tube and γ is the ratio of specific heats. Note that the temperature used in the last term is the temperature at the cold end and not the average temperature. The phasor diagram representing the pulse-tube is shown in figure 3.6(c).

3.5 Phasor analysis of regenerator

In an optimized regenerator there must be very good heat exchange between the gas and the material. At any cross-section in the regenerator the temperature is assumed to be constant. However, the regenerator spans a large temperature gradient along the length. To account for this large temperature gradient, average temperature is used in equation 3.16 to relate the mass flow between the warm and cold ends of the regenerator. The $\dot{\boldsymbol{P}}$ in equation 3.16 is related to the oscillating pressure as,

$$\dot{\boldsymbol{P}} = j2\pi f \boldsymbol{P} \tag{3.22}$$

where j is the imaginary unit and f is the frequency of operation. From equation 3.16 and 3.22 the relationship between mass flow at the warm $\dot{\boldsymbol{m}}_{\boldsymbol{h}}$ and cold end $\dot{\boldsymbol{m}}_{\boldsymbol{c}}$ for a regenerator is given by,

$$\dot{\boldsymbol{m}}_{\boldsymbol{h}} = \dot{\boldsymbol{m}}_{\boldsymbol{c}} + \frac{i2\pi f \boldsymbol{P} V_{rg}}{R T_a} \tag{3.23}$$

The vertical phasor given by the second term increases proportionally with either increase in gas volume V_{rg} or frequency f of operation. For a fixed $\dot{\boldsymbol{m}}_{\boldsymbol{c}}$ (both magnitude and phase θ with respect to the pressure) $\dot{\boldsymbol{m}}_{\boldsymbol{h}}$ increases when the compliance term increases. Increase in mass flow has primarily two negative effects;

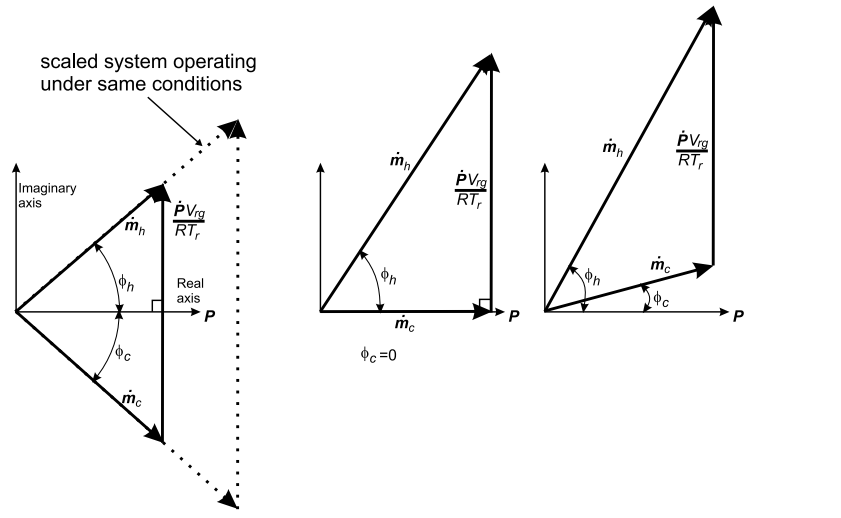

Figure* 3.7: Phasor representation of the regenerator which is locally isothermal along the length of the regenerator. (a) The desired phase relationship is to have the mass flow in phase with pressure at the center of the regenerator to reduce mass flow at the two ends. The phasor represented by the dotted line is for a scaled up system (larger cooling power) operating under the same conditions. (b) The phasor representation of the regenerator with the flow in phase with pressure at the cold end of the regenerator for maximum cooling power. However the flow at the warm end would increase without much gain in the cooling energy reducing the COP. (c) The phasor representation of typical orifice type pulse-tube refrigerators. The flow is in phase with pressure at the orifice which is located at the warm end of the pulse-tube. The pulse-tube would increase the phase of flow as shown in 3.6 (c) and at the cold end of the regenerator the phase would be positive. The losses in this case are the highest and is the reason to use inertance tube (to have negative angle at the pulse-tube warm end) instead of orifice.*

One, for effective heat transfer with increased mass flow, we would need a larger heat exchanger resulting in an increase in the pressure drop and decreasing the overall system efficiency. The second is that increased mass flow, increases the volume-flow proportionally (for a fixed average pressure), leading to the requirement of larger compressor with higher swept volume. Both these effects decrease the overall efficiency of the system. Hence, we would like to have very small gas volume for a certain operating frequency, but with very effective heat exchange and small pressure drop.

The optimum phase relationship between flow and pressure is that in which the flow is in phase with the pressure at about the midpoint of the regenerator as shown in figure 3.7 (a). With such a phase relationship the magnitude of flow at each end is minimized for a given acoustic power at the coldend of the regenerator. Note that the mass flow $\dot{m}$ is not exactly in phase with pressure at the center of the regenerator because viscosity is higher at higher temperatures so we like to keep $\dot{m}_h$ slightly small. Figure 3.7 (b), (c) shows the phasor diagram of the regenerator with zero and positive phase of flow at the cold end with respect to pressure. The mass flow at the warm end of the regenerator increases with more positive angle without much increase in the acoustic power at the cold end leading to lower overall efficiency. The phasor diagram represented by figure 3.7 (c) is typical for orifice type of pulse-tube refrigerators [4] and is the reason for the use of inertance tubes in modern pulse-tube coolers.

Radebaugh et al. [6] have performed REGEN simulations with varying phase angle between pressure and flow at the cold end of the regenerator and their results are shown in figure 3.8. The figure shows how regenerator losses vary with the phase angle between flow and pressure at the cold end of the regenerator. The losses are minimum when the flow lags the pressure by 30^0. Such a phase relationship is easily achieved in a Stirling refrigerators by selecting the appropriate phase of the displacer and in pulse-tube cryocooler, by an inertance tube at the warm end of the pulse-tube [7].

3.5.1 Scaling of regenerative systems with cooling power

The magnitude of the mass flow at the cold end of the regenerator is proportional to the cooling power, for a fixed average pressure, pressure ratio, cold end temperature and the phase of flow with respect to pressure at the cold end (see equation 3.7). In the next section, we will see that the specific area (ratio gas cross-sectional area to massflow) is constant for an optimized regenerator under certain operating conditions. Hence, the regenerator cross-sectional area is proportional to the cooling power desired. The phasor diagram representing scaling of the regenerator with cooling power is shown in figure 3.7 (a). The dotted phasor diagram represents a scaled up regenerator operating under the same conditions as the regenerator represented by the solid lines. It is significant to note that the phase relationship between flows and pressure must be maintained in scaling the

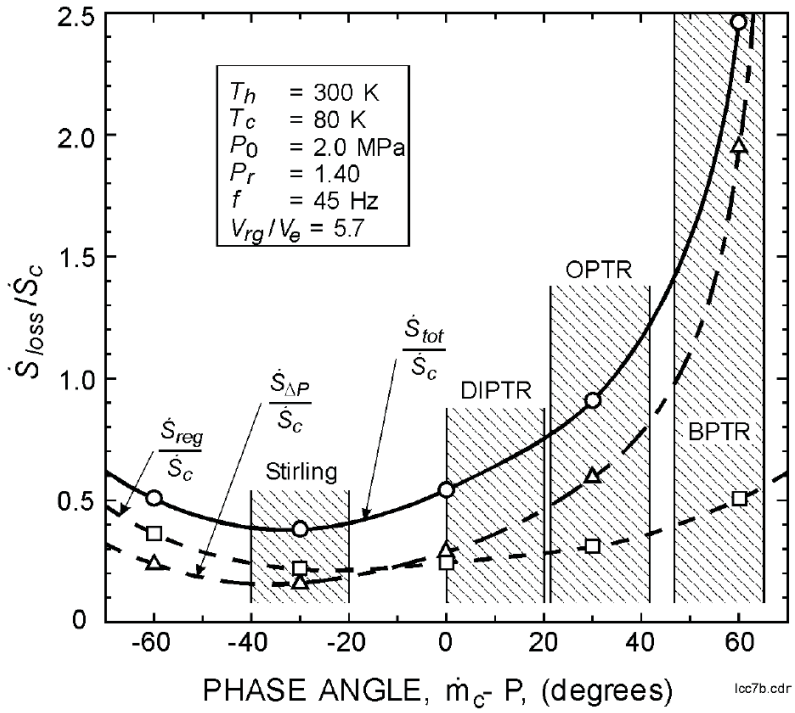

Figure* 3.8: Regenerator losses associated with ineffectiveness and pressure drop for various phase angles by which flow leads pressure. This plot is obtained from Radebaugh et al. DIPTR, OPTR, BPTR refers to double inlet, orifice and basic pulse-tube refrigerator respectively. [6]. Various losses in the regenerator can be expressed as entropy flows. For an efficient regenerator the sum of entropy flow losses should be minimum. [5]*

system.

3.6 Parameter Analysis

This section formulates various losses in the regenerator such as the pressure drop ΔP, enthalpy flow $\dot{H}_{hx}$ (inefficient heat transfer between gas and the material), conduction losses along the length $\dot{Q}_c$ and the acoustic power lost due to the void volume $\dot{W}_{PV,loss}$, as a function of regenerator geometry and operational parameters. These losses are expressed as fractional losses $\frac{\Delta P}{P_1}$, $\frac{\dot{H}_{hx}}{\dot{Q}_r}$, $\frac{\dot{Q}_c}{\dot{Q}_r}$, $\frac{\dot{W}_{PV,loss}}{\dot{W}_{PV,ideal}}$ and the objective is to minimize the fractional losses because some of them conflict with the others.

3.6.1 Pressure drop and enthalpy flow

The pressure drop ΔP of gas flow in a channel with gas cross-sectional area A_g $A.n_g$ (A is the cross-sectional area and n_g is the porosity), length L and hydraulic diameter D_h $\frac{4A_g}{O}$ (O is the perimeter) is given by,

$$\Delta P = 2 \cdot f_r \frac{1}{\rho} \left(\frac{\dot{m}}{A_g} \right)^2 \frac{L}{D_h} \tag{3.24}$$

where f_r is the Fanning friction factor, ρ is the average density of the gas and $\dot{m}$ is the mass flow rate of the gas. It should be noted that the mass flow in the regenerator is an oscillating parameter with its average value equal to zero. Steady flow correlations for the friction factor are normally used in the regenerator optimization and in that case the root mean square value (amplitude/$\sqrt{2}$) of the mass flow must be used. We refer to chapter 7 for a detailed study on the friction factor correlations for a regenerator.

In the heat exchanger design, the pressure drop is often expressed by a non-dimensional parameter, NPH (Number of Pressure Heads) and is given by [8],

$$NPH = \frac{\Delta P}{\frac{1}{2\rho}\left(\frac{\dot{m}}{A_g} \right)^2} = f_r \frac{L}{D_h} \tag{3.25}$$

The ineffectiveness $(1 - \epsilon)$ of the regenerator is defined as the ratio of the enthalpy flow $\dot{H}_{hx}$ to the thermodynamically limited, maximum possible heat transfer rate ($\dot{Q}_{max}$ which is equal to average mass flow over a half cycle $\dot{m}$ times the enthalpy change of the gas Δh between the both ends of the regenerator),

$$1 - \epsilon = \frac{\dot{H}_{hx}}{\dot{m} \Delta h} \tag{3.26}$$

The number of heat transfer units (NTU) is a non-dimensional expression that is related to the heat exchanger's, heat transfer size [9]. When the NTU is small the exchanger effectiveness is low and when the NTU is large the effectiveness is high, but the size of the heat exchangers also increases. Kays and London [9] give a simplified expression relating NTU and ineffectiveness for a regenerator. They show that the ineffectiveness of a regenerator is a function not only of NTU but also of the heat capacity ratio between the matrix and the gas that passes through the regenerator (see figure 3.9). However, for temperatures of 80 K and above the volumetric heat capacity of nearly all matrix materials is much larger than that of the helium gas. The relationship between ineffectiveness and the NTU can in that case be written as,

$$1 - \epsilon = \frac{\dot{H}_{hx}}{\dot{m}\Delta h} \approx \frac{B}{NTU} \tag{3.27}$$

where B is a constant that depends on the heat capacity of the regenerator, and that of the warm and cold gas (see figure 3.9).

From equation 3.27, the NTU can be expressed in terms of $\dot{H}_{hx}$ as,

$$NTU = \frac{B\dot{m}\Delta h}{\dot{H}_{hx}} \tag{3.28}$$

Equation 3.25 and 3.28 describe the hydraulic and thermal performance of the regenerator, respectively. However, these equations are not coupled to describe the effects of both pressure drop and heat transfer in the regenerator. In order to describe the combined effects of the pressure drop and heat transfer, Ruehlich et al. [8] proposes to use the ratio of NPH to NTU. The NPH to NTU ratio with Reynolds number Re for several geometries is shown in figure 3.10. This ratio does not vary a lot with Reynolds number and is a characteristic of the geometry of the regenerator material. The Reynolds number expresses non-dimensional flow and is defined as,

$$Re = \frac{\left(\frac{\dot{m}}{A_g}\right) D_h}{\mu} \tag{3.29}$$

where μ is the viscosity of the gas. Note that the ratio of NPH to NTU is a very weak function of Reynolds Number, Re.

Using the definition of NPH in equation 3.25, the NPH/NTU ratio can be written as,

$$\frac{NPH}{NTU} = \frac{\frac{\Delta P}{\frac{1}{2\rho}\left(\frac{\dot{m}}{A_g}\right)^2}}{NTU} \tag{3.30}$$

Rewriting the terms in equation 3.30, the specific area (ratio of gas cross-sectional area to mass flow) $\frac{A_g}{\dot{m}}$ is given by,

$$\frac{A_g}{\dot{m}} = \left[\left(\frac{NPH}{NTU}\right)\frac{NTU}{2\rho\Delta P}\right]^{\frac{1}{2}} \tag{3.31}$$

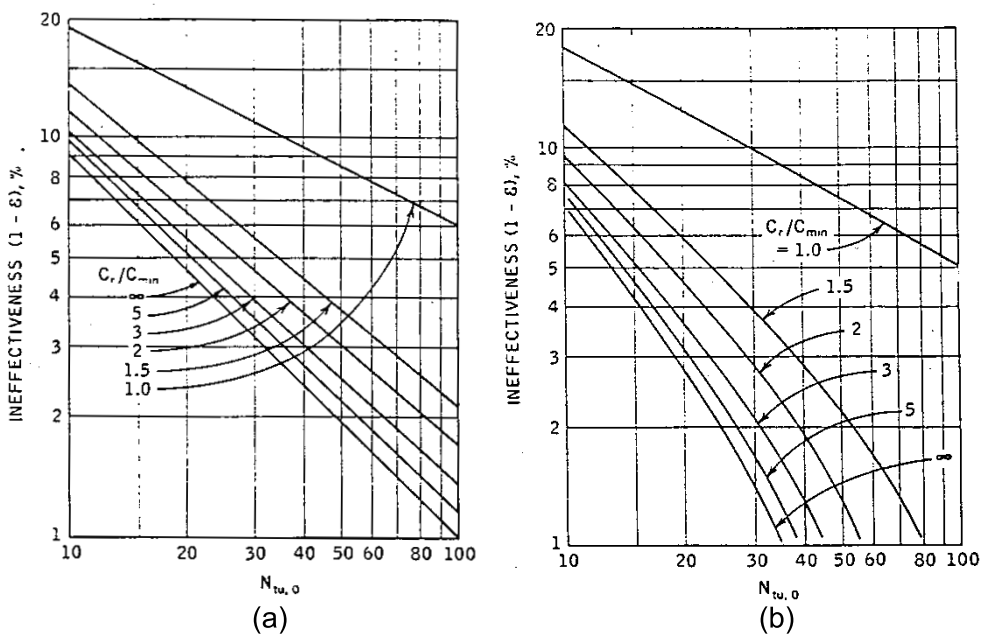

Figure* 3.9: Heat transfer ineffectiness as a function of number of transfer units and matrix capacity-rate ratio; periodic-flow exchanger performance for (a)* $\frac{C_{min}}{C_{max}} = 1$ *(b)* $\frac{C_{min}}{C_{max}} = 0.95$ *[9]. C_r is the heat capacity rate of the regenerator which is equal to frequency times mass and specific heat of regenerator material. C_{max} and C_{min} are the products of massflow of gas times the specific heat of warm or cold gas whichever is maximum or minimum.*

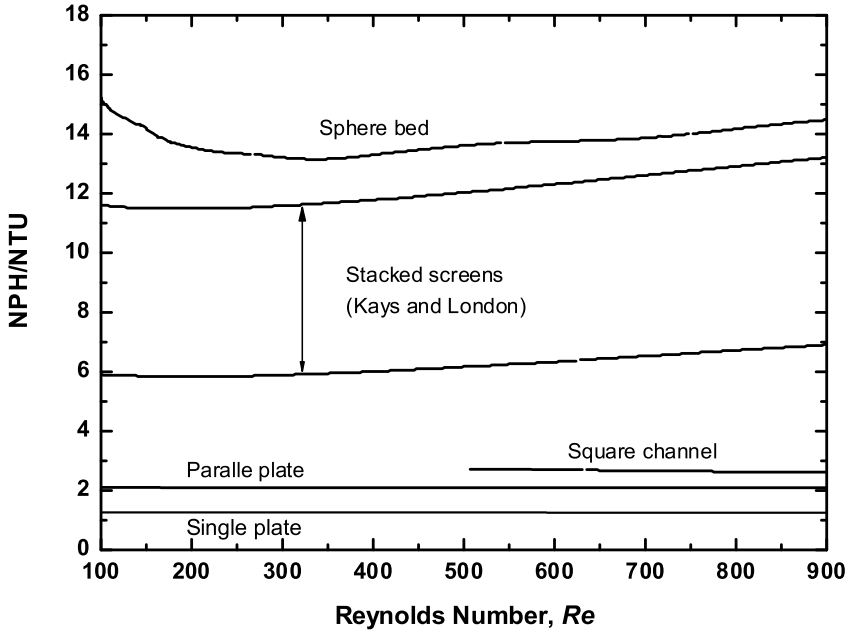

Figure* 3.10: The NPH/NTU for various geometries typically used in a regenerator which is obtained from Ruehlich et al. [8]. The ratio is almost constant with Reynolds number. The analytically derived ratios for parallel and single plate are also shown and represent the lowest ratio that can be achieved.*

It is interesting to note that for a certain ΔP, equation 3.31 relates the specific area to NTU. The higher the NTU required for the heat exchanger, the larger is the specific area.

Using the definition of NTU from equation 3.28 and expressing the enthalpy flow as a fractional loss of refrigeration power $\frac{\dot{H}_{hx}}{\dot{Q}_r}$ and pressure drop as a fractional loss of pressure amplitude $\frac{\Delta P}{P_1}$ the specific area in equation 3.31 becomes,

$$\frac{A_g}{\dot{m}} = \left[\frac{\left(\frac{NPH}{NTU}\right) T_0 \Delta h B}{{P_0}^2 T_c \left(\frac{P_1}{P_0}\right)^2 \cos\phi \left(\frac{\Delta P}{P_1}\right) \left(\frac{\dot{H}_{hx}}{\dot{Q}_r}\right)} \right]^{\frac{1}{2}} \tag{3.32}$$

where T_0 is mean temperature. For a certain operating condition of the regenerator, it is interesting to note that the specific area should increase to keep the fractional pressure drop and heat transfer losses low. However, we will later show that the increase in specific area would increase the fractional conduction and void volume losses.

3.6.2 Heat conduction

The primary source of heat conduction $\dot{Q}_c$ in the regenerator is through the regenerator material and is given by,

$$\dot{Q}_c = \frac{A_s}{L} \int \lambda dT = \left(\frac{1-n_g}{n_g}\right) \left(\frac{A_g}{L}\right) \int \lambda dT \tag{3.33}$$

where A_s is the solid cross-sectional area, L is the length, n_g is the porosity of the regenerator material and λ is the thermal conductivity of the material. The thermal conductivity should be corrected to include the interfacial contact between the regenerator material [10] (which is often lower than the solid material itself). The fractional conduction loss is given by,

$$\frac{\dot{Q}_c}{\dot{Q}_r} = \left(\frac{1-n_g}{n_g}\right) \left(\frac{A_g}{\dot{m}}\right) \frac{1}{L} \frac{\int \lambda dT}{\frac{1}{2} R T_c \left(\frac{P_1}{P_0}\right) \cos\phi} \tag{3.34}$$

For a fixed length L, the fractional conduction loss increase with specific area. The scaling of conduction losses contradict with the fractional pressure drop and heat transfer losses with specific area.

3.6.3 Void-volume pressure loss

In order to formulate fractional void volume loss we refer to section 3.5 in which we have shown that the optimum phasor relationship in the regenerator is to have

pressure and mass flow to be in phase at the center of the regenerator (see figure 3.7). If there were to be zero gas volume the phase between pressure and mass flow would be zero at the cold end of the regenerator and the PV power would be maximum represented by $\dot{W}_{PV,ideal}$. However because of the gas volume V_{rg} in the regenerator the mass flow phase at the cold end must lag the pressure by ϕ degrees. The fractional PV power lost due to this phase shift can be expressed as,

$$\frac{\dot{W}_{PV,loss}}{\dot{W}_{PV,ideal}} = 1 - \cos\phi_c \tag{3.35}$$

$\cos\phi_c$ can be expressed in terms of the sides of the triangle formed by the mass flow and half of the vertical phasor representing buffered flow inside the regenerator volume (see figure 3.7),

$$\frac{\dot{W}_{PV,loss}}{\dot{W}_{PV,ideal}} \approx 1 - \left[1 - \frac{1}{4}\left(\frac{2\pi f P_1 V_{rg}}{RT_r \dot{m}}\right)^2\right]^{\frac{1}{2}} \tag{3.36}$$

assuming no pressure drop, $\dot{m}_c = \dot{m}_h = \dot{m}$. Ignoring higher order terms and taking $V_{rg} = A_g L$ equation 3.36 can be expressed as,

$$\frac{\dot{W}_{PV,loss}}{\dot{W}_{PV,ideal}} \approx \frac{1}{8}\left(\frac{2\pi f P_1}{RT_r}\right)^2 \left(\frac{V_{rg}}{\dot{m}}\right)^2 = \frac{1}{8}\left(\frac{2\pi f P_1}{RT_r}\right)^2 \left(\frac{A_g}{\dot{m}}\right)^2 L^2 \tag{3.37}$$

It is significant to that in order to have lower fractional void volume losses, the specific area and the length should be smaller which, is conflicting with the pressure drop and heat transfer losses (specific area should be larger for lower losses) and conduction loss (length should be larger for lower loss).

		$\propto (\frac{A_g}{\dot{m}})^\alpha$	$\propto L^\beta$
Heat conduction	$\frac{\dot{Q}_c}{\dot{Q}_r}$	1	-1
Void volume	$\frac{\dot{W}_{PV,loss}}{\dot{W}_{PV,ideal}}$	2	2
Pressure drop	$\frac{\Delta P}{P_1}$	-2	1
Heat transfer	$\frac{\dot{H}_{hx}}{\dot{Q}_r}$	0	-1

Table* 3.1: Variation of fractional losses in the regenerator with specific area and length of the regenerator*

3.6.4 Summary of losses

Table 3.1 shows the order with which various losses scale with specific area and length of the regenerator. Note that the product of pressure drop and enthalpy flow

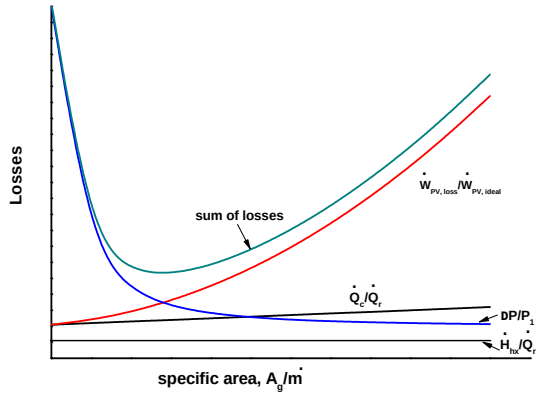

Figure* 3.11: Variation of conduction, pressure drop, enthalpy flow and void volume losses in the regenerator with specific area.*

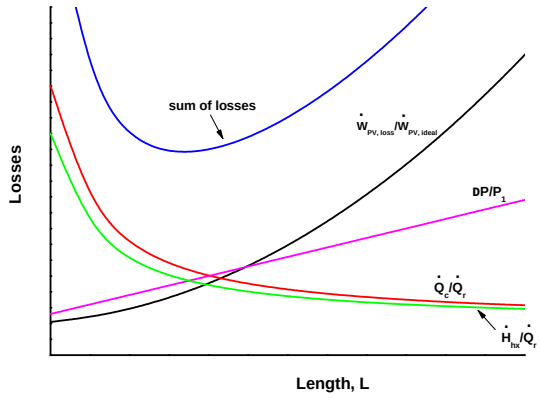

Figure* 3.12: Variation of conduction and void volume losses in the regenerator with length.*

loss is independent of the length and varies as a power of -0.5 with specific area. Figure 3.11 gives a graphical view of the losses with specific area of the regenerator. The plot indicates that there is an optimum specific area resulting from the trade off between heat conduction, enthalpy flow, pressure drop and void volume losses. Figure 3.12 gives a graphical view of the losses with length of the regenerator. The plot indicates that there is an optimum length resulting from the trade off between heat conduction and void volume losses. Another parameter of interest is the hydraulic diameter of the regenerator material.

3.6.5 Hydraulic diameter

For a fully developed laminar flow, the friction factor f_r in equation 3.24 is expressed as,

$$f_r = \frac{C}{Re} \tag{3.38}$$

where C is the coefficient of friction and is a constant for a cross-sectional geometry (see chapter 6). Expressing the ratio of NPH (second term in equation 3.25) to NTU (equation 3.28) and inserting f_r from 3.38, Re from equation 3.29, L from equation 3.34, and $\frac{A_g}{\dot{m}}$ from equation 3.32, the hydraulic diameter becomes,

$$D_h = \left[\frac{C\mu T_0 \left(\frac{1-n_g}{n_g}\right) \int \lambda dT}{{P_0}^2 T_c \left(\frac{P_1}{P_0}\right)^2 \cos\phi \left(\frac{\Delta P}{P_1}\right) \left(\frac{\dot{Q}_c}{\dot{Q}_r}\right)} \right]^{\frac{1}{2}} \tag{3.39}$$

It is significant to note that the hydraulic diameter does not depend on the heat transfer losses or the frequency of operation. However, the hydraulic diameter varies inversely with fractional pressure drop and conduction losses.

3.6.6 Frequency effects

As discussed in section 3.5, increasing the frequency of operation would increase the losses in the regenerator (both pressure drop and heat transfer) due to increase in mass flow at the warm end of the regenerator for the same acoustic power at the cold end. The void volume losses given by equation 3.37 suggest that the ratio of volume of the regenerator V_{rg} to mass flow $\dot{m}$ should decrease if the frequency increases in order to have a reasonable value of void volume loss.

The ratio $\frac{V_{rg}}{\dot{m}}$ can be obtained by multiplying the specific area (from equation 3.32) and length (from equation 3.34) and is given by,

$$\frac{V_{rg}}{\dot{m}} = \frac{A_g}{\dot{m}} L = \frac{\left(\frac{NPH}{NTU}\right) \left(\frac{1-n_g}{n_g}\right) T_0 \Delta h B \int \lambda dT}{{P_0}^2 \frac{{P_1}^3}{{P_0}} (\cos^2\phi)\, {T_c}^2 \frac{1}{2} R \left(\frac{\Delta P}{P_1}\right) \left(\frac{\dot{H}_{hx}}{\dot{Q}_r}\right) \left(\frac{\dot{Q}_c}{\dot{Q}_r}\right)} \tag{3.40}$$

It is significant to note that the volume of the regenerator V_{rg} can be reduced by increasing the average pressure P_0 or the ratio $\frac{P_1}{P_0}$, with the fraction pressure drop and heat transfer losses unchanged. The ratio $\frac{P_1}{P_0}$ is related to the pressure ratio P_r as,

$$\frac{P_1}{P_0} = \frac{P_r - 1}{P_r + 1} \tag{3.41}$$

In practical Stirling cryocoolers the pressure ratio P_r is limited to values less than 1.5. Hence, the average pressure P_0 has to be increased to efficiently operate the regenerator at higher frequencies. Decreasing the volume of the regenerator would increase the enthalpy flow losses because the heat transfer area would decrease. The heat $\dot{Q}_{conv}$ transferred to the gas from the material with a temperature difference ΔT is given by,

$$\dot{Q}_{conv} = h.A_w.\Delta T \tag{3.42}$$

where A_w is the heat transfer area between gas and solid and h is the heat transfer coefficient. The Nusselt number Nu is a non-dimensional number related to the heat transfer effectiveness of the geometry and is related to h as,

$$Nu = \frac{hD_h}{\lambda_g} \tag{3.43}$$

where λ_g is the thermal conductivity of the gas. The hydraulic diameter D_h is related to the heat transfer area A_w and gas volume V_g as,

$$D_h = \frac{4V_g}{A_w} \tag{3.44}$$

Replacing h and A_w in equation 3.42 with definitions from equations 3.43 and 3.44 results in,

$$\dot{Q_{conv}} = 4Nu\lambda_g \frac{V_g}{D_h^2}\Delta T \tag{3.45}$$

Equation 3.45 suggests that for a certain quantity of heat flow and geometry fixed (Nusselt number depends on the geometry such as screen, sphere etc.), the hydraulic diameter D_h varies with gas volume V_g as $D_h \propto \sqrt{V_g}$. Hence, in order to decrease the gas volume, the hydraulic diameter should also be decreased. To conclude, for efficient high frequency operation of the regenerator, the average pressure should increase and a smaller hydraulic diameter regenerator material should be used, as suggested by Radebaugh and O'Gallagher [11].

3.7 Numerical optimization of the regenerator

The phasor and parameter analysis described in the previous sections provide a useful insight into the influence of various parameters on the performance of the

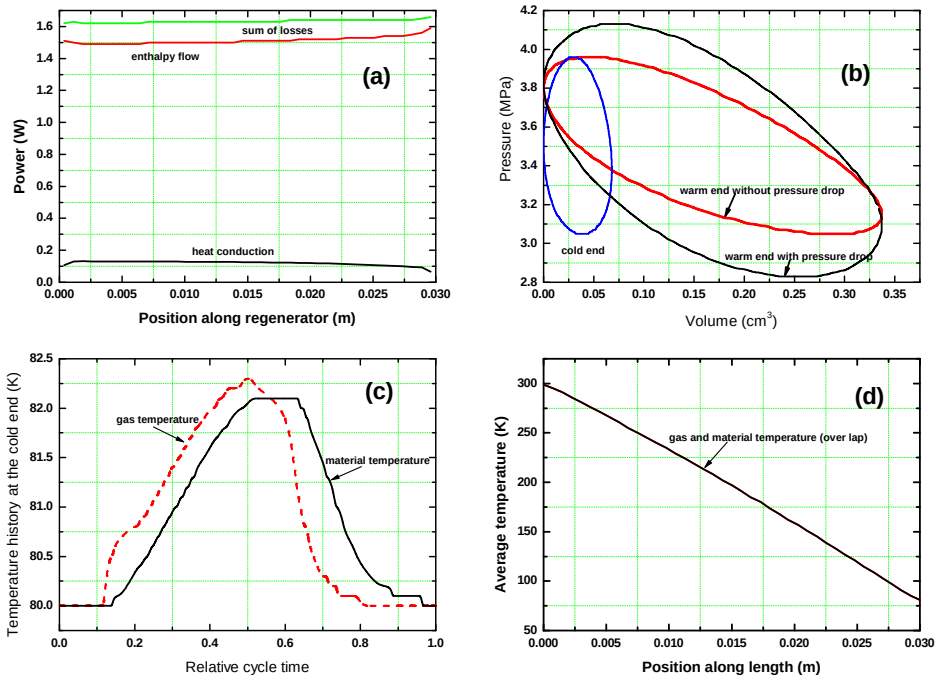

***Figure* 3.13:** *Typical output graphs from REGEN3.2 simulations. (a) Conservation of energy in a regenerator. The total energy should be equal to the sum of the heat conduction and the enthalpy flow. From this plot the convergence of the numerical solution can be seen. (b) The PV or indicator diagram at the warm and cold ends of the regenerator. The area of the PV diagram at the cold end is smaller than the warm end due to reduced volume with temperature. The plot also shows the PV diagram at the warm end with pressure drop in the regenerator. (c) The instantaneous temperature of the gas and the material at the cold end of the regenerator. (d) The temperature profile of the gas and the material along the length of the regenerator. Note that the two lines overlap in the figure. From (b), (c) and (d) decision on specific area, hydraulic diameter and length can be made on the subsequent runs to accommodate more pressure drop or heat exchange.*

regenerator. To have a simple formulation, the properties of materials and fluid such as specific heat capacity c_p, thermal conductivity λ, density ρ, viscosity μ were taken to be constant in the parameter analysis. In practice, the regenerator spans a large temperature gradient between the cold end (typically about 80 K) and the warm end (about 300 K). The material and fluid properties are very strong functions of temperature [12, 13]. The friction factor and heat transfer data are strong functions of Reynolds number which depends on the fluid properties. Numerical tools such as REGEN3.2 [2, 14] developed at the National Institute of Standards and Technologies, SAGE [15], DELTAE [16], solve simultaneously the conservation equations for the regenerator [17], taking into account the fluid properties. We have used REGEN3.2 for numerical modeling of the regenerator. In REGEN 3.2, the mass flow at the cold end and its phase with respect to the pressure at the cold end are input parameters, along with the desired average pressure, pressure ratio at the cold end of the regenerator, frequency, and the geometrical parameters of the regenerator matrix (porosity, hydraulic diameter and the type of the matrix). The program finds the solution to the conservation equations that satisfies the input conditions. The mass flow at the warm end (both magnitude and phase) is calculated by the model. Losses associated with regenerator ineffectiveness (enthalpy flow), conduction through the matrix, and pressure drop are calculated by the model. Conduction loss through the tube wall containing the regenerator material is calculated separately. The conduction loss along the regenerator tube wall of cross-sectional area A_{wall} is given by,

$$\dot{Q}_{c,wall} = \frac{A_{wall}}{L} \int \lambda dT \tag{3.46}$$

The wall area A_{wall} is approximately equal to $\pi D_{reg} t_{reg}$, when the tube diameter D_{reg} is much larger than wall thickness t_{reg}. A small wall thickness is required to limit the conduction loss. However, the minimum wall thickness depends on the maximum tensile strength of the material σ_{max} and the tube dimensions and is given by

$$\sigma_{max} = \frac{P_{max} D_{reg}}{2 t_{reg}} \tag{3.47}$$

where P_{max} is the maximum pressure in the regenerator. A mechanical safety factor is normally used for the tensile strength of the material. Equation 3.47 indicates that the wall thickness t_{reg} is proportional to the regenerator diameter D_{reg}. So, the wall area $A_{wall} \propto D_{reg}^2 \propto A_s \propto A_g$. Hence, the wall conduction losses scale similar to the conduction heat flux through the regenerator material given by equation 3.33.

Some of the graphical output from a typical REGEN3.2 run is shown in figure 3.13. These plots are helpful in making choices of parameters for further runs. The convergence of a particular run was determined from the conservation of energy across the cross-section of the regenerator which, is shown in figure 3.13a. To satisfy, the first law of thermodynamics for open systems [18], the energy flow at any

cross-section of the regenerator must be equal to the sum of enthalpy flow and heat conduction (there is no work done or heat input from the surroundings). Figure 3.13 b is the PV diagram or the so-called indicator diagram for a gas volume at the cold end and warm end of the regenerator. In the same figure the PV diagram of a gas parcel including the pressure drop is shown. From the difference in PV area of the gas volume with and without pressure drop at the warm end of the regenerator a qualitative measure of the pressure drop can be ascertained. Figure 3.13c is the trace (instantaneous) of the gas and material temperature at the cold end of the regenerator. Figure 3.13d is the plot of gas and material temperature along the length of the regenerator. From the instantaneous and steady gas temperature plots, a qualitative measure of the ineffectiveness of heat transfer can be ascertained. If the temperature difference between the gas and the material is large, the next subsequent run could be with a smaller hydraulic diameter regenerator material (better heat transfer, but larger pressure drop). On the other hand, if the temperature difference is rather small but the difference in PV area with and without pressure drop is large a larger hydraulic diameter could be used in the subsequent run (smaller pressure drop, but worse heat transfer).

Figure 3.14 shows the coefficient of performance, COP (ratio of net refrigeration power to input PV power at the warm end) for an example regenerator optimization for several REGEN3.2 runs. The corresponding data is shown in table 3.2. The regenerator geometry used is that of stainless steel screen with the cold end at 80 K and the warm end at 300 K. The average pressure, pressure ratio at the cold end and the frequency of operation was 3.5 MPa, 1.3 and 120 Hz respectively. The flow at the cold end lags the pressure by 30 deg. The frequency, average pressure, and pressure ratio were kept constant for all the runs. Several runs of REGEN3.2 were carried out while varying the specific area (ratio of regenerator gas cross-sectional area to mass flow at the cold end), length of the regenerator and the hydraulic diameter of the matrix. For the above operating conditions, the COP is found to be maximum for a specific area of 0.054 $m^2.s/kg$, length of 30 mm and hydraulic diameter of about 35 μm.

Optimum length

There is an optimum regenerator length for certain operating conditions for a fixed hydraulic diameter. Figure 3.14 shows the REGEN3.2 runs for various lengths of the regenerator and the optimum length was about 30 mm. The optimum length of the regenerator can be explained from the trade off between the conduction and void volume losses in the regenerator which are both functions of length. For a fixed specific area, the relative conduction losses decrease (see equation 3.34) and

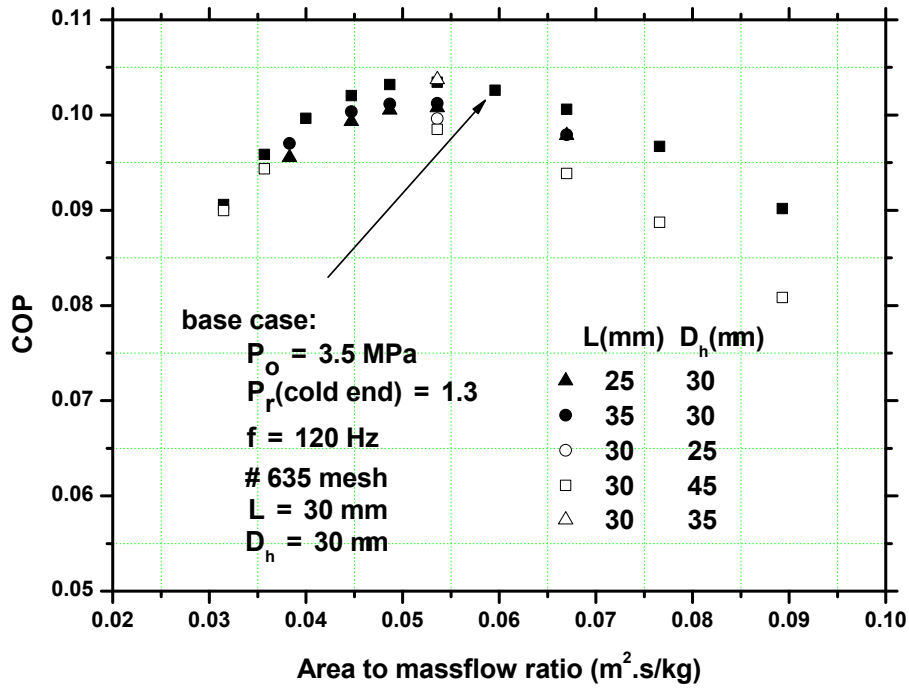

Figure* 3.14: Several REGEN3.2 runs to illustrate regenerator optimization procedure.*

Run	L (mm)	$\dot{m}$ [a] (g/s)	D_h (μm)	ϕ [b] (deg.)	$A_g/\dot{m}$ ($m^2.s/kg$)	$\dot{W}_{PV}$ [c] (W)	$\dot{Q}_r$ (W)	COP	ΔP (MPa)	$\dot{Q}_{c,wall}$ (W)	$\dot{H}_{hx}$ (W)	$\dot{Q}_c$ (W)
6301	30	0.6	30.6	-46.63	0.045	28.41	2.898	0.102	0.102	0.436	1.118	0.050
6302	30	0.55	30.6	-50.41	0.049	25.53	2.634	0.103	0.092	0.436	1.003	0.053
6303	30	0.67	30.6	-42	0.040	32.78	3.266	0.100	0.117	0.436	1.282	0.047
6304	30	0.5	30.6	-54.63	0.054	22.82	2.360	0.103	0.082	0.436	0.897	0.057
6305	35	0.55	30.6	-57.45	0.049	27.52	2.784	0.101	0.112	0.373	0.918	0.049
6306	25	0.55	30.6	-42.35	0.049	24.02	2.414	0.101	0.074	0.523	1.137	0.060
6307	30	0.45	30.6	-59.34	0.060	20.28	2.080	0.103	0.074	0.436	0.796	0.061
6308	30	0.5	25	-54.85	0.054	24.91	2.481	0.100	0.114	0.436	0.780	0.053
6309	30	0.5	35	-54.41	0.054	21.8	2.261	0.104	0.066	0.436	0.995	0.060
6310	30	0.5	45	-53.82	0.054	20.44	2.013	0.098	0.045	0.436	1.242	0.065
6399	30	0.4	45	-63.63	0.067	16.19	1.519	0.094	0.035	0.436	0.969	0.075
6398	30	0.35	45	-69.31	0.077	14.18	1.258	0.089	0.032	0.436	0.844	0.082
6397	30	0.3	45	-75.5	0.089	12.25	0.990	0.081	0.028	0.436	0.725	0.092
6396	30	0.75	45	-36.86	0.036	32.91	3.104	0.094	0.076	0.436	2.070	0.052
6395	30	0.85	45	-32.42	0.032	38.97	3.505	0.090	0.092	0.436	2.471	0.050
6394	35	0.5	45	-60.87	0.054	21.49	2.180	0.101	0.055	0.373	1.136	0.059
6393	35	0.6	45	-52.83	0.045	26.25	2.685	0.102	0.067	0.373	1.390	0.053

continued..

***Table* 3.2:** *Data for the REGEN3.2 runs shown in figure 3.13. In these runs the regenerator cold end temperature T_C = 80 K, warm end temperature T_W = 300 K was taken. The filling pressure P_0 = 3.5 MPa, pressure ratio at the cold end P_r = 1.3, frequency f = 120 Hz. The phase of the mass flow with respect to the pressure at the cold end of the regenerator was taken as -30 deg. The regenerator geometry was screen mesh with a porosity of 0.6.*

[a] magnitude at the cold end
[b] phase difference of cold end flow with the warm end flow
[c] at the warm end of the regenerator

continuation of table 3.2

Run	L (mm)	$\dot{m}$ [a] (g/s)	D_h (μm)	ϕ [b] (deg.)	$A_g/\dot{m}$ ($m^2.s/kg$)	$\dot{W}_{PV}$ [c] (W)	$\dot{Q}_r$ (W)	COP	ΔP (MPa)	$\dot{Q}_{c,wall}$ (W)	$\dot{H}_{hx}$ (W)	$\dot{Q}_c$ (W)
6392	25	0.5	45	-45.49	0.054	19.65	1.768	0.090	0.036	0.523	1.404	0.073
6391	25	0.6	45	-38.06	0.045	24.12	2.160	0.090	0.046	0.523	1.776	0.067
6390	30	0.4	30.6	-64.59	0.067	17.88	1.798	0.101	0.066	0.436	0.697	0.067
6389	30	0.35	30.6	-70.38	0.077	15.63	1.511	0.097	0.059	0.436	0.599	0.075
6388	30	0.3	30.6	-76.7	0.089	13.5	1.217	0.090	0.053	0.436	0.508	0.084
6387	30	0.75	30.6	-37.55	0.036	38.33	3.674	0.096	0.137	0.436	1.489	0.044
6386	30	0.85	30.6	-33.09	0.032	46.28	4.192	0.091	0.165	0.436	1.765	0.041
6385	35	0.5	30.6	-61.71	0.054	24.7	2.501	0.101	0.101	0.373	0.821	0.052
6384	35	0.6	30.6	-53.56	0.045	30.54	3.065	0.100	0.123	0.373	1.016	0.046
6383	25	0.5	30.6	-46.33	0.054	21.44	2.160	0.101	0.066	0.523	1.011	0.064
6382	25	0.6	30.6	-38.87	0.045	26.76	2.658	0.099	0.083	0.523	1.271	0.057
6381	25	0.7	30.6	-33.16	0.038	32.8	3.133	0.096	0.104	0.523	1.562	0.053
6380	25	0.4	30.6	-56.13	0.067	16.67	1.631	0.098	0.051	0.523	0.774	0.075
6379	35	0.4	30.6	-71.43	0.067	19.59	1.919	0.098	0.084	0.373	0.640	0.062
6378	35	0.7	30.6	-46.78	0.038	37.23	3.612	0.097	0.148	0.373	1.226	0.041

[a] magnitude at the cold end
[b] phase difference of cold end flow with the warm end flow
[c] at the warm end of the regenerator

the relative void volume losses increase (see equation 3.37) with increase in length and vice versa.

Optimum hydraulic diameter

Similar to the length, there is an optimum hydraulic diameter of the material. Figure 3.14 shows the REGEN3.2 runs for various hydraulic diameter and the optimum was about 30 μm. The optimum hydraulic diameter of the regenerator can be explained from the trade off between the pressure drop losses and void volume losses. If the hydraulic diameter is made smaller the pressure drop losses increase (see equation 3.39). If the hydraulic diameter is very large, to transfer a quantity of heat for regeneration the volume of the regenerator increases (heat transfer area decreases with larger hydraulic diameter, to compensate for this, we have to use more regenerative material). Increase in volume of the regenerator would increase the void volume losses.

Optimum specific area

The REGEN3.2 runs also suggest that there is an optimum specific area for a given set of input parameters. The optimum specific area is because of the trade off between pressure drop, enthalpy flow, conduction and void volume losses. For smaller specific areas the pressure drop and enthalpy flow losses increase (see equation 3.32). If the specific area is large, conduction and void volume losses increase (see equation 3.34 and 3.37). The optimum specific area is an important parameter because it determines the diameter of the regenerator for a certain mass flow (cooling power is proportional to mass flow).

3.8 Conclusions

In this chapter, phasor analysis for oscillating systems was introduced and was used to represent the oscillating flow and pressure of the regenerator. Phasor analysis provides powerful insight into the influence of various parameters on the performance of the regenerator. The optimum phase angle for a regenerator is to have the mass flow in phase with pressure at the center of the regenerator. Pressure drop, enthalpy flow (inefficient heat transfer), conduction and void volume losses were derived as function of operating and geometrical parameters of the regenerator. Although graphical and parameter analysis provide useful inputs, the final design of the regenerator relies on numerical tools which solve the conservation equations for energy, momentum and mass simultaneously. For a set of input parameters for the regenerator (average pressure, pressure ratio, frequency, phase angle at the cold end of the regenerator) the following conclusions can be made:

1. There exists an optimum specific area (gas cross-sectional area to mass flow

at the cold end of the regenerator). For values smaller than the optimum specific area the pressure drop and enthalpy flow losses dominate and for values greater than the optimum specific area, the void volume and conduction losses dominate.

2. There exists an optimum length of the regenerator. For values of length smaller than the optimum the conduction losses dominate and for larger lengths the pressure drop and void volume losses dominate.
3. The hydraulic diameter of the regenerator material has an optimum value. For lower hydraulic diameters the pressure drop losses dominate and for larger hydraulic diameters the void volume losses dominate and viceversa for enthalpy flow losses.

Conclusion on high frequency regenerator operation

Operating the regenerator at a frequency higher than the designed value would increase the losses in the regenerator due to increase in mass flow without any increase in the acoustic power (hence refrigeration power). The increase in mass flow is because of the increase in the buffered mass flow (similar to a capacitor in electrical systems) at higher frequency which is proportional to the product of frequency and regenerator gas volume. High frequency operation of the regenerator is possible by decreasing the gas volume. It was shown from parameter analysis that the average pressure should increase in order to decrease the gas volume. A second effect of decreasing the volume of the regenerator is the decrease in heat transfer area. In order to increase the heat transfer at smaller volumes the hydraulic diameter of the regenerator material must be made smaller. Hence, efficient high frequency operation of the regenerator is possible by increasing the average pressure and to use a smaller hydraulic diameter regenerator material.

Bibliography

[1] R. Radebaugh. Thermodynamics of regenerative refrigerators. *Generation of low temperature and its applications: edited by T. Ohtsuka and Y. Ishizaki, Shonam Tech. Center, Kamakura Japan*, 1–20, 2003.

[2] J. Gary, D. E. Daney, and R. Radebaugh. A computational model for a regenerator. *Proc. 3rd cryocooler conf.:NIST special pulication*, 698:199–211, 1985.

[3] H. J. M. ter Brake, and G. F. M. Wiegerinck Low-power cryocooler survey *Cryogenics*, 42:705-718, 2002.

[4] F. Kuriyama and R. Radebaugh. Analysis of mass and energy flow rates in an orifice pulse-tube refrigerator. *Cryogenics*, 39:85–92, 1999.

[5] M. E. Will and A. T. A. M. de Waele. Heat exchanger versus regenerator: A fundamental comparison. *Cryogenics*, 45:473–480, 2005.

[6] R. Radebaugh, M. Lewis, E. Luo, J. M. Pfotenhauer, G. F. Nellis, and L. A. Schunk. Inertance tube optimization for pulse tube refrigerators. *Advances in cryogenic engineering*, 51, 2006.

[7] R. Radebaugh. *Pulse tube cryocoolers*, pages 415–434. 2003. edited by S. Kakac, H. Smirnov, and M.R. Avelino, Kluwer academic publishers, Dordrecht, The Netherlands.

[8] I. Ruhlich and H Quack. Investigations on regenerative heat exchangers. *Cryocoolers*, 10, 1999.

[9] W. M Kays and A. L. London. *Compact Heat Exchangers*. New York: McGraw-Hill, 1964.

[10] M. A. Lewis and R. Radebaugh. Measurement of heat conduction through bonded regenerator matrix materials. *Cryocoolers*, 12, 2003.

[11] R. Radebaugh and A. O´ Gallagher. *Advances in cryogenic engineering*, **51**,1919 (2006).

[12] Cryocomp - thermal properties of materials, version 3.01, Cryodata Inc., Niwot, CO, USA, www.sni.net.

[13] Gaspak- Gas properties, version 3.32, Horizon technologies, 7555 South webster st., Littleton, Colorado 80128, USA, www.htess.com.

[14] J. Gary and R. Radebaugh. An improved model for the calculation of regenerator performance (regen3.1). *Proc. 4th Interagency Meeting on Cryocooler: David Taylor Research Center Technical Report DTRC91/003*, pages 165–176, 1991.

[15] Sage - Object-oriented software for Stirling machine design , Gedeon Associates, Athens, OH.

[16] DeltaE-Design Environment for low-amplitude thermoacoustic engines, Los Alamos National Laboratory, New Mexico, USA.

[17] Ackermann R A. *Cryogenic Regenerative Heat Exchangers*. New York: Plenum, 1997.

[18] R. Radebaugh. *Thermodynamics of regenerative refrigerators*, pages 1–20. Shonan Tech. Center, Kamakura, Japan, 2003.

Chapter 4

Systematic design of a Pulse-tube Refrigerator

The design of a pulse-tube refrigerator (PTR) combines the numerical optimization of the regenerator and few rules of thumb obtained from experiments and investigations. In this chapter a systematic design procedure of a pulse-tube refrigerator is given with some practical issues if not implemented may prove detrimental to the efficient operation of the refrigerator.

4.1 Introduction

The schematic of a pulse-tube refrigerator (PTR) is shown in figure 4.1. The function of the regenerator is the same as in Stirling and GM refrigerators in that it precools the incoming high pressure gas before it reaches the cold end. The function of the pulse-tube is to insulate the processes at its two ends. So it must be large enough that the gas flowing from the warm end traverses only part way

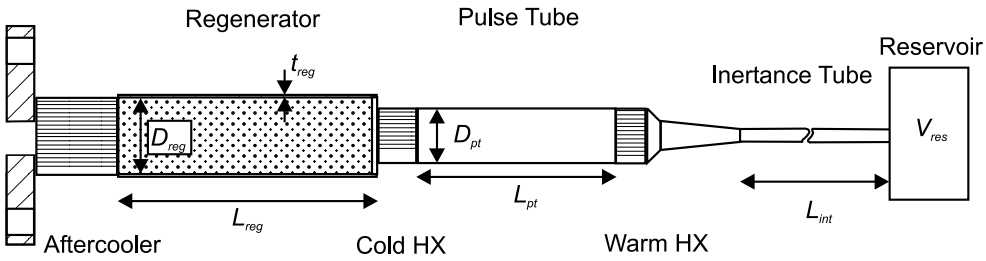

Figure* 4.1: Schematic of a pulse-tube refrigerator*

through the pulse-tube before flow is reversed. Likewise, flow in from the cold end should never reach the warm end. Gas in the middle portion of the pulse-tube never leaves the pulse-tube and forms a temperature gradient that insulates the two ends. For this gas plug to effectively insulate the two ends of the pulse-tube, turbulence in the pulse-tube must be minimized. Thus, flow straightening at the two ends is crucial to the successful operation of the pulse-tube refrigerator. The heat exchangers are the only places where heat is exchanged between the working gas and the environment. The inertance tube is used to have proper phase of mass flow with respect to pressure in the regenerator. Helium is almost always used as the working fluid in the regenerative cycles because of its ideal gas properties, high thermal conductivity and high ratio of specific heats.

The pulse-tube cryocooler is theoretically inefficient compared to a displacer type of Stirling cooler because work obtained during the cooling process is not recovered and is rejected as heat at the warm end of the pulse-tube. The COP of an ideal pulse-tube refrigerator COP_{ptr} is given by,

$$COP_{ptr} = \frac{\dot{Q}_r}{\dot{W}_{PV,w}} = \frac{\dot{W}_{PV,c}}{\dot{W}_{PV,w}} = \frac{T_c}{T_w} \tag{4.1}$$

where $\dot{Q}_r$, $\dot{W}_{PV,c}$, $\dot{W}_{PV,w}$ is the gross refrigeration power, PV power at the cold end and warm end respectively. The relationship between $\dot{W}_{PV,c}$, $\dot{W}_{PV,w}$ was given in the previous chapter (equation 3.8).

For a PTR operating between 300 K and 290 K (near ambient temperature) the COP_{ptr} is equal to 0.96 whereas the Carnot COP is (equation 3.10) is equal to 29. Hence the PTR is very inefficient near ambient temperature. However, a PTR operating between 300 K and 80 K has a COP_{ptr} equal to 0.26 whereas the Carnot COP equals 0.36. Hence, PTR's are used only at cryogenic temperatures. Practical PTR's have efficiencies in the range of 10 to 20 % of Carnot which is almost as good as a practical displacer type Stirling cooler [1]. The advantage of pulse-tube refrigerator over Stirling cooler are given in chapter 1.

This chapter describes a systematic design procedure of a PTR operating around 80 K. The regenerator is the most critical component of the PTR and the optimization procedure described in chapter 3 will be used. The pulse-tube dimensions are determined from rules of thumb which, evolved from rigorous experimentation. Inertance tube and reservoir are optimized based on the transmission line model for electrical systems with mass flow, pressure analogous to current and voltage [2, 3]. Practical aspects in the design of a PTR are briefly discussed in this chapter. Finally, the constraints and challenges in the miniaturization of the PTR are presented.

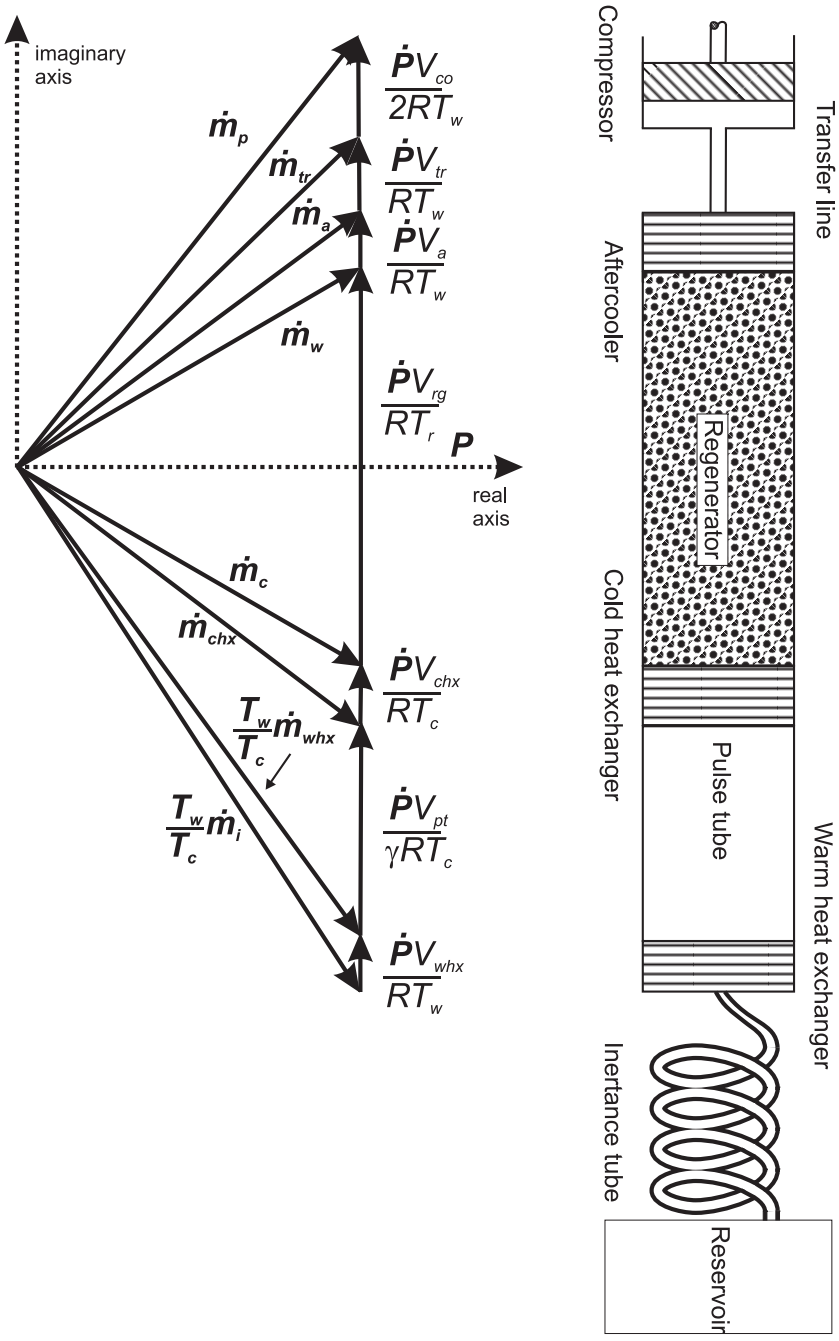

***Figure* 4.2:** *Phasor representation of a pulse-tube cryocooler with an inertance tube*

4.2 Phasor representation of PTR

In this section, a simple approach to calculate the mass flows at various sections in the PTR is discussed. The amplitude and phase of flow are important parameters in the design of heat exchangers and in determining the choice of compressor and the phase shifting component such as an inertance tube.

Figure 4.2 shows a phasor diagram representing oscillating pressure and mass flow in the various components of a pulse-tube refrigerator. The pressure at the cold end of the regenerator is taken as the reference phasor. The pressure drop in all the components is neglected for simplicity. The mass flow (magnitude and phase) at the cold end $\dot{\boldsymbol{m}}_{\boldsymbol{c}}$ and that at the warm end $\dot{\boldsymbol{m}}_{\boldsymbol{w}}$ of the regenerator are outputs from the REGEN3.2 optimization run. From the volume of the aftercooler V_a and the transferline V_{tr}, the vertical phasor representing flow buffered into these volumes is calculated. From the vertical phasors, the mass flows at the aftercooler $\dot{\boldsymbol{m}}_{\boldsymbol{a}}$ and in the transfer line $\dot{\boldsymbol{m}}_{\boldsymbol{tr}}$ is determined. Similarly, the mass flow in the cold heat exchanger $\dot{\boldsymbol{m}}_{\boldsymbol{chx}}$ is determined. The vertical phasor in the pulse-tube is calculated from the volume of the pulse-tube V_{pt} and the heat capacity ratio of the gas γ. Note that the temperature used in the calculation is the cold temperature T_c. From the vertical phasor and the warm temperature to cold temperature ratio the mass flow in the warm heat exchanger is determined $\dot{\boldsymbol{m}}_{\boldsymbol{whx}}$ (see figure 4.2). The mass flow into the inertance tube $\dot{\boldsymbol{m}}_{\boldsymbol{i}}$, is determined similar to the heat exchangers.

4.3 Design procedure

The design procedure described in this section assumes cylindrical cross-section of the regenerator, pulse-tube, heat exchangers and the inertance tube. The refrigeration power $\dot{Q}_{r,net}$ at cold temperature T_c and the warm temperature T_w for heat rejection are often the design requirements of a pulse-tube refrigerator. The warm temperature T_w is usually ambient temperature. There could be practical constraints such as the size of the cold head, frequency of operation, maximum average pressure and pressure ratio. The last three parameters are very much dependent on the availability of the pressure oscillator which, can operate efficiency under those conditions. The systematic design procedure described in this section is valid only for a cold temperature about 80 K. Because below temperatures of 80 K the material properties vary significantly and the losses do not scale proportionately. A multistage PTR is often used to reach temperatures of 4 K and lower.

The design procedure is schematically shown in figure 4.3. Based on the above mentioned input parameters the dimensions of the various PTR elements are determined. All symbols used in the diagram of figure 4.3 were defined before and/or are defined in following sections. Furthermore, the symbols and the separate routines will be discussed in more detail in the next subsections.

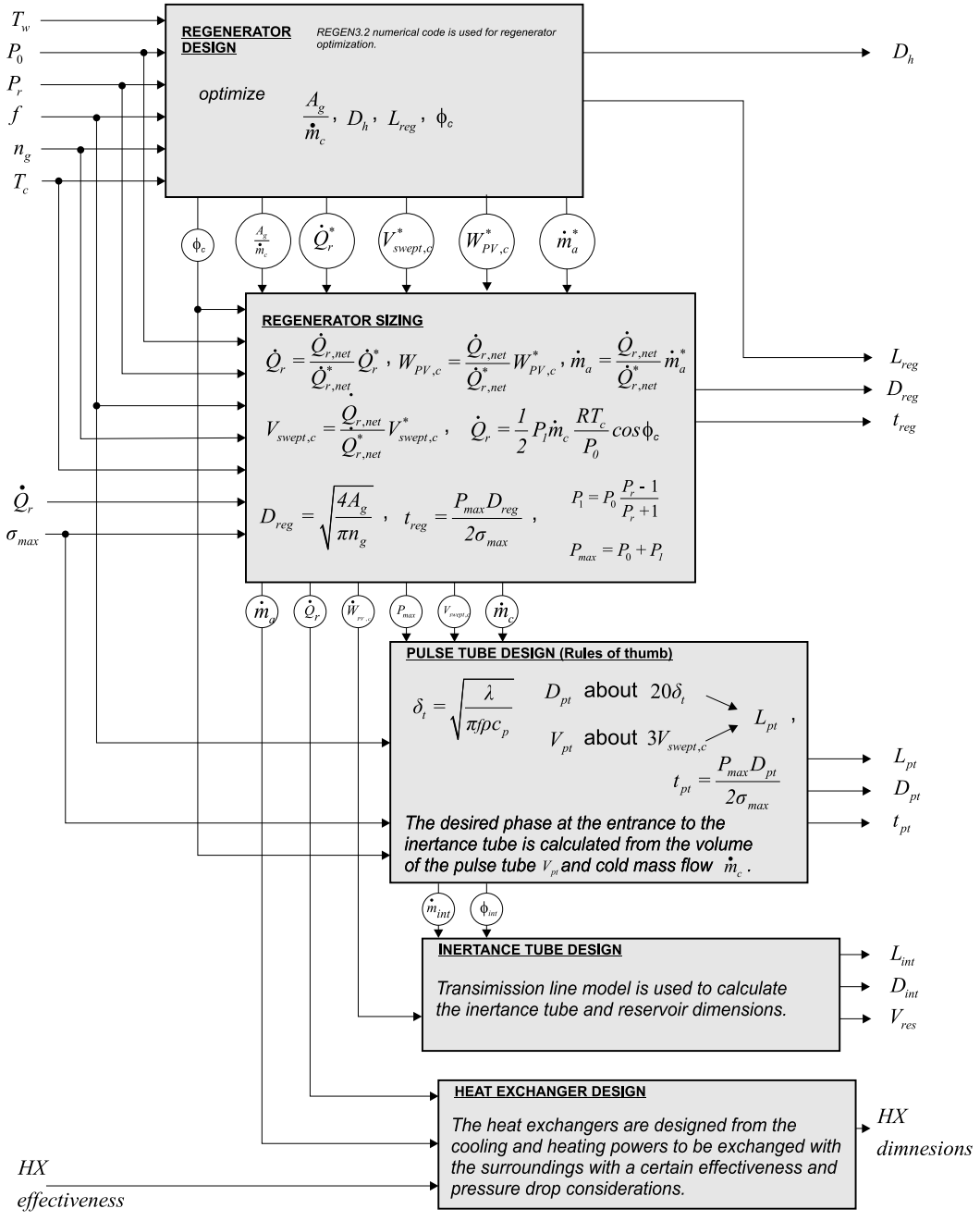

***Figure* 4.3:** *Diagram representing sequential design of a PTR.*

4.3.1 Regenerator Optimization

The input parameters for the optimization of the regenerator are as follows:

1. The average pressure P_0, pressure ratio P_r, and frequency of operation f which, are determined from the operational constraints of the compressor and/or other practical constraints.
2. Temperatures at the cold end T_c and warm end T_w of the regenerator.
3. The hydraulic diameter D_h and porosity n_g of the regenerator material.

It is interesting to note that the regenerator optimization does not need refrigeration power and diameter of the regenerator as an input. The parameter of interest is the specific area which is a ratio of the gas cross-sectional area to mass flow at the cold end. However, in a numerical simulation model such as REGEN3.2, we need to provide dimensions of the regenerator as an input parameter. Hence the diameter and mass flow are chosen randomly so as to vary the specific area. Once the optimum specific area is determined (as for instance shown in figure 3.12) the regenerator is scaled depending on the requirements of the cooling power. The output from the optimized REGEN3.2 run consist of parameters that do not scale with refrigeration power and the rest that scale with refrigeration power which, are indicated by a '*' superscript. Some of the output parameters from the numerical optimization are,

1. Specific area $\frac{A_g}{\dot{m}}$, length of the regenerator L_{reg} and the phase between flow and pressure at the cold end of the regenerator ϕ_c.
2. The gross refrigeration power $\dot{Q}_r^*$, the net refrigeration power $\dot{Q}_{r,net}^*$, swept volume at the cold end of the regenerator $V_{swept,c}^*$, acoustic power at the cold end $\dot{W}_{PV,c}^*$ and mass flow at the aftercooler $\dot{m}_a^*$.

4.3.2 Regenerator sizing

From the optimized output of REGEN3.2 runs and the desired refrigeration power, the dimensions of the regenerator are calculated. Since the parameters $V_{swept,c}^*$, $\dot{W}_{PV,c}^*$, $\dot{Q}_r^*$, $\dot{Q}_w^*$ and $\dot{Q}_{r,net}^*$ are proportional with the refrigeration power $\dot{Q}_{r,net}$, the scaled values of these parameters are given by,

$$V_{swept,c} = \frac{\dot{Q}_{r,net}}{\dot{Q}_{r,net}^*} V_{swept,c}^* \tag{4.2}$$

$$\dot{W}_{PV,c} = \frac{\dot{Q}_{r,net}}{\dot{Q}_{r,net}^*} \dot{W}_{PV,c}^* \tag{4.3}$$

$$\dot{m}_a = \frac{\dot{Q}_{r,net}}{\dot{Q}_{r,net}^*} \dot{m}_a^* \tag{4.4}$$

$$\dot{Q}_r = \frac{\dot{Q}_{r,net}}{\dot{Q}^*_{r,net}} \dot{Q}^*_r \tag{4.5}$$

The swept volume at the cold end $V_{swept,c}$ is used in the calculation of the pulse-tube volume. The acoustic power at the cold end $\dot{W}_{PV,c}$ is required for calculation of inertance tube dimensions. The mass flow at the aftercooler $\dot{m}_a$ is required for designing the aftercooler. From the gross refrigeration power $\dot{Q}_r$, the mass flow at the cold end of the regenerator $\dot{m}_c$ is calculated using the equation for the cooling power (see chapter 2 equation 1.4), repeated here for completeness,

$$\dot{Q}_r = \frac{1}{2} P_1 \dot{m}_c \frac{RT_c}{P_0} \cos\phi_c \tag{4.6}$$

where ϕ_c is obtained from the REGEN3.2 optimization. The gas cross-sectional area of the regenerator A_g is calculated from the optimum specific area (output of REGEN3.2 run) and the mass flow $\dot{m}_c$. The diameter of the regenerator D_{reg} is calculated from the gas cross-sectional area A_g and the porosity n_g of the regenerator material and is given by,

$$D_{reg} = \sqrt{\frac{4A_g}{\pi n_g}} \tag{4.7}$$

The wall thickness t_{reg} of the regenerator tube is calculated from the maximum tensile strength of the material σ_{max} (including a safety margin) which, is given by,

$$\sigma_{max} = \frac{P_{max} D_{reg}}{2t_{reg}} \tag{4.8}$$

where P_{max} is the maximum pressure in the regenerator tube. The maximum pressure P_{max} in the regenerator is at the warm end of the regenerator. P_{max} is equal to the sum of the average pressure P_0 and the amplitude of the dynamic pressure P_1. The amplitude of the dynamic pressure P_1 is calculated from the pressure ratio P_r and the average pressure P_0 and is given by,

$$P_1 = P_0 \frac{P_r - 1}{P_r + 1} \tag{4.9}$$

Stainless steel with a yield strength of 250 MPa [4] is normally used for the regenerator tubing. The conduction losses across the regenerator wall is proportional to the thickness of the tubing. Using, titanium with a yield strength of 830 MPa [4] and comparable thermal conductivity, the thickness of the tubing can be reduced by about a factor of 3, but titanium is a more expensive material. The diameter D_{reg}, length L_{reg} and thickness of the wall t_{reg} completely define the regenerator geometry.

The material that is typically used for the regenerator is wire mesh screens which are commercially designated with a number. This number represents the number of

wires in an inch. For example #400 mesh screen has 400 wires in an inch. Chapter 6 explains in detail the equations for calculating the hydraulic diameter and porosity of the screen. An experimental comparison of various screen materials (stainless steel, phosphor bronze) based on the losses in the regenerator was discussed by Lewis and Radebaugh [5] and they concluded that stainless steel material was a good choice. The choice of the regenerator mesh screen is then made from the optimum hydraulic diameter and porosity calculated from REGEN3.2.

4.3.3 Pulse-tube design

The pulse-tube also known as thermal buffer tube, isolates the cold end of the regenerator from the warm end of the phase shifting component (inertance tube). Ideally, the processes in the pulse-tube is adiabatic (thermally isolated). For adiabatic conditions in the pulse-tube, the tube radius must be large (by one order) compared to the thermal penetration depth δ_{th} in the helium gas which is given by,

$$\delta_{th} = \sqrt{\frac{\lambda}{\pi f \rho c_p}} \tag{4.10}$$

where λ is the thermal conductivity of the gas, f is the frequency of operation, ρ is the density of the gas and c_p is the specific heat capacity of gas. As a rule of thumb the diameter D_{pt} should be greater than 20 times δ_{th}.

In the PTR, part of the gas in the pulse-tube traverses into the cold heat exchanger and another part of the gas into the warm heat exchanger located near the inertance tube. In order to isolate the cold and warm parts of the pulse-tube, the volume of the pulse-tube must be chosen such that it is larger than the swept volume of the gas in the cycle, so that the cold gas does not arrive at the warmer parts of the tube and vice versa. As a rule of thumb, the volume of the pulse-tube is taken to be about three times the swept volume of the gas at the cold end of the regenerator (output from REGEN3.2 run) [6]. From the above two rules of thumb, the length L_{pt} and the diameter D_{pt} of the pulse-tube are calculated. The thickness of the pulse-tube wall t_{pt} is calculated from the maximum stress σ_{max}, maximum pressure and diameter of the tube which is similar to the calculations discussed above for the regenerator. The diameter D_{pt}, length L_{pt} and wall thickness t_{pt} completely define the dimensions of the pulse-tube.

4.3.4 Inertance tube design

A relatively new passive flow element, known as the inertance tube, utilizes the inertia of the oscillating flow to bring about a shift in the phase between the flow and the pressure. The location of this inertance tube is shown in figure 4.1. In order to achieve the optimum phase angle of flow lagging pressure by about 30^0. at the cold end means that the inertance tube will need to lag the flow at its inlet

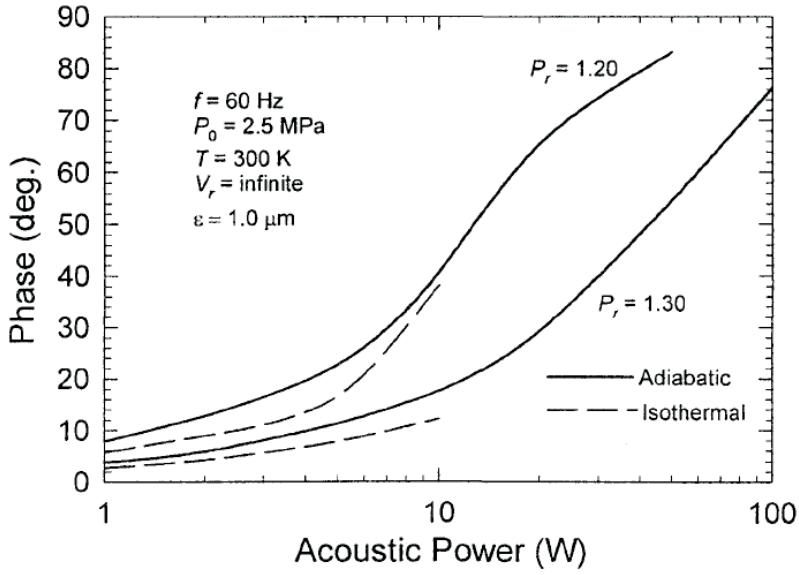

***Figure* 4.4:** *Maximum phase shift in inertance tubes optimized for a given acoustic power [8].*

by about 60^0 to accommodate the change in phase through the pule tube. Such a large phase shift produces a large magnitude of flow for a given acoustic power flow (projection of the flow phasor on the pressure phasor in figure 4.2). However, because the pulse-tube is an open tube, large flows there do not contribute to large loss. For small pulse-tube refrigerators where the mass flow in the inertance tube is small, the phase shift may be only a few degrees [8, 9]. Figure 4.4 shows the maximum phase shift produced by an optimized inertance tube as a function of acoustic power. For decreasing acoustic powers the phase shift decreases. In the 120 Hz pulse-tube refrigerator, described in the next chapter, the flow was taken in phase with pressure at the cold end because the maximum phase shift that could be obtained from the inertance tube at the warm end of the pulse-tube for an acoustic power of about 10 W was about 30^0.

4.3.5 Heat exchanger design

The heat exchanger design is based on classical models [7] in which, a choice of dimensions has to be made based on the trade off between the efficient heat transfer

and pressure drop. The gas volume should be kept to a minimum to reduce void volume losses. The design is similar to the regenerator design with the exceptions, that the temperature of the material along the length is uniform and the heat capacity of the material is less important. The heat exchangers are normally embedded in the regenerator and the pulse-tube as shown in figure 4.2. Hence, the diameter of the heat exchangers are determined by the regenerator and pulse-tube diameter. Conventionally, copper (Cu) wire mesh screen is used as heat exchanger geometry. Finally, the length of the heat exchanger is determined from the numerical model.

4.4 Practical aspects

In a practical PTR, the pulse-tube does not always have the same diameter as the regenerator. Because of the difference in the diameter the flow entering or leaving the connecting part can create turbulence in the pulse-tube. Turbulent increases the loss in the pulse-tube. The turbulence can be avoided by placing flow straightners (made of wire screens or sintered material) at the cold and warm end of the pulse-tube [10].

The flow velocities at the entrance to the inertance tube are very high because of smaller cross-sectional diameter of the inertance tube compared to the pulse-tube. An abrupt change in cross-sectional area will create turbulence in the flow. The subsequent turbulent flow will have two consequences: first, it will increase the resistance to flow in the inertance tube and second, it will lead to mixing of fluid at the pulse-tube warm end. The second effect will increase the losses in the pulse-tube and will reduce the cooling power. To overcome this rapid change in velocity, the connecting flange between the pulse-tube and inertance tube should be gradually tapered as shown in figure 4.1.

4.5 Miniaturization

The pulse-tube refrigerator is a good candidate for micro miniaturization because it does not have any moving parts in the cold stage of the refrigerator (namely regenerator, pulse-tube). However, for a certain operating frequency of the refrigerator, the minimum size of the pulse-tube refrigerator is determined by the lateral dimensions of the pulse-tube (for a circular tube it is the diameter). As discussed in the section 4.3 on the pulse-tube design, the diameter of the tube must be about an order greater than the penetration depth of the gas. The thermal penetration depth varies with frequency as $\delta_{th} \propto 1/\sqrt{f}$, hence increasing the frequency of operation of the refrigerator would enable decreasing the size (diameter) of the pulse-tube. Increasing the frequency of operation of the PTR would have implications on the design of regenerator as discussed in chapter 2. For efficient operation of the regenerator at high frequency, the filling pressure must increase and a smaller hydraulic

diameter regenerator material must be used.

4.6 Conclusions

The design of a pulse-tube refrigerator follows from the numerical optimization procedure of the regenerator. The actual size of the refrigerator depends on the desired refrigeration power at a given operating frequency. Extensive experiments and investigations by researchers lead to rules of thumb for determining the dimensions of the pulse-tube. The inertance tube is determined from transmission line models. Miniaturization of pulse-tube refrigerators implies high operating frequencies in order to have adiabatic condition in the smaller pulse-tubes.

Bibliography

[1] R. Radebaugh. *Pulse tube cryocoolers*, pages 415–434. 2003. edited by S. Kakac, H. Smirnov, and M.R. Avelino, Kluwer academic publishers, Dordrecht, The Netherlands.

[2] P. C. Magnusson. *Transmission lines and wave propagation.* Allyn and Bacon, Boston, 1970.

[3] H. H. Skilling. *Electric transmission lines.* McGraw Hill, New York, 1951.

[4] Cryocomp - thermal properties of materials, version 3.01, cryodata inc., niwot, co, usa, www.sni.net.

[5] M. A. Lewis and R. Radebaugh. Measurement of heat conduction through bonded regenerator matrix materials. *Cryocoolers*, 12, 2003.

[6] J. M. Pfotenhauer, Z. Gan, and R. Radebaugh. Approximate deisgn method for single stage pulse tube refrigerators. *to be pulished in Advances in cryogenic engineering*, 2008.

[7] W. M Kays and A. L. London. *Compact Heat Exchangers.* New York: McGraw-Hill, 1964.

[8] R. Radebaugh, M. Lewis, E. Luo, J. M. Pfotenhauer, G. F. Nellis, and L. A. Schunk Inertance tube optimization for pulse tube refrigerators. *Advances in Cryogenic Engineering*, 51:59–67, 2006.

[9] M. Lewis, P. E. Bradley, and R. Radebaugh Impedance measurements of inertance tubes. *Advances in Cryogenic Engineering*, 51:1557–1563, 2006.

[10] I. Tanaeva PhD thesis, Technische Universiteit Eindhoven, isbn: 90-386-2005-5 chapter 3, 2004.

Chapter 5

120 Hz Pulse-tube Cryocooler

We report on the efficient operation of a pulse-tube cryocooler at 120 Hz with an average pressure of 3.5 MPa. A no-load temperature of 49.9 K was achieved. This is the first time such low temperatures have been achieved for operating frequencies above 100 Hz. The net refrigeration power at 80 K was 3.37 W. The input acoustic power at the aftercooler was 66.0 W, which yields a cooler efficiency of 14.0 % of Carnot with an aftercooler temperature of 298.7 K. The background loss consisting of heat conduction and radiation, was about 0.93 W. A numerical model was used to optimize the dimensions of the regenerator, which used #635 mesh stainless steel screen. The cryocooler size is reduced at high frequencies and high pressures for a given input acoustic power, which is important to many applications and can enable development of microcryocoolers for MEMS applications. The cryocooler cooled from room temperature to 80 K in 5.5 minutes. The fast cooldown is the combined result of the small regenerator volume and the large cooling power.

5.1 Advantages of high-frequency operation

The size of Stirling-type pulse-tube cryocoolers is dominated by the size of the pressure oscillator. Typically, such coolers operate at about 60 Hz for cold-end temperatures of about 80 K. The acoustic power (see equation 3.5) delivered by the pressure oscillator is given by (repeated here for completeness),

$$\dot{W}_{PV} = \frac{1}{2} P_1 \dot{V}_1 \cos\phi \tag{5.1}$$

The amplitude of the volume flow rate $\dot{V}_1$ is related to the volume amplitude V_1 by,

$$\dot{V}_1 = j2\pi f V_1 \tag{5.2}$$

The PV power then becomes,

$$\dot{W}_{PV} = \pi f V_1 P_0 \left(\frac{P_1}{P_0}\right) \cos\phi \tag{5.3}$$

The ratio of P_1 to P_0 is related to the pressure ratio by,

$$\frac{P_1}{P_0} = \frac{P_r - 1}{P_r + 1} \tag{5.4}$$

so the PV power can be written as,

$$\dot{W}_{PV} = \pi f V_1 P_0 \frac{P_r - 1}{P_r + 1} \cos\phi \tag{5.5}$$

From equation 5.5, we can see that, for a certain PV power delivered by the compressor, the volume amplitude V_1 can be reduced by increasing the frequency. The size of the compressor is usually a function of the swept volume and hence increasing the frequency of operation would reduce the size of the compressor.

The size of the pulse-tube and regenerator would also be reduced at higher frequencies for a given cooling power because the swept volume at the cold end is reduced (see equation 5.1 and 5.2), enabling the use of pulse-tubes in military infrared applications, in which dewars for the infrared sensors were originally designed for the small cold-finger diameter of Stirling coolers. Reduction in size and mass is a huge advantage for portable and space applications. The high cooling power density in the small cold finger also leads to a very fast cooldown time, which is an added advantage. However, simply increasing the frequency in a cryocooler designed for 60 Hz operation will lead to higher regenerator losses as shown in chapter 3. Radebaugh and O'Gallagher [1] have shown that by the right combination of regenerator geometry and higher pressures, operating frequencies as high as 1 kHz could be used while maintaining high efficiency. Recently, researchers from the Chinese Academy of Sciences in Beijing reported achieving a temperature of about 70 K at a frequency of 300 Hz and a pressure of 4.13 MPa [2]. In this chapter we present experimental verification of the theoretical predictions in chapter 3 for a pulse-tube cryocooler operating at 120 Hz. The frequency which is twice the line frequency (60 Hz) was chosen randomly. This frequency is higher than the resonance frequency of commercially available linear compressors, so at this time we focus only on the efficiency of the cold head. The inline type of pulse-tube configuration was chosen for easy instrumentation.

5.2 Design

The design of a 120 Hz inline pulse-tube refrigeration follows from the systematic design procedure described in the previous chapter.

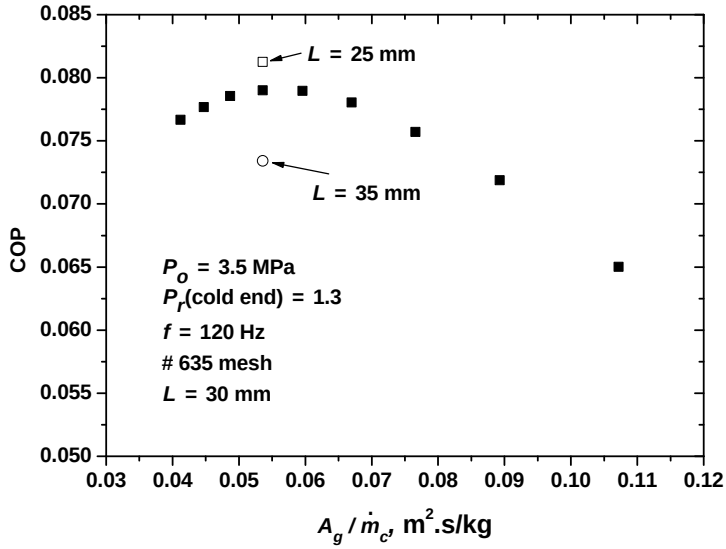

Figure* 5.1: Optimization results with REGEN3.2 assuming $\phi_c = 0$ and including conduction in the regenerator tube wall.*

5.2.1 REGEN3.2 calculations

Optimization of the regenerator for 120 Hz operation was carried out with REGEN3.2. In chapter 3, (section 3.5), we have noticed that in order to efficiently operate the regenerator at high frequency, the average pressure should increase and the hydraulic diameter of the regenerator material must be made smaller. Conventional Stirling type refrigerators operate at a frequency of about 60 Hz with an average pressure of 2.5 MPa and a pressure ratio of 1.3, using a #400 mesh stainless steel screen (see table 5.1). For the 120 Hz operation of the refrigerator, we have chosen an average pressure of 3.5 MPa and a pressure ratio of 1.3 at the cold end, because of the current limitations of commercially available pressure oscillators [3]. For the regenerator matrix, #635 mesh screen (see table 5.1) was used because it was the finest (smallest hydraulic diameter) commercially available screen. In chapter 4 section 4.3.4, we have noticed that for small (low acoustic power) pulse-tube refrigerators it was not feasible to have very large phase shift between flow and pressure with an inertance tube. Typically a well optimized large (high acoustic power) regenerator has a phase of flow lagging pressure at the cold

Mesh	Wire dia. (μm)	Opening (μm)	Spacing (μm)	Porosity [a]	Hydr. Dia. (μm)
635	20.3	19.7	40.0	0.6010	30.6
500	19.8	31.0	50.8	0.6939	44.88
500	25.4	25.4	50.8	0.6073	39.28
400	25.4	38.1	63.5	0.6858	55.44
325	35.6	43.2	78.2	0.6425	63.98
250	40.6	61.0	101.6	0.6861	88.74
200	53.3	73.7	127.0	0.6704	108.41

Table* 5.1: Commercially available wire mesh screen characteristics.*

[a] $1 - n_g = \frac{\pi}{4}\frac{d}{s}$, where d: wire dia. ; s: spacing

end by 30^0. In our design, the flow was taken to be in phase with pressure. The cold and warm end temperatures of the regenerator were taken to be 80 K and 300 K, respectively.

For the REGEN runs, the frequency, average pressure, and pressure ratio were kept constant. Several runs of REGEN3.2 were carried out while varying the ratio of regenerator gas cross-sectional area to mass flow at the cold end, to find the optimum geometry under the operating conditions discussed above. A loss associated with the expansion process (pulse-tube) was taken to be 20 % of the gross refrigeration power. The resulting coefficient of performance, COP (ratio of net refrigeration power to input PV power at the warm end) is shown in figure 5.1. The maximum COP is for the area-to-flow ratio (specific area) of about 0.053 m^2.s/kg (see figure 5.1). REGEN runs were performed for lengths of 25, 30 and 35 mm for this specific area. The variation of COP (see figure 5.1) is less than 5 %. The length of the regenerator was chosen as 30 mm.

The next step in the design is the sizing of the regenerator for the optimum specific area (ratio of gas cross-sectional area to mass flow). Since, the objective of the design was to study 120 Hz operation of the PTR, we could have chosen either the diameter of the regenerator (gives gas cross-sectional area) or the mass flow (can be calculated from desired refrigeration power, see chapter 3). In our case, an inner diameter of 9.017 mm (3/8" outer diameter and wall thickness of 0.010"), was chosen from the standard commercially available stainless steel tubes. Some of the results of the REGEN3.2 run for the optimum case are shown in Table 5.2.

Parameter	REGEN3.2 run (optimum case)	REGEN3.2 run (experimental)	Experimental
Cold-end temperature (K)	80	80	80
Warm-end temperature (K)	300	300	298.7
PV power at aftercooler (W)	81.3	64.2	66.0
PV power at regenerator warm end (W)	78.6	62.6	-
PV power at cold end (W)	13.79	10.89	-
Net Refrigeration Power (W)	6.21	4.69	3.35
Coefficient of performance [a]	0.0764	0.0731	0.051
Coefficient of Performance [b]	0.078	0.075	-
Phase of mass flow [c] (deg.)	41.0	34.7	-
Mass flow at the cold end (g/s)	1.19	1.19	-
Mass flow at the warm end (g/s)	1.52	1.39	1.54
Mass flow at reservoir entrance (g/s)	0.69	0.55	0.757
Phase of mass flow [d] (deg.)	-60.0	-64.0	-68.7
Pressure ratio at the warm end	1.421	1.372	1.40
Pressure ratio at the cold end	1.3	1.23	1.23
Swept volume at cold end (cm^3)	0.162	0.161	-

***Table* 5.2:** *Results of REGEN 3.2 calculations for the designed optimum case at T_c = 80 K, with a pressure ratio of 1.3 at the cold end of the regenerator (run #6312) and with the experimental pressure ratio of 1.23 at the cold end of the regenerator (run #7312). Also shown are the experimentally measured parameters.*

[a] referred to PV power at aftercooler
[b] referred to PV power at the warm end of the regenerator
[c] at regenerator warm end relative to pressure at cold end
[d] at reservoir entrance relative to pressure at pulse-tube warm end

Component	Length (mm)	Outside Diameter (mm)	Wall thickness (mm)
Regenerator	30	9.5	0.25
Pulse-tube	30	4.7	0.15
Inertance Tube (double dia.)			
Small dia.	864	2.37	0.50
Large dia.	746	2.37	0.30

Table* 5.3: Component geometry in pulse-tube cryocooler. (All components stainless steel).*

5.2.2 Pulse-tube design

The swept volume at the cold end of the regenerator calculated by the model was about 0.161 cm^3 (see table 5.2). The pulse-tube volume was chosen to be about three times the swept volume. The thermal penetration depth in helium at 300 K, pressure of 3.5 MPa and frequency of 120 Hz was about 100 μm. The radius of the pulse-tube must be greater than 1 mm (10 times penetration depth, see chapter 4 section 4.3.3). The tube inner diameter was chosen from the standard commercially available tube catalog and is equal to 4.457 mm (outer diameter of 3/16", wall thickness of 0.006"). The length of the pulse-tube is about 30 mm.

5.2.3 Inertance tube calculations

The transmission line model was used to find the unique diameter and length of the inertance tube which gives the maximum phase shift. A double inertance tube model (a smaller diameter tube connected to a larger diameter tube) was considered because it can provide larger phase shift compared to a single tube [4]. The input parameters to the model were acoustic power flow at the entrance to the inertance tube is equal to 13.79 W (see table 5.2), pressure ratio of 1.3 and average pressure of 3.5 MPa. The model predicts the flow to lag the pressure by 31^0, for the dimensions of the tubes given in table 5.3. The reservoir volume was 50 cm^3.

5.2.4 Heat exchanger calculations

The dimensions of the cold and warm heat exchangers located at the ends of the pulse-tube were calculated from the NIST heat exchanger model. This model is based on the standard heat exchanger calculations found in any heat transfer text book [5]. The geometry used was #100 mesh copper screen with a porosity of about 0.600 and a wire diameter of 0.114 mm. The matrix radial thermal conductivity and matrix axial thermal conductivity were of 500 W/K.m and 50 W/K.m respectively for cold heat exchanger, wheres for the warm heat exchanger the values were 400

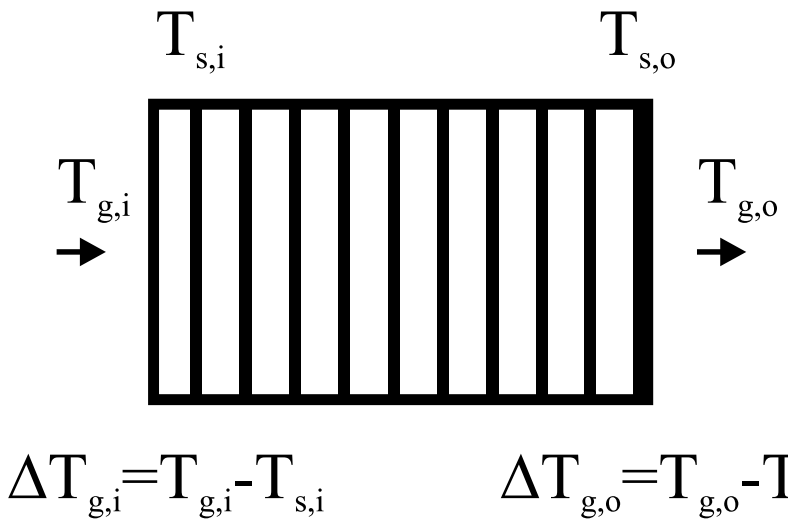

***Figure* 5.2:** *Definitions of the temperature difference in the heat exchanger calculations.*

W/K.m and 40 W/K.m. The input to the model for the cold heat exchanger was a mass flow of 1.19 g/s (from table 5.2), temperature of 80 K and diameter of 4.46 mm (pulse-tube inner diameter). A similar procedure was followed for the warm heat exchanger with a mass flow of 0.371 g/s (calculated from the mass flow at the cold end and the vertical phasor of the pulse-tube), temperature of 300 K and diameter of 4.46 mm (pulse-tube inner diameter) as inputs. The relative pressure drop and the ratio of temperature difference between flow and screen at the outlet and inlet for the cold and warm heat exchangers is shown in figure 5.3 and 5.4 respectively. The data of simulation results with varying lengths is shown in tables 5.4 and 5.5 respectively. The lengths of the cold and warm heat exchangers were chosen 4.4 mm and 3.4 mm, respectively.

5.2.5 Phasor diagram

The phasor diagram representing the designed pulse-tube refrigerator is shown in figure 5.5. The method to calculate the amplitude and phase of the mass flow at various sections of the refrigerator was described in chapter 4 section 4.2. The

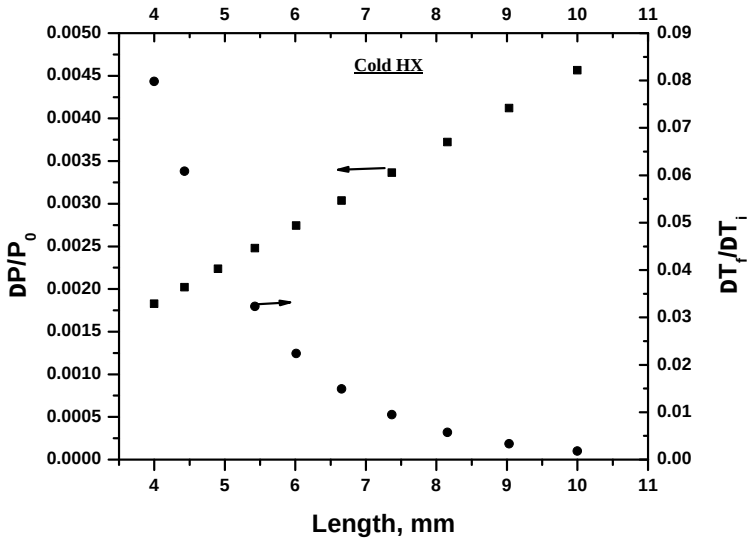

Figure* 5.3: Variation of relative pressure drop and the ratio of temperature difference between gas and solid at the outlet to the inlet of cold heat exchanger. In the calculations, the average pressure P_0 was 3.5 MPa, mass flow of 1.19 g/s and temperature of 80 K. The heat exchanger geometry was flow through screens with a wire diameter of 0.114 mm (#100 mesh), porosity of 0.60 (calendered). The diameter of the heat exchanger was 4.76 mm. The matrix radial and axial thermal conductivity was 500 and 50 W/K.m respectively.*

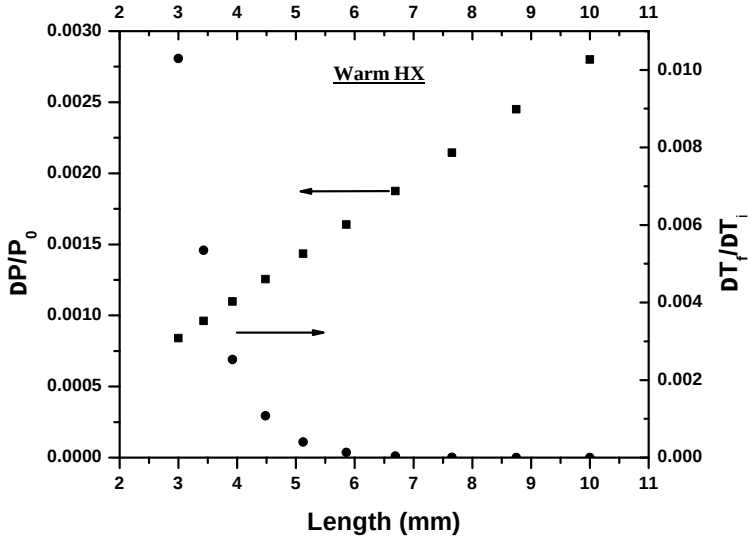

***Figure* 5.4:** *Variation of relative pressure drop and the ratio of temperature difference between gas and solid at the outlet to the inlet of cold heat exchanger. In the calculations, the average pressure P_0 was 3.5 MPa, mass flow of 0.371 g/s and temperature of 300 K. The heat exchanger geometry was flow through screens with a wire diameter of 0.114 mm (#100 mesh), porosity of 0.60 (calendered). The diameter of the heat exchanger was 4.76 mm. The matrix radial and axial thermal conductivity was 400 and 40 W/K.m respectively.*

Length	NTU	$\Delta T_f/\Delta T_i$	$\Delta P/P_0$	Gas Volume (cm^3)
4.000	2.528	0.7979E-01	0.1826E-02	0.4271E-01
4.429	2.799	0.6085E-01	0.2021E-02	0.4729E-01
4.903	3.099	0.4508E-01	0.2238E-02	0.5235E-01
5.429	3.432	0.3234E-01	0.2478E-02	0.5796E-01
6.011	3.799	0.2239E-01	0.2743E-02	0.6418E-01
6.655	4.207	0.1490E-01	0.3037E-02	0.7105E-01
7.368	4.657	0.9492E-02	0.3363E-02	0.7867E-01
8.158	5.156	0.5762E-02	0.3723E-02	0.8710E-01
9.032	5.709	0.3316E-02	0.4122E-02	0.9644E-01
10.00	6.321	0.1798E-02	0.4564E-02	0.1068

Table* 5.4: Simulation results for optimizing the cold heat exchanger. The Reynolds number of the flow was 2164.*

important distinction between 4.2 and 5.5 is that the pressure drop in the regenerator is taken into account in calculating the mass flow phasor's. The mass flows at the cold end and warm end of the regenerator are obtained from the output of REGEN3.2 runs. From the gas volume and other parameters, the mass flows in the cold heat exchanger, pulse-tube, warm heat exchanger and aftercooler are calculated.

5.2.6 PTR layout

The layout diagram of the in-line pulse-tube refrigerator used in the experiments is shown in figure 5.6. Pressure taps were provided at the aftercooler and the warm heat exchanger. Since the diameter of the pulse-tube is rather large, the pressure drop in the pulse-tube can be neglected. Hence, the pressure measured at the warm heat exchanger gives the pressure at the cold end of the regenerator. The flanges where the thermometer holes were located, were made of copper to have low thermal resistance between the thermometer and the gas. Rubber O-ring provided sealing on the warm end of the pulse-tube and the aftercooler flanges. Indium was used to seal the cold end of the pulse-tube and the regenerator flanges. Indium is a soft material and spreads on the surface under pressure (when bolted). To confine the indium ring, the mating flanges of the pulse-tube and the regenerator have a step as shown in the figure 5.6. The flange connecting the pulse-tube and the inertance tube has a taper to ensure gradual change in cross-sectional area from the pulse-tube to the inertance tube. This is required to decrease turbulence at the pulse-tube warm end.

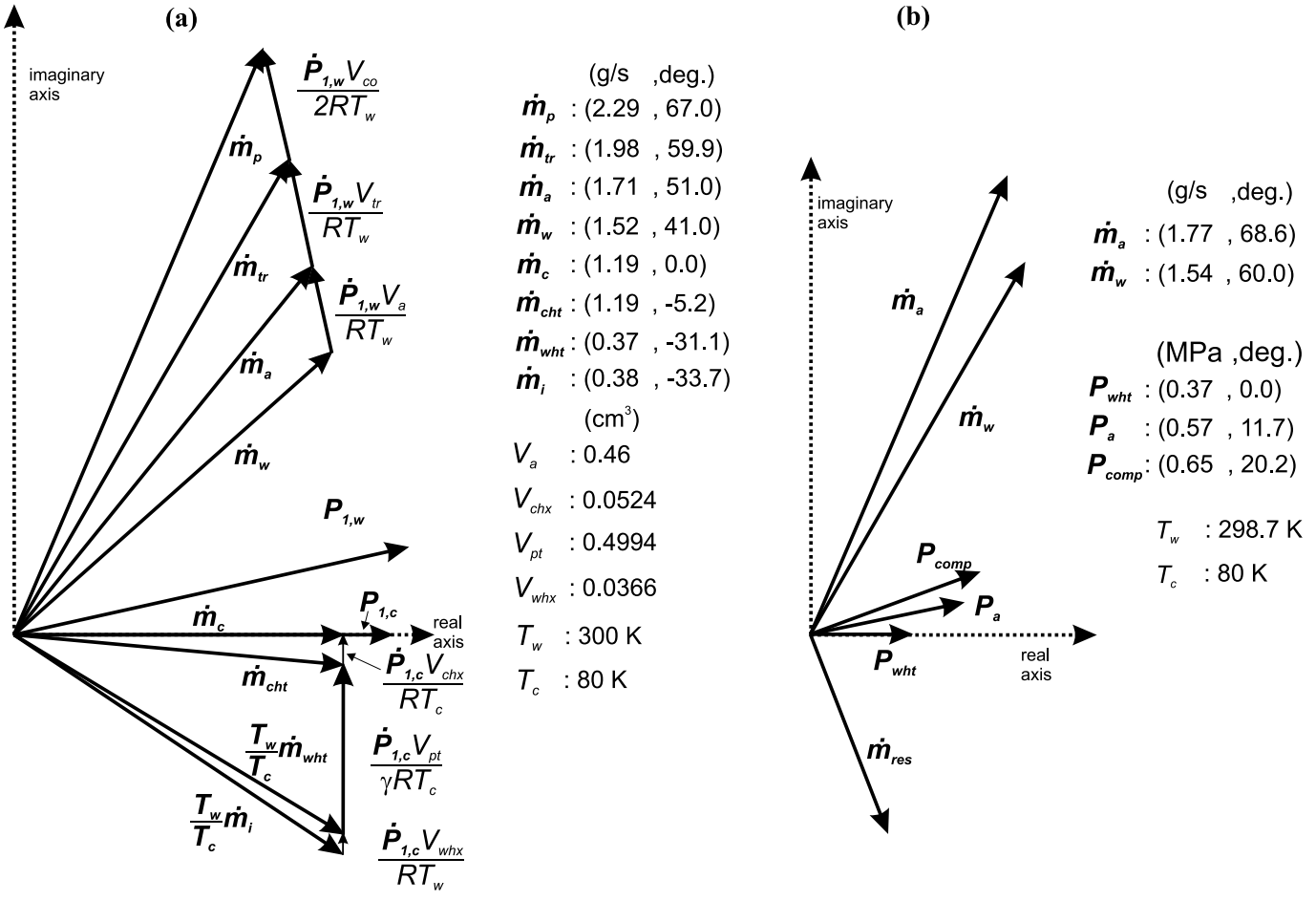

Figure* 5.5: (a) Phasor diagram representing pressures and mass flow under design conditions. (b) Experimental pressure phasors and calculated mass flow phasors.*

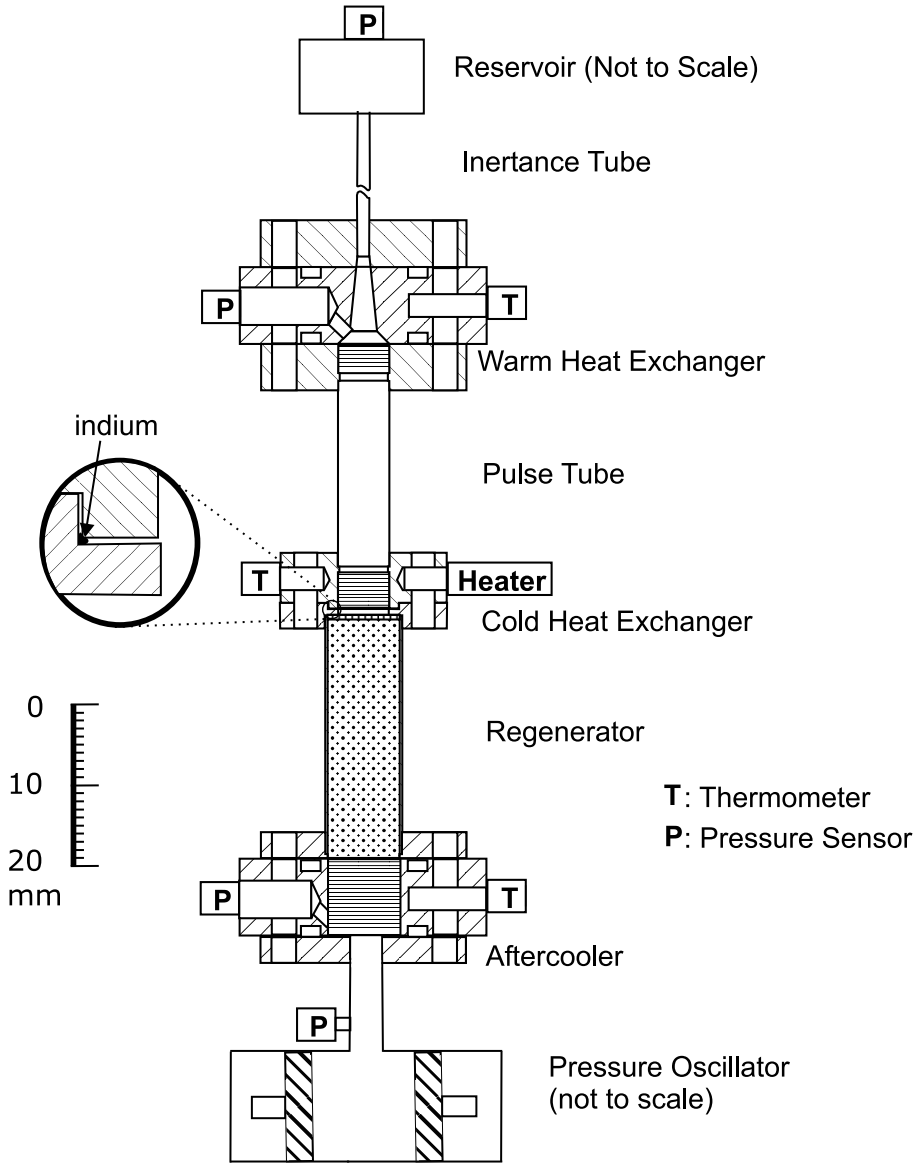

***Figure* 5.6:** *Layout drawing of the in-line pulse-tube cryocooler used in the experiments.*

Length	NTU	$\Delta T_f/\Delta T_i$	$\Delta P/P_0$	Gas Volume (cm^3)
3.000	4.576	0.1029E-01	0.8404E-03	0.3203E-01
3.429	5.232	0.5345E-02	0.9607E-03	0.3662E-01
3.920	5.980	0.2528E-02	0.1098E-02	0.4186E-01
4.481	6.836	0.1074E-02	0.1255E-02	0.4785E-01
5.123	7.815	0.4037E-03	0.1435E-02	0.5470E-01
5.856	8.933	0.1319E-03	0.1640E-02	0.6253E-01
6.694	10.21	0.3672E-04	0.1875E-02	0.7148E-01
7.653	11.67	0.8514E-05	0.2144E-02	0.8171E-01
8.748	13.34	0.1601E-05	0.2450E-02	0.9340E-01
10.00	15.25	0.2371E-06	0.2801E-02	0.1068

Table* 5.5: Simulation results for optimizing the warm heat exchanger. The Reynolds number of the flow was 296.*

5.3 Experimental setup

5.3.1 Pulse-tube refrigerator

Figure 5.7 shows the fabricated regenerator and the matrix material. The regenerator was made by brazing machined flanges on to the stainless steel tube. The regenerator matrix consists of circular discs which were punched with a punch and a die from a stainless steel screen. The microscopic picture of the regenerator matrix is also shown in figure 5.7. The circular discs are stacked into the regenerator.

The pulse-tube was made from a standard stainless steel tube with flanges brazed on to the ends of the tube. Circular discs of copper mesh screen were punched and stacked into the flanges of the pulse tube and diffusion bonded to the flanges at 950^0 for 1 hour in a vacuum furnance to form heat exchangers on either end.

The braze used in brazing of the flanges of the regenerator and the pulse-tube was 65 % Cu - 35 % Au (melting point of 1010 ^oC). This braze material is typically used for brazing to stainless steel or between stainless steel and copper. Stainless steel must be heated to atleast 950 ^oC in the vacuum furnace to remove the oxide layer. In the vacuum braze operation the part is placed in the vacuum furnace with a vacuum pressure less than about <0.1 Pa and heated slowly to the melting temperature. After heating, the furnace is turned off and cooled to atmospheric temperature. A close look at the brazed section is shown in figure 5.7.

Figure 5.8 shows the assembled in-line pulse tube refrigerator. The compressor, inertance tube and reservoir are not shown in the figure. The warm heat exchanger and the aftercooler are cooled by circulating water. Several layers of MLI (Multi Layer Insulation) were wrapped on to the refrigerator to reduce radiation falling on the cold parts. The refrigerator is enclosed in a chamber and pumped to high vacuum to reduce convective and conduction losses with the gas.

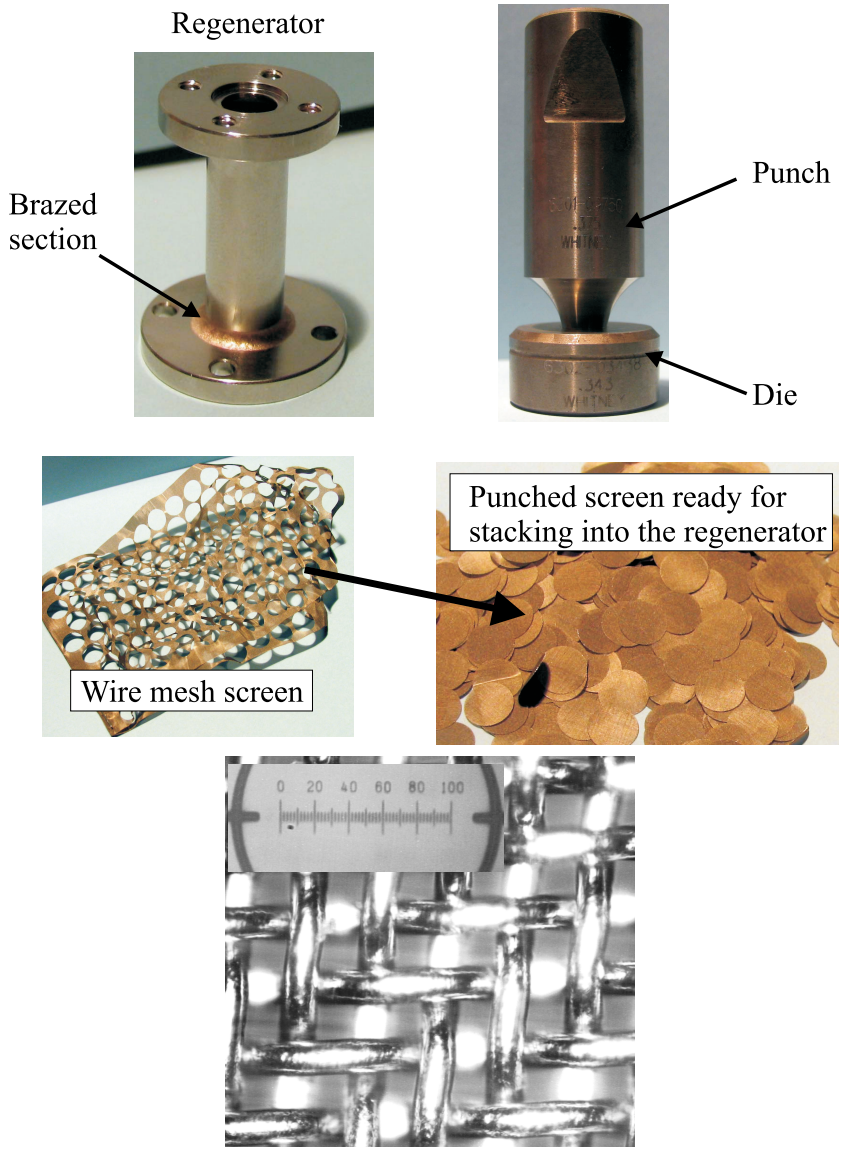

***Figure* 5.7:** *The regenerator was made of stainless steel tube. Fine machined flanges were brazed on the either ends. The regenerator material was made of stainless steel wire mesh screen. Discs of wire mesh screens were made with a die and a punch. The microscopic picture of the wire mesh screen is also shown.*

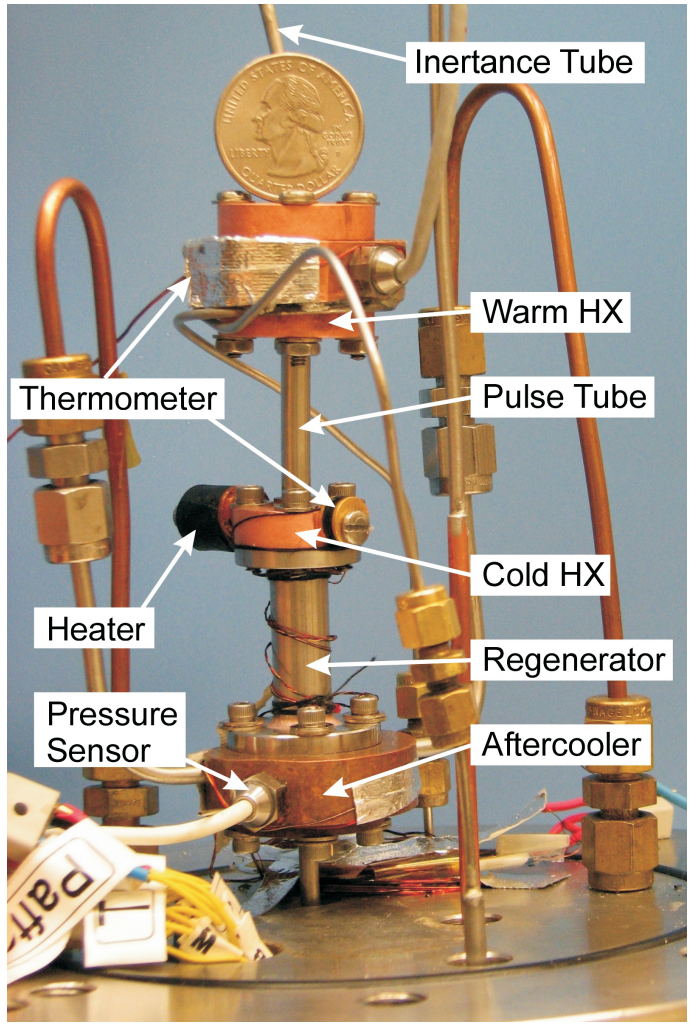

***Figure* 5.8:** *The high frequency pulse-tube cryocooler showing various components. The compressor, most of the inertance tube, and reservoir are not shown. A U.S. quarter (24.3 mm) is shown for size comparison.*

5.3.2 Instrumentation

Measurement and control of the PTR was done at several locations, as indicated in Figure 5.6. The pressure was measured at the warm end of the pulse-tube, near the compressor end of the transfer-line, the aftercooler inlet and outlet(warm end of the regenerator) and the reservoir. The absolute pressure was measured at the back side of the compressor. The sensors used were miniature semiconductor piezoresistive sensors manufactured by Endevco, model #8510B-500 [6]. The sensors have a small dead volume, low sensor mass, and a rated frequency response of 500 kHz. The fast response allows these sensors to easily follow the pressure oscillations in the system. The differential pressure measured across the transfer-line connecting the compressor and the aftercooler was used to calculate the mass flow rates at these locations as described below. The oscillating pressure signals were read by a lockin amplifier [7]. The electronics for energizing and detecting the outputs for these pressure transducers is manufactured by Validyne [8]. A linear compressor manufactured by Q-Drive [3] was used to power the cryocooler.

Temperature measurement points are also indicated in Figure 5.6. The temperatures are determined by diode thermometers by measuring the temperature dependent voltage drop across a diode while maintaining constant current through the diode. The diode thermometers and the electronics which provide the constant current are manufactured by Lake Shore Cryotronics, Inc [9]. The diode sensors are model #DT-470. These thermometers have a response time of approximately 0.3 s and are only used to provide mean temperatures at these locations.

The heater is made of manganine wire and was bolted to the cold heat exchanger flange. Vacuum grease was used to have good thermal contact. A turbo pump manufactured by Peiffer [10] was used to achieve high vacuum (<0.1 Pa). Labview [11] data acquisition hardware and the software was used to record the temperature history.

Mass-flow calibration

Assuming adiabatic behavior in the reservoir, the mass flow into the reservoir can be determined from the oscillating pressure in the reservoir by the equation

$$\dot{m} = \frac{\dot{\boldsymbol{P}} V_{res}}{\gamma R T_{res}} \tag{5.6}$$

where V_{res} and T_{res} are the volume and temperature of the reservoir, respectively. The mass flow at the aftercooler entrance was determined from the pressure difference measured across the transfer line connecting the compressor and the aftercooler. The transfer line inside diameter was 2.5 mm with a length of 100 mm. To determine the amplitude and phase of the mass flow, the pressure difference across the transfer line was calibrated against mass flow by connecting a known reservoir volume directly to the aftercooler as shown in figure 5.9, and using the dynamic pressure measured in the reservoir to determine the instantaneous mass flow at the reservoir entrance from equation 5.6. The calibration curve is shown in

figure 5.10. The PV power $\dot{W_{PV}}$, at the aftercooler entrance is determined from the amplitudes of the mass flow $\dot{m_1}$ and the pressure P_1 measured at the aftercooler entrance by the equation,

$$\dot{W_{PV}} = \frac{1}{2} R T_a \left(\frac{P_1}{P_0} \right) \dot{m_1} \cos\theta \tag{5.7}$$

The term P_0 is the average pressure, T_a is the temperature at the aftercooler, and θ is the phase between $\dot{m_1}$ and P_1. Extensive experiments were later performed by Lewis and Radebaugh at the National Institute of Standards and Technologies to estimate the accuracy of the mass flow measurement [12, 13].

5.4 Experimental results

Several experiments were performed on the designed pulse-tube refrigerator, by varying the compressor power, driving frequency and the filling pressure in the system.

5.4.1 Cooldown curve

Figure 5.11 shows the cooldown curve for the cryocooler operating at an average pressure P_0 of 3.5 MPa, pressure ratio at the cold-end of 1.23 (1.4 at the aftercooler), and an operating frequency of 120 Hz. The cooldown times from ambient temperature of 299 K to 80 K and 50 K are about 5.5 and 11 minutes, respectively. This very fast cooldown is a result of the small regenerator volume and low heat capacity for a given refrigeration power, which is an advantage of operating the cryocooler at high frequencies. Note that in the cooldown experiments, the compressor power or the pressure ratio were not monitored. The fast cooldown was studied in greater detail and is the topic of the next chapter.

5.4.2 Load curve

The net refrigeration power (applied to the heater) as a function of temperature is shown in figure 5.12 for several operating conditions. For an average pressure of 3.5 MPa and a pressure ratio of 1.4 at the aftercooler (1.23 at the cold end) the net refrigeration power at 80 K was 3.37 W with an input PV power at the aftercooler of 66.0 W. For an aftercooler temperature of 298.7 K the efficiency is about 14.0 % of Carnot when referred to the input PV power.

5.4.3 Background losses

The background loss, consisting of the heat conduction through the walls of the regenerator, the pulse-tube, regenerator matrix, and radiation heat losses are

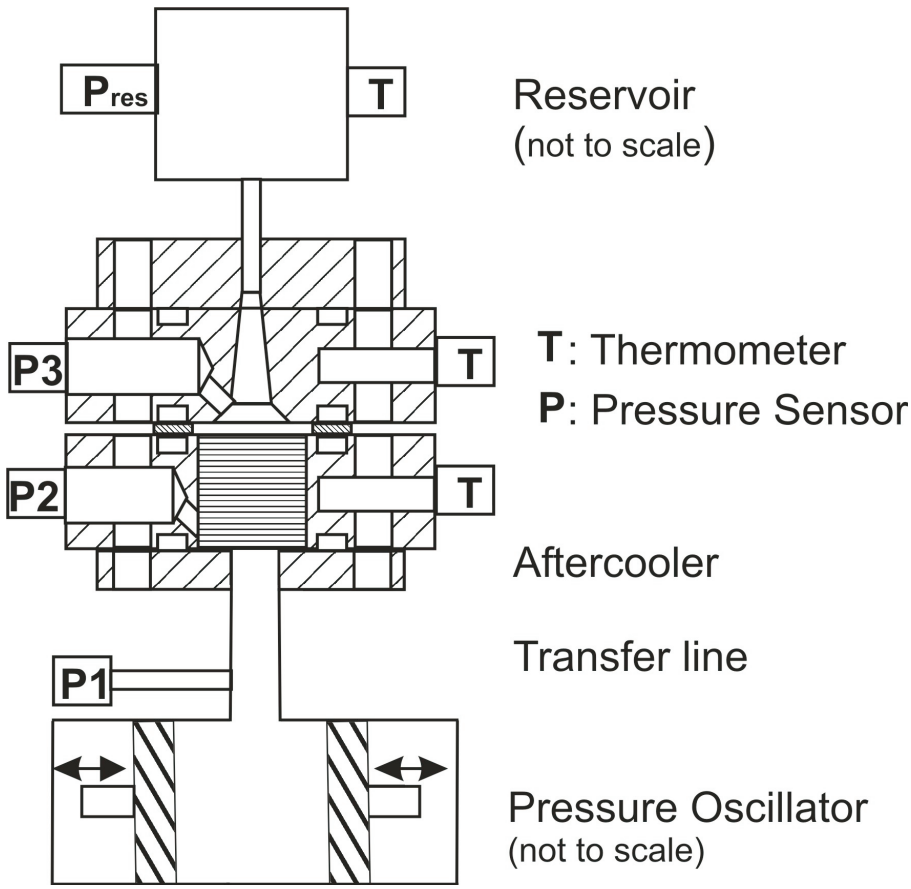

Figure* 5.9: 5. Layout of the apparatus to calibrate mass flow in the transferline. The pressure difference across the transferline, $P_1 - P_2$ is calibrated against the mass flow into the reservoir, which is determined from the reservoir pressure P_{res} by using equation 5.6*

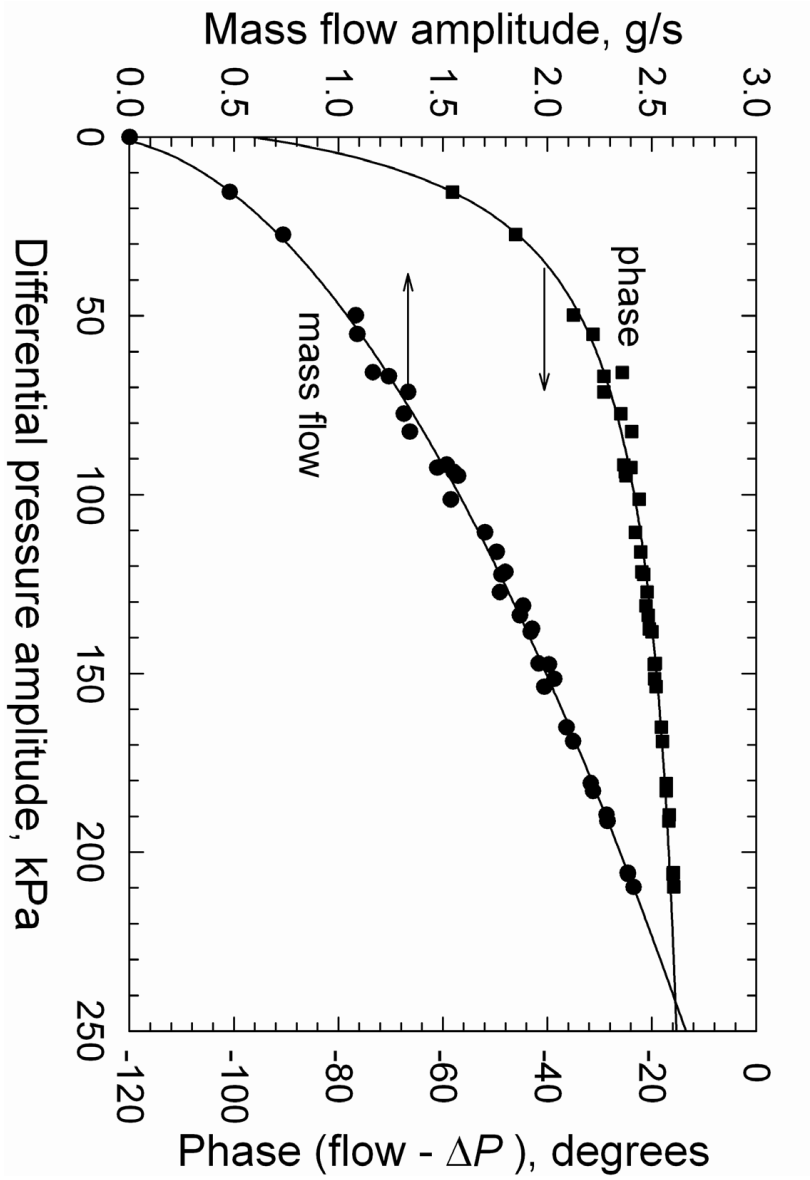

Figure* 5.10: Calibration curve for mass flow in the transfer line. A flow amplitude of 1.40 g/s was measured with a pressure ratio of 1.23 at the cold end.*

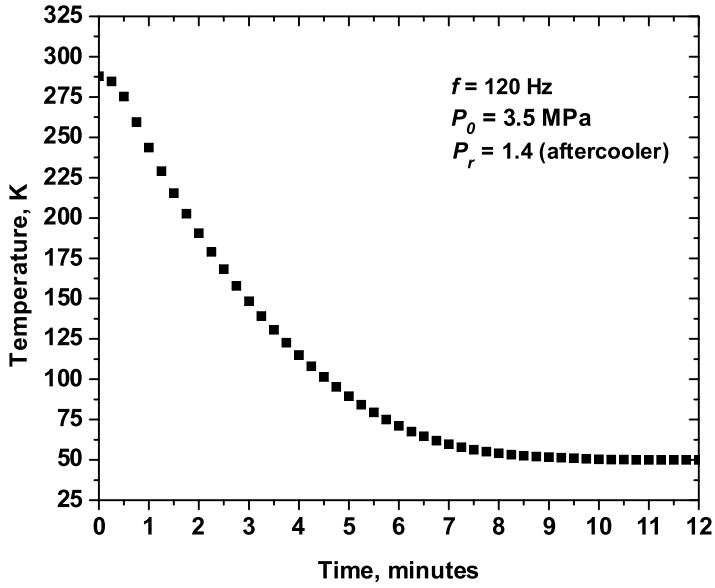

Figure* 5.11: Cooldown curve of the cryocooler. Cooldown times to 80 K and 50 K are about 5.5 and 11 minutes, respectively.*

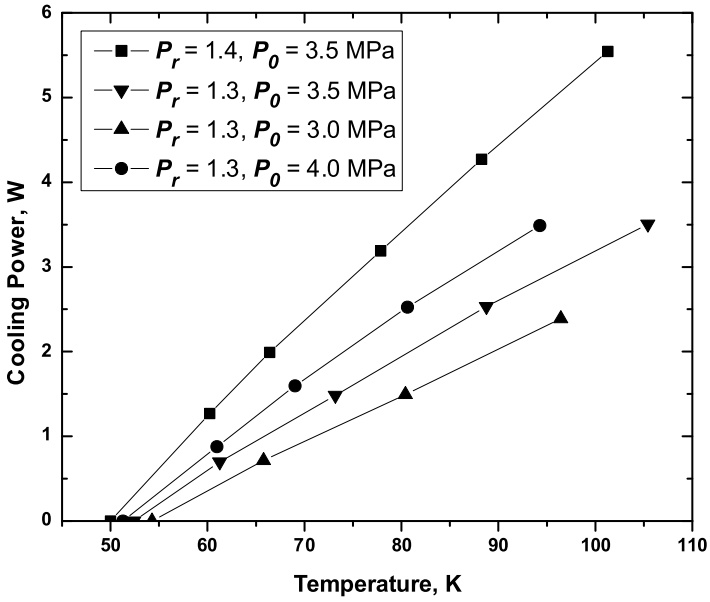

Figure* 5.12: Net refrigeration power of the pulse-tube cryocooler with different warm end pressure ratios and average pressures.*

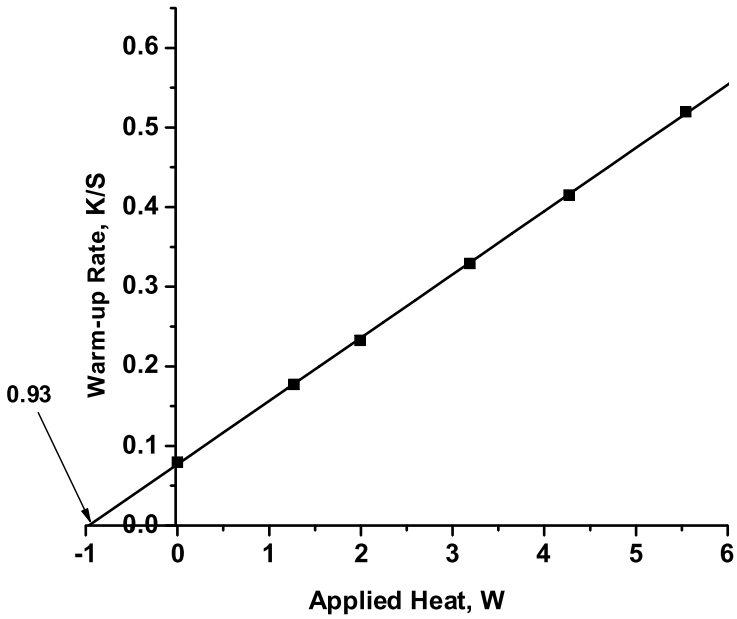

Figure* 5.13: Determination of background leak in the cryocooler from the warm-up rate at 120 K with variable applied heat.*

measured by finding the slope of the warm-up curve at 120 K with different heating powers. Figure 5.13 shows the plot of the warm-up rate at 120 K versus the applied heat. The background losses are obtained by extrapolating the warm-up rate to zero, which is found to be about 0.93 W at 120 K. The losses are not expected to increase significantly (will probably increase linearly) between 120 K and 80 K. The computed conduction losses along the tube walls of regenerator and pulse-tube with the cold end at 120 K and the warm end at 300 K is about 0.8 W. The conduction losses in the matrix is obtained from the REGEN3.2 run for the experimental case with the cold end temperature at 80 K and warm end at 300 K and was about 0.14 W. The sum of the losses was 0.94 W which is in close agreement with the experimentally measured losses.

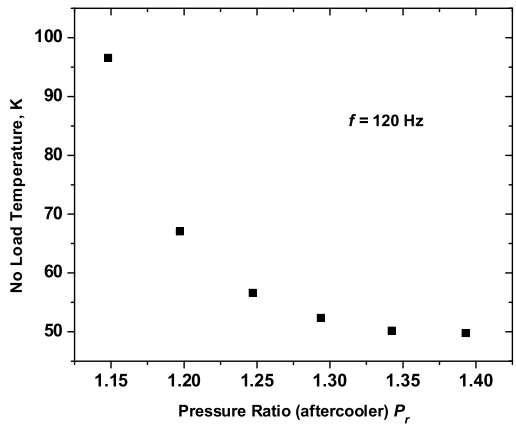

Figure* 5.14: No-load temperature versus pressure ratio at the aftercooler.*

5.4.4 Variation of pressure ratio and frequency

Figure 5.14 is a plot of no-load temperature versus pressure ratio P_r at the aftercooler for a frequency of 120 Hz. Figure 5.15 shows how the no-load temperature varies with frequency for a pressure ratio of 1.3 at the aftercooler and an average pressure of 3.5 MPa. In both figures the no-load temperature does not show a significant decrease with increase in pressure ratio or frequency beyond the design values of P_r equal to 1.4 and f equal to 120 Hz. The phasor representing the rate of change of mass in the regenerator is proportional to dynamic pressure and frequency. Both higher dynamic pressure and frequency increase this phasor resulting in higher mass flow in the regenerator and greater losses, which tends to dominate the increased gross refrigeration power at higher dynamic pressures and frequencies.

5.4.5 Performance comparison with REGEN3.2 calculations

Figure 5.5 (b) shows an example of the phasor representation of pressures and mass flows measured with respect to the pressure at the pulse-tube warm heat exchanger. The experimental and calculated data of amplitudes for this example case are shown in table 5.2. The pulse-tube is a large open tube, hence the pressure at the warm heat exchanger is very close to the pressure at the cold end of regenerator. The mass flow at the aftercooler is determined from the pressure difference across

Cold-end temperature (K)	60.2	66.4	77.9	88.3	101.3	80 [a]
Transfer line data						
Transfer line volume (cm^3)	0.56					
Transfer line temperature (K)	320					
Aftercooler data						
Aftercooler gas volume (cm^3)	0.46					
Aftercooler temperature (K)	298.7					
Amplitude						
Delta P (rms) across transfer line (kPa)	76.34	82.89	79.65	73.72	68.45	
Delta P (ampl.) across transfer line (kPa)	107.94	117.21	112.63	104.24	96.79	
Mass flow amplitude [b] (g/s)	1.649	1.73	1.69	1.616	1.547	1.67
RMS of P at aftercooler (kPa)	417.8	420.3	415.3	418.1	417.6	
Amplitude of P at aftercooler (P3) (kPa)	590.77	594.30	587.23	591.19	590.49	588.05
Phase						
delta P phase referenced to reservoir P (deg)	224.7	228.84	229.62	234.28	233.4	
Phase of P at pulse tube (deg)	160.13	159.39	158.76	158	157.3	
delta P phase referenced to P at pulse tube (deg)	64.57	69.45	70.86	76.28	76.1	
Phase of calibration (deg)	-22.46	-23.76	-21.98	-22.86	-23.76	
Phase of mass flow [c] (deg)	42.11	45.69	48.88	53.42	52.34	
Phase of P at aftercooler (P3) (deg)	171.87	171.28	170.43	169.94	169.6	
Phase of P at aftercooler referenced to P at pulse tube (deg)	11.74	11.89	11.67	11.94	12.3	
Phase of mass flow [d] (deg)	30.37	33.8	37.21	41.48	40.04	38.09

***Table* 5.6:** *Experimentally measured and calculated data for several operating conditions of the 120 Hz pulse-tube cryocooler. The massflow calibration data is obtained from figure 5.10.*

[a] interpolated data
[b] at transfer line center (from calibration)
[c] at center of transfer line referenced to P at pulse tube
[d] at center of transfer line referenced to P at aftercooler

continuation of table 5.6

Correction for 1/2 of transfer line						
Frequency	120					
Amplitude of half phasor (g/s)	0.19	0.19	0.19	0.19	0.19	0.19
Mass flow amplitude at aftercooler (g/s)	1.50	1.57	1.52	1.44	1.38	1.50
Delta mass flow phase across half transfer line (deg)	6.20	5.74	5.61	5.61	5.99	5.61
Phase of mass flow [a] (deg)	24.17	28.06	31.60	35.87	34.05	32.64
Phase of mass flow [b] (deg)	35.91	39.95	43.27	47.81	46.35	32.64
Correction for aftercooler						
Amplitude of half phasor	0.17	0.17	0.16	0.17	0.17	0.16
Mass flow amplitude at regenerator warm end (g/s)	1.43	1.49	1.44	1.34	1.29	1.42
Delta mass flow phase across aftercooler (deg)	6.03	5.65	5.59	5.72	6.10	5.62
Phase of mass flow [c] (deg)	29.89	34.30	37.69	42.08	40.25	26.86
Power and efficiency						
Aftercooler temperature (K)	298.7	298.7	298.7	298.7	298.7	298.7
Average pressure (kPa)	3500	3500	3500	3500	3500	3500
Ratio of pressure amplitude to average pressure at aftercooler	0.17	0.17	0.17	0.17	0.17	0.17
PV power at aftercooler (W)	71.65	72.85	67.41	61.07	59.67	66.00
Net refrigeration power (W)	1.27	1.991	3.19	4.27	5.54	3.37
COP	0.02	0.03	0.05	0.07	0.09	0.05
efficiency	0.07	0.10	0.13	0.17	0.18	0.14

[a] at aftercooler referenced to P at aftercooler
[b] at aftercooler referenced to P at pulse tube
[c] at regenerator warm end referenced to P at pulse tube

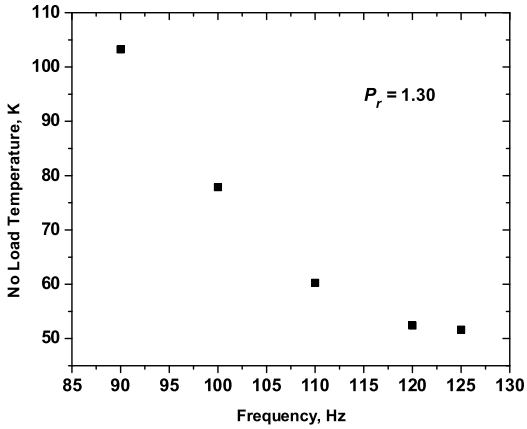

Figure* 5.15: No-load temperature versus frequency.*

the aftercooler $P_{comp} - P_a$. The mass flow into the reservoir is determined from the pressure measured in the reservoir. The maximum pressure ratio that could be reached at the cold end of the regenerator was 1.23. The measured cooling power, calculated PV power flow, and COP for this experimental case are shown in table 5.2. The measured and calculated parameters for several operating conditions of the cryocooler are shown in table 5.6. The calculated parameters agree rather well with the measured parameters.

5.5 Conclusions

A 120 Hz pulse-tube cryocooler was designed and built which cooled to a no-load temperature of 49.9 K. This is for the first time such low temperature was achieved for a pulse-tube cryocooler operating above 100 Hz. We have also experimentally verified the theoretical prediction that by using a higher average pressure, a smaller hydraulic diameter in the regenerator matrix, and a smaller regenerator volume, a pulse-tube cryocooler operating at 120 Hz can achieve high efficiency at 80 K. A pulse-tube cryocooler operating at 120 Hz, with an average pressure of 3.5 MPa, and a pressure ratio of 1.23 at the cold end produced a net cooling power of 3.37 W at 80 K with an efficiency of 14.0 % of Carnot when referred to the PV power at the aftercooler. The small regenerator volume resulted in a reduced heat capacity and a faster cooldown time compared with pulse tube cryocoolers operating at 60

Hz. A cooldown time of 5.5 minutes to 80 K was achieved.

Bibliography

[1] R. Radebaugh and A. O´ Gallagher. Regenerator operation at very high frequencies for microcryocoolers. *Advances in cryogenic engineering*, 51:1919, 2006.

[2] S. Zhu, G. Yu, X. Zhang, W. Dai, E. Luo and Y. Zhou. A 300 Hz high frequency thermoacoustically driven pulse tube cryocooler. *Advances in Cryogenic Engineering*,in press 53, 2008.

[3] compressors, Q-Drive resonant power systems, CFIC inc., 302 10th street, troy, NY 12180. www.qdrive.com.

[4] M. Lewis. Impedance measurements of inertance tubes at high frequency and pressure. *Advances in cryogenic engineering*, 53, 2008.

[5] *Heat transfer*. John Wiley & Sons, Inc.,, 1993.

[6] Endevco corporation, www.endevco.com.

[7] Lock-In amplifiers, Stanford Research Systems, Inc, 1290-D Reamwood Ave., Sunnyvale, CA 94089, www.thinksrs.com.

[8] Validyne Engineering Corp., 8626 Wilbur Avenue, Northridge, CA 91324, www.validyne.com.

[9] LakeShore 575 McCorkle Blvd, Westerville, OH 43082, www.lakeshore.com.

[10] Pfeiffer Vacuum, 24 Trafalgar Square Nashua, NH 03063 www.pfeiffer-vacuum.com.

[11] National instruments corp., www.ni.com.

[12] private communication Radebaugh, R. and Lewis, M.

[13] Lewis, M. et al. to be published in Advances in Cryogenics engineering, 2008.

Chapter 6

Fast cooldown modeling and experiments

High frequency operation of a pulse-tube cryocooler leads to reduced regenerator volume, which results in a reduced heat capacity and a faster cooldown time. A pulse-tube cryocooler operating at a frequency of 120 Hz and an average pressure of 3.5 MPa achieved a no-load temperature of 50 K. The cooling power at 80 K was about 3.37 W with a cooldown time from 285 to 80 K of about 5.5 minutes, even though the additional thermal mass at the cold end due to flanges, screws, heater, and thermometer was 4.2 times that of the regenerator. This fast cooldown is about two to four times faster than that of typical pulse-tube cryocoolers and is very attractive to many applications. In this study we measure the cooldown time to 80 K for different cold-end masses and extrapolate to zero cold-end mass. We also present an analytical model for the cooldown time for different cold-end masses and compare the results with the experiments. The model and the extrapolated experimental results indicate that with zero cold-end mass the cooldown time to 80 K with this 120 Hz pulse-tube cryocooler would be about 32 s.

6.1 Introduction

Fast cooldown is often desired for cryocoolers. Conventionally, Joule- Thomson (JT) cryocoolers have been used for fast cooldown. Open-cycle JT cryocoolers operate at very high pressure (5-16 MPa) and have a very high flow impedance at the cold end that is susceptible to clogging. Gifford-McMahon (GM), Stirling and pulse tube cryocoolers[1] are alternatives to reach temperatures of about 50 K. Mullie et al. [3] reported improvements in cooldown time of resonant Stirling cryocoolers by matching the regenerator material heat capacity to the temperature profile that would exist at steady state in the regenerator. However, the improvements in the cooldown time were not significant. Radebaugh et al. [2] proposed a fast cooldown technique for pulse-tube cryocooler that makes use of the resonance phenomenon that occurs with an appropriately sized inertance tube and reservoir volume. With a small reservoir, the resonance condition can occur, which allows for higher PV power flows (higher refrigeration power). That concept applies to fast cooldown of large masses at the cold end. In this paper we discuss another method of fast cooldown that relies on high frequency and high pressure to reduce the thermal mass of the regenerator. This method is useful for applications with small cold-end masses where the regenerator heat capacity has a large influence on the cooldown time.

6.2 Refrigeration power density

For an ideal Stirling and Stirling-type pulse-tube cryocooler, the cooling power is equal to the acoustic power (PV power) at the cold end and is given by

$$\dot{W}_{PV} = \frac{1}{2} P_1 \dot{V}_1 \cos\phi_c, \tag{6.1}$$

where P_1 and $\dot{V}_1$ are the amplitudes of the sinusoidal pressure and the volume flow, and ϕ_c is the phase by which the volume flow leads the pressure. The volume flow amplitude is related to the instantaneous volume amplitude V_1 at the cold end by

$$\dot{V}_1 = 2\pi f V_1. \tag{6.2}$$

The PV power is then given by

$$\dot{W}_{PV} = \pi f V_1 P_0 \left(\frac{P_1}{P_0}\right) \cos\phi_c, \tag{6.3}$$

where P_0 is the average pressure and f is the frequency. The term in parentheses is the relative pressure amplitude, which is usually not varied. From this equation

1. Commercial Stirling coolers have a typical cooldown time to 80 K from ambient temperature of about 300 s [3]. Note that these coolers do not have flanges at the cold side of the regenerator. The heat capacity ratio between the cold part and the regenerator is less than one.

we see that by increasing the frequency the PV power can be increased for fixed size of the refrigerator and operating conditions. However, simply increasing the frequency of a cryocooler designed for operating at 60 Hz would lead to higher losses because of ineffective heat transfer in the regenerator. We have shown that to efficiently operate the cryocooler at higher frequencies it is necessary to increase the average pressure and to use a regenerator matrix with a smaller hydraulic diameter (see chapter 3, section 3.6.5) [4], [5]. High frequency operation of the cryocooler would also reduce the required regenerator volume. According to equation 6.3, for a certain PV power, increasing the frequency reduces the volume flow at the cold end for a fixed pressure ratio and phase ϕ_c. The pulse-tube volume is generally chosen to be about three times the swept volume at the cold end. Reduction in swept volume due to high frequency operation of the cryocooler also reduces the pulse tube volume. Hence, high frequency operation of the cryocooler reduces the volumes of the regenerator and the pulse-tube for a given cooling power, which increases the power density and leads to a faster cooldown.

6.3 120 Hz Pulse-tube cryocooler

A pulse-tube cryocooler was designed to operate at a frequency of 120 Hz with an average pressure of 3.5 MPa [5], [6] and was described in the previous chapter. Figure 6.1 shows the assembled cryocooler with an added mass attached to the cold end for cooldown experiments. For the cooldown experiments reported here the pressure ratio at the cold end (measured at the pulse-tube warm end) was held constant at 1.23 during the entire cooldown process. For comparison, one test was performed with the input power to the compressor held constant. To determine the effect of the cold-end mass on the cooling process, various copper masses were mounted at the cold end and the cooling times were recorded. The average heat capacities of the copper masses and other components are given in table 6.1.

6.4 Experimental results

Experiments were performed on the cryocooler for several cold-end masses given in table 6.2. For all the tests the average pressure was 3.5 MPa, the frequency was 120 Hz, and the pressure ratio was 1.23 at the cold end (measured at the warm end of the pulse-tube), except for test 6 where the input power to the compressor was held constant at 275 W. Figure 6.2 is the plot of cooldown curves for tests 1 to 5 in table 6.2. The tests at constant pressure ratio were chosen to provide a constant cold-end acoustic power in order to simplify the comparison with analytical models. As shown in table 3 the cooldown time for test 6, which was performed with a constant compressor input power of 275 W, was significantly less than test 5 made with the same mass but with a constant pressure ratio. The 275 W is the steady-

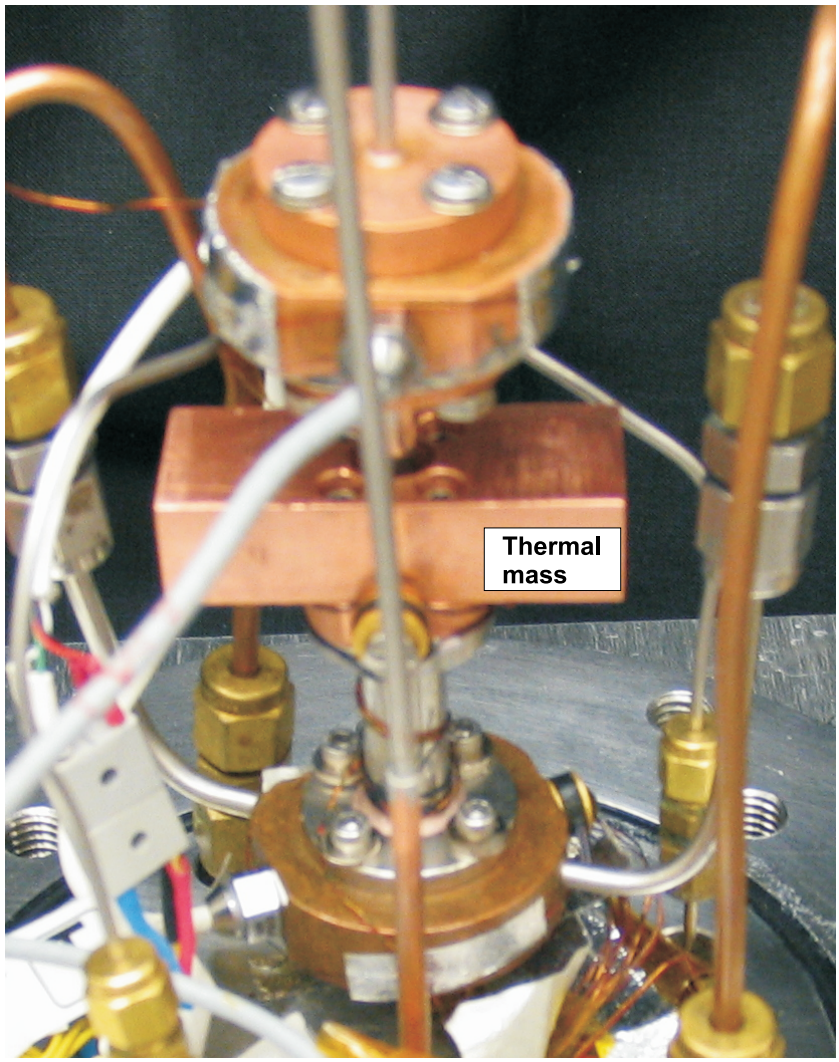

Figure* 6.1: 120 Hz pulse-tube cryocooler showing the thermal mass attached to the cold heat exchanger.*

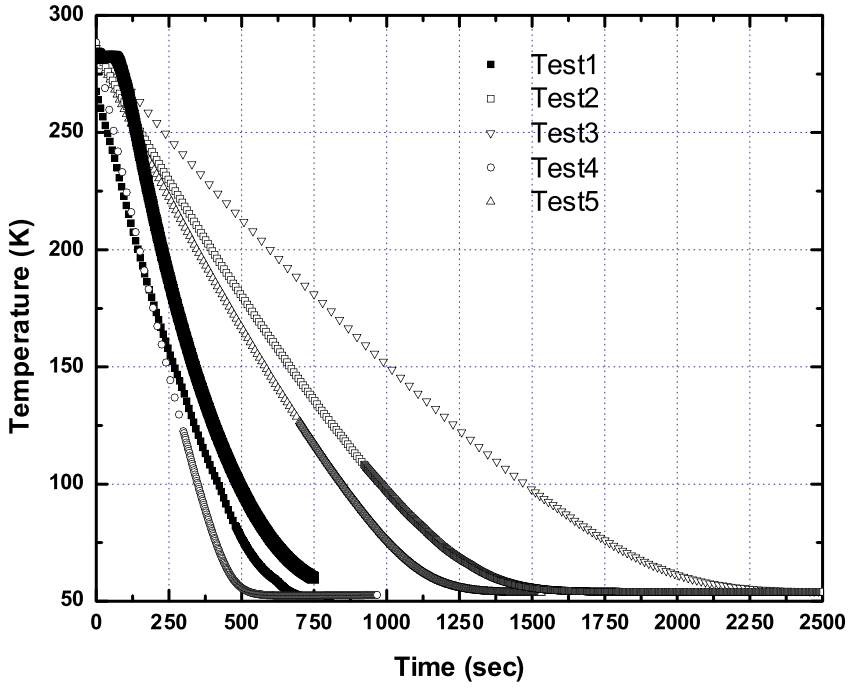

Figure* 6.2: Cooldown curves under various conditions.*

state input power required when the cold end is at 50 K with a pressure ratio of 1.23 at the cold end. The high input power is a result of the compressor operating far from resonance conditions at the 120 Hz frequency. A constant input power would be more realistic for cooldown during actual applications.

Cold Item	Mass (g)	Average heat capacity (J/K)
Built-in mass, M_0	26.1	9.26
(cold HX, flanges and thermometer)		
Heater + screw and washer	9.2	3.10
Mass 1, M_1 (Cu)	41.7	13.88
Mass 2, M_2 (Cu)	83.9	27.93
Regenerator, (SS)	7.7	2.95

Table* 6.1*: *Average heat capacities (80-285 K) of various masses at the regenerator cold end.*

Test	Cold item	Mass (g)	Heat capacity ratio, C_r	Cooldown time [a](s)
1	M_0 + heater	35.3	4.19	517
2	M_0 + heater + M_1	77.0	8.89	1133
3	M_0 + heater + M_2	119.2	13.66	1692
4	M_0	26.1	3.14	394
5	M_0 + M_1	67.8	7.84	970
6 [b]	M_0 + M_1	67.8	7.84	585

Table* 6.2*: *Experimental conditions and cooldown time with various capacities. Tests 1-5 were for a constant pressure ratio of 1.23 at the warm end.*

[a] 285-80 *K*
[b] Constant input power, 275 W.

6.5 Analysis

6.5.1 Analytical Model

The experimental cold stage (consisting of the regenerator, cold heat exchanger, pulse-tube, warm heat exchanger) was maintained in a high vacuum, which

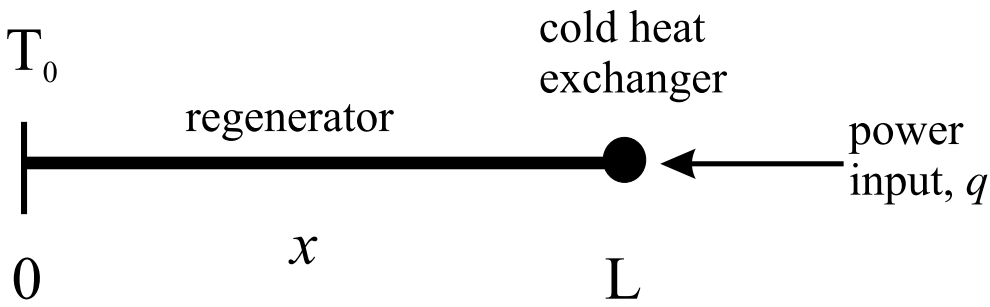

Figure* 6.3: Schematic of a one-dimensional thermal model of the regenerator and the cold heat exchanger.*

essentially eliminates conduction as a means of heat transfer. The cold stage was wrapped with several layers of multi-layer insulation, which substantially reduces the heat radiation gain from ambient. The main sources of heat transfer to the cold end are enthalpy flow, heat conduction through the regenerator material, and heat conduction through the tube walls of the regenerator and the pulse-tube. To simplify the analytical model, the enthalpy flow and heat conduction were assumed to be proportional to the temperature difference between the hot and cold ends for cold-end temperatures between 80 and 285 K. An effective thermal conductivity is defined as

$$\lambda_{eff} = f_c.\lambda + \lambda_h \tag{6.4}$$

The factor f_c is the conductivity degradation factor accounting for packing of the screens [7], λ_h is the simulated conduction to account for enthalpy flow, and λ is the thermal conductivity of the material. The density and specific heat are taken to be independent of temperature and equal to the average value between 80 and 285 K.

The one-dimensional thermal model is illustrated in figure 6.3. Because of the high thermal conductivity of copper, the cold heat exchanger can be modeled as a uniform temperature thermal mass with a total heat capacity C_M. The warm-end heat sink is assumed to be at a constant temperature T_0 and the heat flows by the effective thermal conductivity given in Eq. 6.4 through the regenerator and pulse-tube simulating conduction through a solid rod of the same solid cross-sectional area. If the temperature of the regenerator and the cold heat exchanger were initially at the heat sink temperature T_0 and a step power q is applied ($q <$ 0 for refrigeration) at the cold heat exchanger at $t > 0$, the cold heat exchanger temperature T is given by [8],[9],

$$T(t) = T_0 + \frac{qL}{\lambda_{eff} A_c} \left[1 - \sum_{n=1}^{\infty} \frac{4 \sin^2 \xi_n}{\xi_n (2\xi_n + \sin 2\xi_n)} \exp(-\frac{t}{\tau_n}) \right] \tag{6.5}$$

where A_c is the solid cross-sectional area, L is the regenerator length, and the time constants are

$$\tau_n = \rho c_p L^2 / \lambda_{eff} \xi_n^2, \tag{6.6}$$

where ρ is the solid density, c_p is the specific heat of the regenerator matrix and the eigenvalues ξ_n are determined by the positive solutions to the equation

$$\xi_n \tan \xi_n = \frac{\rho A_c L c_p}{C_M} = \frac{1}{C_r}. \tag{6.7}$$

where C_M is the heat capacity of the cold-end mass and C_r is the ratio between the heat capacity of cold-end mass and that of the regenerator mass. When C_M approaches zero the result gives the intrinsic cooldown time when there is no cold-end mass. For the intrinsic case of zero cold-end mass we derived an alternative analytical model that gives the temperature as a function of both time and position x between the warm and cold ends. The result is given by

$$T(x,t) = T_0 + \frac{qx}{\lambda_{eff} A_c} - \sum_{n=1}^{\infty} A_n \sin\left[\frac{(2n-1)\pi x}{2L}\right] \exp\left(-\frac{t}{\tau_n^*}\right), \tag{6.8}$$

where the constants are,

$$A_n = \frac{8qL \sin[(2n-1)\pi/2]}{\lambda_{eff} A_c \pi^2 (2n-1)^2} = \frac{8qL(-1)^{n+1}}{\lambda_{eff} A_c \pi^2 (2n-1)^2}, \tau_n^* = \frac{4L^2}{\pi^2 (2n-1)^2 \alpha_m}, \alpha_m = \frac{\lambda_{eff}}{\rho c_p} \tag{6.9}$$

Equation 6.8 is similar to the equation derived by Reese and Tucker [10] for use in measuring specific heats, except for a small error in their published equation. Note that in our case $q < 0$. The analytical equations rely on the use of the effective thermal conductivity given by eq. 6.4 that takes into account the enthalpy flow in the regenerator. We rely on a numerical model described in next section to calculate this enthalpy flow loss.

6.5.2 Numerical Analysis

The NIST numerical model, known as REGEN3.2 and based on finite difference equations for the conservation equations, was used for the calculations discussed here. In REGEN3.2 the mass flow at the cold end and its phase with respect to the pressure at the cold end are input parameters, along with the desired average pressure, pressure ratio, frequency, and the geometrical parameters of the regenerator matrix. The mass flow at the warm end (both magnitude and phase) is calculated by the model. Losses associated with regenerator ineffectiveness, conduction through the matrix, and pressure drop are calculated by the model. Conduction loss through the tube containing the screen matrix is calculated separately. A loss associated with the expansion process (pulse-tube) was taken to be 20 % of the gross refrigeration power [11].

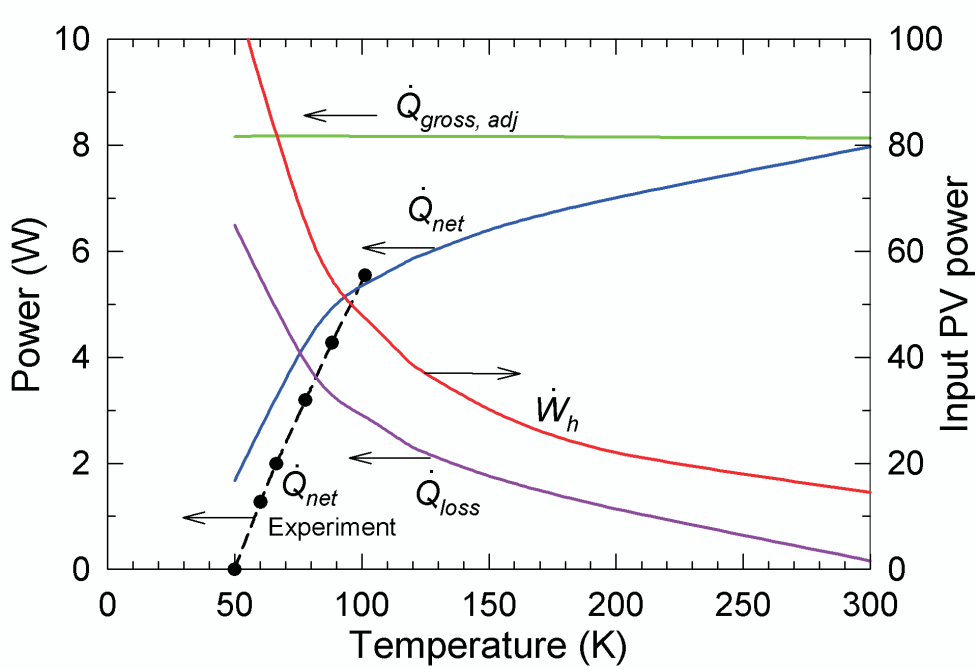

***Figure* 6.4:** *Output from REGEN3.2 calculations compared with experimental results.*

The enthalpy flow loss in the regenerator is not linear with the temperature difference between the two ends of the regenerator. The enthalpy flow tends to increase rather rapidly as the cold end cools below about 100 K, which for a constant input PV power causes the net refrigeration power to decrease rapidly below 100 K. To estimate the net cooling power as a function of cold end temperature, REGEN runs were performed with the dimensions of the regenerator given in table 6.1 with varying cold end temperatures. The average pressure of 3.5 MPa, a pressure ratio of 1.23 at the cold end and a frequency of 120 Hz were taken to match with the experimental data. The flow at the cold end was made to be in phase with the pressure ($\phi_c = 0$, see chapter 5 section 5.2) for all the runs. Since the mass flow is a function of temperature, the mass flow for various runs was adjusted from the mass flow value of 1.9 g/s at 80 K. The warm end temperature was taken to be 300 K.

Heat conduction loss through the pulse-tube and regenerator walls as well as a radiation heat loss of about 0.06 W was subtracted from the net cooling power calculated by REGEN3.2. Figure 6.4 is the plot of the adjusted gross refrigeration power (gross minus the 20 % pulse-tube loss), net refrigeration power, input PV power and heat loss as a function of temperature. The heat loss takes into account the enthalpy flow as well as the conduction and radiation losses. The adjusted gross refrigeration power was about 8.17 W. The heat loss was approximated by a straight line between 300 K and 80 K, and the effective thermal conductance was found to be 0.014 W/K. The equivalent conductivity due to enthalpy flow in eq. (6.4) was adjusted to yield this effective thermal conductance. The appropriate enthalpy factor was found to be $\lambda_h / f_c \lambda = 10.27$, with $fc = 0.13$, and $\lambda = 11.32$ W/(K.m) (for stainless steel from www.cryogenics.nist.gov). This effective thermal conductivity from equation 6.4 was then used in the analytical equations for the cooldown time.

6.6 Comparison of experimental and calculated results

Figure 6.4 also shows the measured net refrigeration power as compared with that calculated by REGEN3.2. We see that the experimental values in the range between 80 and 100 K are close to, but slightly less than, the calculated values. That could indicate the pulse-tube ineffectiveness may be slightly larger than 20 %, thereby reducing the adjusted gross refrigeration power. If we maintain the enthalpy factor at 10.27 and use a single adjusted gross refrigeration power q (equal to $\dot{Q}_{gross,adj}$ in figure 4) in eq. 6.5 to give the best agreement between the calculated cooldown times and the experimental results, we find q to be -6.63 W (minus indicates refrigeration) instead of -8.17 W from REGEN3.2. The dashed curve in figure 6.5 represents the cooldown times calculated from eq. (6.5) with q = -6.63

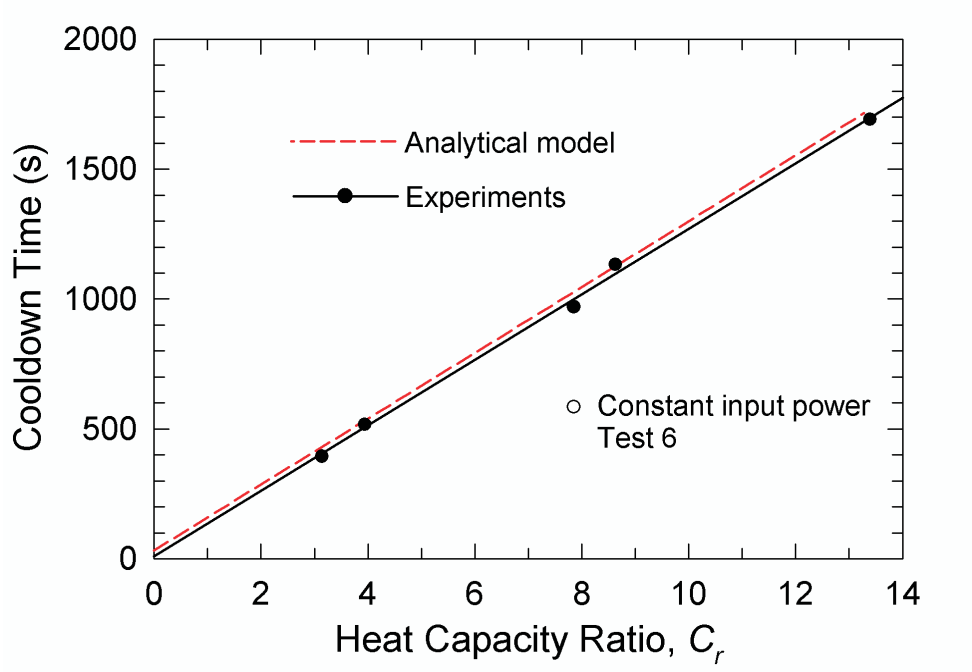

Figure* 6.5: Measured and calculated cooldown times for various ratios of cold-end heat capacity to regenerator heat capacity.*

W. When q = -6.63 W is used in eq. 6.5 or 6.8 for the intrinsic cooldown time from 285 K to 80 K a value of 31.5 s is obtained. The experimental data are also shown in Figure 6.5 for comparison. The solid line is a least squares linear fit to the experimental data. That fit extrapolates to a cooldown time from 285 K to 80 K of 29.7 ± 59.7 s for zero cold-end mass. In practice a small but finite cold-end mass is required to accommodate a heat exchanger, a small thermometer, and some device to be cooled. Heat capacity ratios C_r less than 1.0 would be reasonable in some applications. The major uncertainty in the experimental results is that of the built-in cold-end mass, M_0. Small variations in the pressure ratio during cooldown result in an uncertainty for the experimental cooldown times of about 5 %.

6.7 Conclusion

We have shown that increasing the frequency and average pressure in an optimized pulse-tube cryocooler leads to shorter cooldown times. A pulse-tube cryocooler with a significant cold-end mass operating at 120 Hz and 3.5 MPa average pressure was shown to cool from 285 to 80 K in 5.5 minutes. Cooldown times for various cold-end masses attached to this cryocooler were measured under the condition of a constant cold end pressure ratio of 1.23. A linear extrapolation of these times to zero cold-end mass showed a cooldown time to 80 K of about 29.7 ± 59.7 s, which agrees within experimental error with the value of 31.5 s found by the use of an analytical model. The uncertainty of 59.7 s for the intrinsic cooldown time is due mostly to the 5 % uncertainty in the measured cooldown times for a fixed input power discussed in section 6.6.

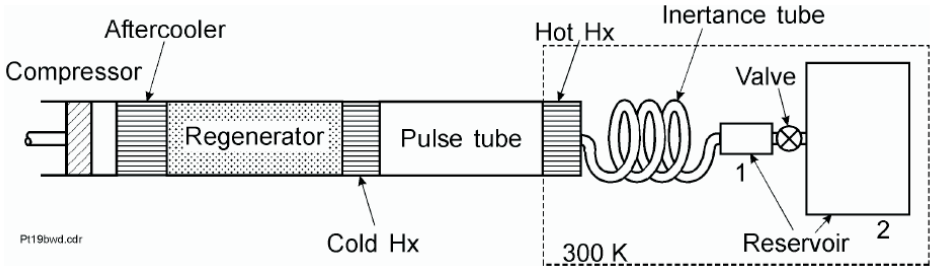

Figure* 6.6: Schematic of a pulse-tube cryocooler with two reservoirs and a control valve that is closed to give a small impedance of the inertance tube and provide for fast cooldown.*

Addendum

This chapter has been adapted from the published article titled, "Modeling and experiments on fast cooldown of a 120 Hz pulse-tube cryocooler" [1]. Section 6.3 is different from the published article to avoid repetition on the description of the 120 Hz cryocoooler which was dealt in greater detail in the previous chapter.

Fast cooldown by tuning the impedance

The proposed improvement in cooldown time of pulse-tube refrigerators for large masses described by Radebaugh et al. [2] is shown in figure 6.6. The impedance of the inertance tube and reservoir volume is determined by the proper combination of inertance tube and reservoir dimensions. For low reservoir volume the system can be tuned to be in resonance similar to a LC electrical circuit. This will increase the PV power flow and hence the refrigeration power. However, the phase angle between mass flow and pressure will not be favorable (an optimum phase angle is mass flow lagging pressure by 30^0) under these conditions which is not a disadvantage when the regenerator is operating till about 100 K. Below this temperature the valve is opened to have a favorable phase relationship to reduce losses in the regenerator.

Mixed regenerator to improve efficiency and decrease cooldown time

Mullie et al. [3] at the Thales Cryogenics in the Netherlands have reported on the development of mixed regenerator. In the mixed regenerator[2], the properties of the regenerator material (wire mesh, regenerator material, filling factor) are

2. The meaning of mixed regenerator is to use different regenerator material along the length of the regenerator.

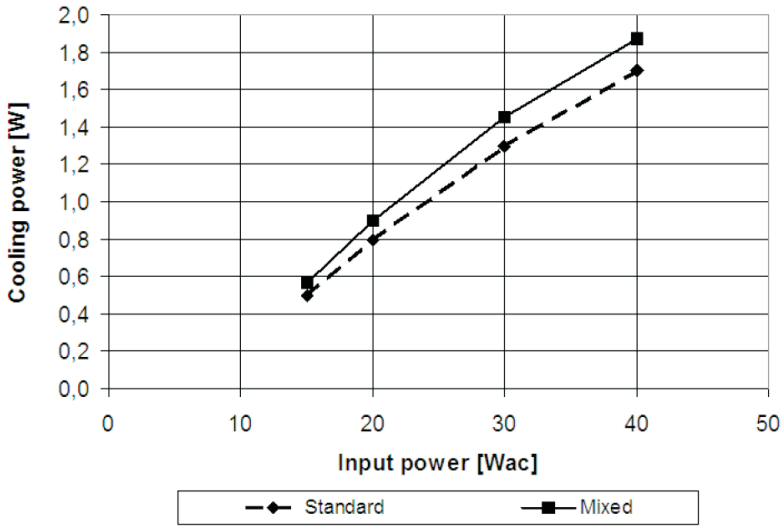

***Figure* 6.7:** *Comparison of performance of mixed with normal regenerator [3].*

varied along the regenerator. The aim is to optimize the regenerator in such a way that at each cross-section the regenerator matrix has the proper heat capacity and pressure drop characteristics to fully match the properties of the gas at that point. Figure 6.7 shows the cooling power vs input power of a pulse-tube refrigerator with mixed regenerator compared to a uniformly filled regenerator. The performance improvement with a mixed regenerator is not very significant.

Comment on extrapolation to obtain intrinsic cooldown time

In section 6.6 we have obtained the intrinsic (zero coldend mass) cooldown time of the 120 Hz cryocooler by extrapolating the cooldown time vs heat capacity ratio plot to zero heat capacity ratio. It must be noted that the error margin in this particular case is quite large about 1 minute when compared to the cooldown time of 29.7 s because the heat capacity ratio in the experiments are also (large greater than 3) significantly larger due to large cold heat exchanger flanges. Hence to compare experimental results with the analytical model we are interested in the order of cooldown time and not the exact values.

Implications of fast cooldown with increasing frequency of PTR

The predicted intrinsic (no cold end mass) cooldown time was about 32 seconds for the pulse-tube refrigerator operating at 120 Hz. This is a significant improvement compared to the 60 Hz PTR operation. The fast cooldown with higher frequency is due to a small cold end mass (regenerator, heat exchanger and pulse-tube) for the cooling power resulting in high power densities. With good design of the heat exchanger, the heat capacity ratio of the cold end mass (heat exchanger) to regenerator can be made smaller to about 1. This would result in a cooldown time at 120 Hz of about 100 s. Increasing the frequency of operation would even further reduce the cooldown time.

Bibliography

[1] S. Vanapalli, M. Lewis, G. Grossman, Z. Gan, R. Radebaugh, and H. J. M. ter Brake. Modeling and experiments on fast cooldown of a 120 Hz pulse tube cryocooler. *Advances in Cryogenic Engineering*in press, 53, 2007.

[2] R. Radebaugh, A. O'Gallagher, M. A. Lewis, and P. E. Bradley. Proposed rapid cooldown technique for pulse tube cryocoolers. *Cryocoolers*, 14:231–240, 2007.

[3] J. Mullie, G. vd Willem, P. Bruins, T. Benschop, de A. Koning, and J. Dam. Improvement of cooldown time of lsf 9599 flexure bearing sada cooler. *spie*, 2006.

[4] R. Radebaugh and A. O´ Gallagher. Regenerator operation at very high frequencies for microcryocoolers. *Advances in Cryogenic Engineering*, 51:1919, 2006.

[5] S. Vanapalli, M. Lewis, Z. Gan, P. Bradley, and R. Radebaugh. Modelling and experiments of a 120 Hz pulse tube cryocooler operating at 50 K with fast cooldown. *to be published in Cryogenics.*

[6] S. Vanapalli, M. Lewis, Z. Gan, and R. Radebaugh. 120 Hz pulse tube cryocooler for fast cooldown to 50 K. *Applied Physics Letters*, 90(072504), 2007.

[7] M. A. Lewis and R. Radebaugh. Measurement of heat conduction through bonded regenerator matrix materials. *Cryocoolers*, 12, 2003.

[8] Z. M. Zhang, S. R. Lorentz, J. P. Rice, and R. U. Datla. Measurement of thermophysical properties of polyimide and a black paint for future development of cryogenic radiometers. *Metrologia*, 35:511–515, 1998.

[9] B. C. Johnson, A. R. Kumar, and Z. M. Zhang. Heat transfer analysis and modeling of a cryogenic laser radiometer. *J. Thermophysics and Heat Transfer*, 12:575–581, 1998.

[10] W. Reese and J. E. Tucker. Thermal conductivity and specific heat of some polymers between 4.5 K and 1 K. *J. Chem. Phys.*, 43(1):105–114, 1965.

[11] W. Rawlins, R. Radebaugh and P. Bradley. Energy flows in an orifice pulse tube refrigerator. *Advances in Cryogenic Engineering*, 39:1449–1456, 1994.

Chapter 7

Investigations on microregenerators

The pressure drops of gas flows in microchannels, filled with a dense pillar matrix, were investigated with specific attention to the pillar shape. The pillars of 250 μm high and aspect ratio of about 10 were etched in silicon using an optimized Bosch deep reactive ion etching process. The pressure drop head-loss coefficient due to compression and expansion of gas at the inlet and outlet of the pillar matrix was estimated to be about 1.4 for an opening ratio of 10. Comparison of friction factor correlations for circular pillar cross-sections agreed rather good with the correlations proposed for the macroscale. Experimentally determined friction factor correlations for several pillar crosssections for Reynolds numbers in the range of 50-500 are presented. Among various pillar crosssections considered sine shaped pillars have the lowest friction factor. These pillar structures with low pressure drop but rather large wetted area can be used quite effectively as regenerative materials enabling the development of microcryocoolers.

7.1 Introduction

Over the past decade, forced flow across a matrix of micropillars has been a subject of interest in many applications such as microreactors [1], micro heat sinks [2] etc. These pillar matrices can also be used as heat exchangers, such as cross-flow heat exchanger [3] and counter-flow heat exchangers [4] for continuous flows or as regenerator [7, 9] for oscillating flows. The increase in area-to-volume ratio at the smaller scale enhances the heat transfer but it also increases the pressure drop. Numerical simulations done by Radebaugh and O'Gallagher [5] predict the necessity of small hydraulic diameter regenerators in order to efficiently operate regenerative cryocoolers at high frequency. This would enable miniaturization of the regenerator and the development of microcryocoolers for on-chip cryogenic cooling. We have experimentally demonstrated this theoretical prediction on a mesoscale cooler (see chapter 5) [6]. Conventional regenerative cryocoolers operating at 80 K use stainless steel wire screens as the regenerative material. However, currently there is a limitation on the finest screen (smallest hydraulic diameter is about 30 μm) commercially available. Ruehlich and Quack [7] have performed numerical simulations on several geometrical shapes for regenerators and concluded that there could be better alternative geometries to screens. Considering microcryocooler applications and using microsystem technology for production, we have considered investigating micropillars embedded in a flow channel for developing a microregenerator.

The main purpose of this study is to identify a pillar shape with low hydraulic (pressure drop) and thermal (heat transfer) resistance for gas flow in regenerators. As a first step in identifying the optimum geometry, pressure drop characteristics of various pillar shapes were investigated. For a regenerator, the contact area between the gas and the material should be large with low material heat conduction losses in the flow direction. In order to achieve this, the aspect ratio of pillars should be rather large which allows most of the interaction of gas to occur with the pillars and not with the supporting walls that make up the fluidic channel. Several studies on macro scale heat exchangers consisting of a bank (matrix) of circular pillars were performed and empirical correlations were summarized by Zukauskas and Ulinskas [8]. Introductory numerical simulation on various shapes of regenerators was reported by Ruehlich and Quack [7]. They conclude that the optimum geometry consisted of slim elements in a staggered (overlapping) arrangement. However, the authors have not provided the geometrical and friction factor data for all the shapes investigated. In this paper, we follow an experimental approach of measuring the pressure drop across various shapes of pillar matrices. The experimental results were compared with the macro correlations for circle shaped pillars. Rectangular channels were also considered to determine the head loss coefficient attributed to compression and expansion of gas at the inlet and outlet of the pillar matrix, for higher opening ratios.

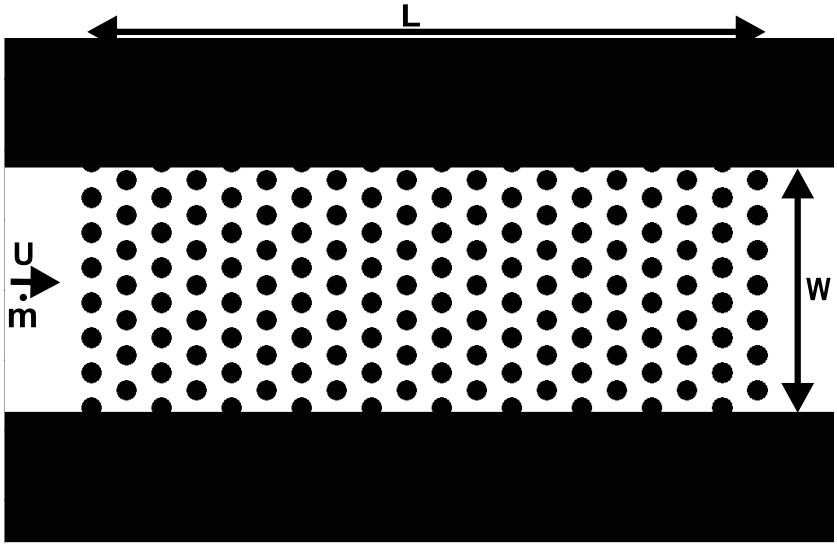

***Figure* 7.1:** *Schematic of a test sample with several pillars embedded in a micro channel. The length L is 1 mm and width W is 0.35 mm.*

7.2 Definitions and design

A schematic cross-section of a test sample is shown in figure 7.1. The pillar structures lie in a rectangular channel perpendicular to the direction of the flow. Circle, square, rhombus, elliptical, eye (formed by intersection of two circles) and sine-shaped pillar cross-sections (see table 7.1) were investigated. For the circle and square pillar cross-sections, aligned and staggered patterns (see inset in figure 7.8) were used and for the rest only staggered patterns were investigated. The cross-sectional area and the height h of all the pillar shapes was kept constant, which yields a constant pillar material volume V_m and a constant porosity of the matrix n_g which is defined as,

$$n_g = 1 - \frac{V_m}{V} \tag{7.1}$$

Where V is the total volume of the rectangular channel containing the pillars. The dimensions of all pillar cross-sections are shown in table 7.1. The porosity of the pillar matrices was 0.75. The longitudinal (in the flow direction) pitch P_L and the transverse pitch P_T (see inset in figure 7.8) was 50 μm for all the pillar cross-sections. Several definitions, for experimental correlations of pressure drop across

Geometry	Hydraulic *Diameter*, D_h	Smallest gap	a	b	Friction factor correlation, f
Circle	84.7	21.8	28.2	-	$Staggered, 70.20Re^{-0.44}$
					$Aligned, 103.50Re^{-0.64}$
Square	75.0	25.0	25.0	-	$Staggered, 96.50Re^{-0.55}$
					$Aligned, 183.02Re^{-0.90}$
Ellipse	34.4	18.6	16.3	49.0	$26.98Re^{-0.82}$
Eye	66.8	20.2	17.4	52.4	$87.10Re^{-0.80}$
Rhombus	58.3	20.5	20.5	61.0	$175.20Re^{-0.94}$
Sine	23.2	18.0	15.6	80.0	$29.65Re^{-0.94}$

***Table* 7.1:** *Geometries and corresponding friction factors considered in the investigation. All dimensions are in microns.*

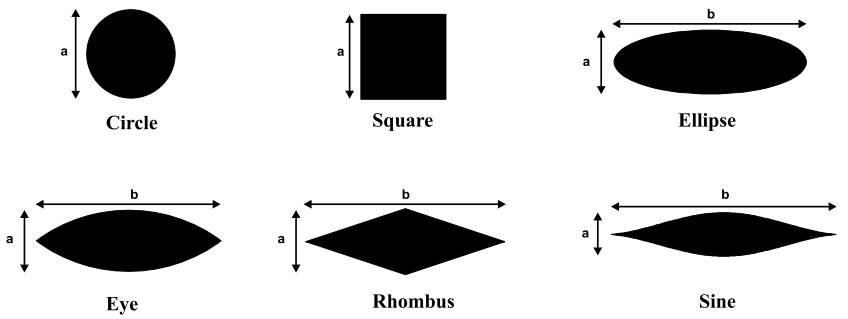

***Figure* 7.2:** *Schematic of the geometrical shapes given in table 7.1.*

a tube bundle matrix can be found in literature. The pressure drop was related to the friction factor f^* by Zukauskas and Ulinskas [8] as,

$$\Delta P = f^* N \frac{1}{2} \rho u_{max}^2 \tag{7.2}$$

Where N is the number of pillar rows, u_{max} is the maximum velocity in the matrix and ρ the density of the gas. However, in regenerator analysis [5, 7, 9] and also in numerical tools for a regenerator such as REGEN [10, 11], a definition based on the theory of porous media was used and is given by [12]

$$\Delta P = \frac{1}{2} \rho u_m^2 \left(f \frac{L}{D_h} + K \right) \tag{7.3}$$

where f is the friction factor, L is the length of the channel. The mean velocity $u_m = u/n_g$, $u = \frac{\dot{m}}{\rho A_f} A_f$ the flow area equal to the width w times the height

h of the channel. The factor K accounts for the head loss due to compression of fluid when it encounters a pillar matrix and expansion of fluid when it flows out of the pillar matrix. To investigate these losses in microscale and to compare them with mesoscale studies, a series of parallel rectangular channels was made and investigated. The hydraulic diameter D_h is defined as,

$$D_h = \frac{4n_g V}{A_w} \tag{7.4}$$

where A_w is the wetted area of the pillars. The friction factor is usually a function of the Reynolds number and is expressed as,

$$f = \frac{C}{Re^m} \tag{7.5}$$

The coefficient C is geometry dependent and the exponent m depends on the flow regime and other fluidic effects. For a laminar, fully developed, incompressible flow the exponent $m = 1$. The Reynolds number Re is given by,

$$Re = \frac{\rho u_m D_h}{\mu} \tag{7.6}$$

Here μ is the dynamic viscosity which is a function of the temperature as is the gas density. The temperature in the regenerator varies along the length L from ambient (about 300 K) at the warm end to cryogenic temperature (< 120 K) at the cold end. Hence, the Reynolds number also varies along the length of the regenerator. Micro regenerative cryocoolers that operate at high frequency (120 - 1000 Hz) have optimum gas cross-sectional areas to mass flow (equal to $1/\rho U_m$) in the range of 0.02 – 0.07 m^2.s/kg [6, 22] and for a hydraulic diameter less than 30 micron, the region of interest of Reynolds number is in the range between Re $\sim$ 50 to 250.

7.3 Experimental details

The high aspect-ratio pillar structures were etched in silicon using a customized Bosch deep reactive ion etching process. The roughness of the surface is less than about 0.3 μm. The accuracy in determining the Reynolds number and the friction factor depends on the accuracy with which the geometrical dimensions and flow parameters can be determined. All the lateral geometrical dimensions were determined using an optical digital microscope which has an accuracy of about 0.1 μm. The vertical height of the pillars was investigated under SEM with a cleaved sample of which an example is shown in figure 7.3(a). The height variation between different pillar structures is less than 5 microns (< 2 %). A silicon wafer with channels containing pillars was closed by anodically bonding a glass wafer with holes sand blasted for fluidic connection. One of the diced samples is shown in figure 7.3(b).

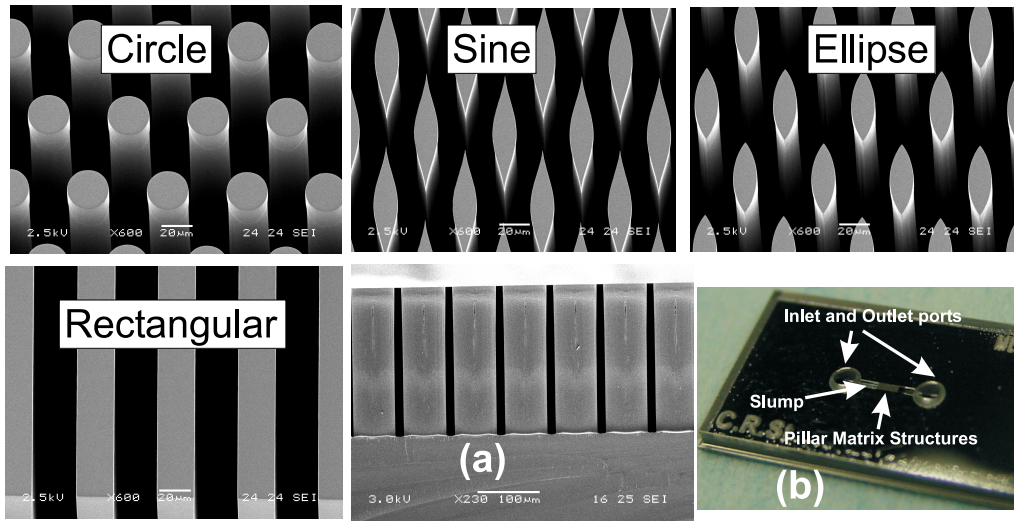

***Figure* 7.3:** *SEM pictures of the circle, sine, ellipse pillar matrix and rectangular channels. (a) Cross-section of the pillars showing vertical pillar walls. (b) Test sample showing inlet and outlet ports for fluidic connections and the pillar matrix.*

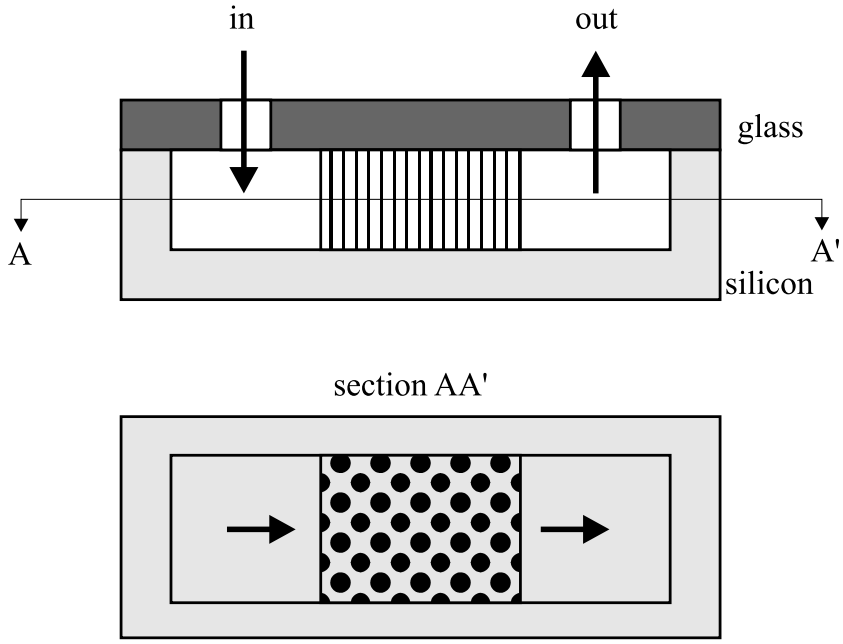

Figure 7.4: *Schematic of the cross-section of a typical sample. The gas flow directions are also marked.*

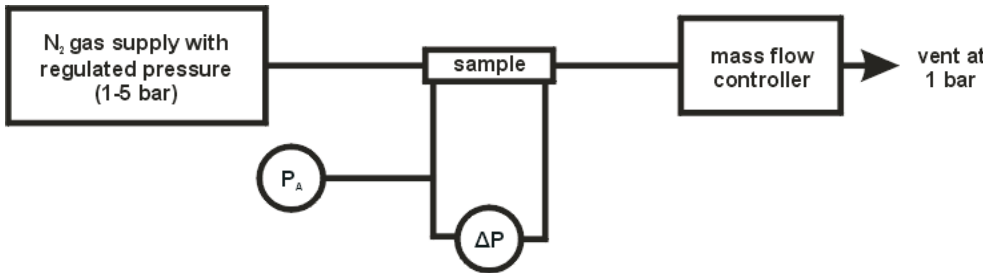

Figure 7.5: *Schematic of the experimental setup. The mass flow and the absolute pressure could be set with this configuration.*

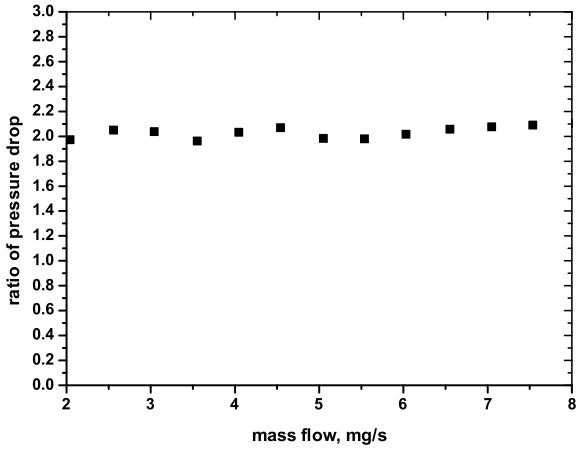

***Figure* 7.6:** *Plot of ratio of pressure drop between sample 1 and 2. The sample 2 has twice the diameter of the circle, pitch of the matrix, length and width of the sample 1. The ratio is close to 2.0 indicating very small influence of the first and last row of pillars on the flow development and most of the losses are frictional.*

The schematic of the cross-section of a sample with gas flow is shown in figure 7.4. The experimental setup is schematically shown in figure 7.5 and consists of a test sample, a nitrogen gas bottle with a pressure regulator, an absolute pressure sensor (range 7 bar, accuracy $\sim$ 1 %), a differential pressure sensor (range 1 bar, accuracy $\sim$ 1 %) and a mass flow controller (range 0-30 mg/s N2, accuracy $\sim$ 0.15%). With this configuration the absolute pressure could be adjusted with the pressure regulator and at the same time the mass flow through the valve could be adjusted with the flow controller. The experimental procedure consists of setting the mass flow to a certain value and then the inlet pressure was set with the pressure regulator. Once the flow has stabilized the pressure drop values were recorded. This procedure was repeated for different values of mass flow in the range of 1-8 mg/s. The gas properties were evaluated at ambient temperature of about 295 K. Experiments were performed on all the samples described in table 7.1 and also on rectangular channels. The absolute pressure P_0 at the inlet to the test device is kept at 5 bar.

The inlet and outlet slumps indicated in figure 7.3(b) also contribute to the pressure drop measured at the inlet and outlet ports of the sample. The total length of the slumps was about 8 mm and the hydraulic diameter was 0.5 mm (two times height of the channel). A test sample with no pillars was used to simulate

the condition of having only inlet and outlet slumps. The measured pressure drop between the inlet and outlet ports of this sample was lower than the resolution of the pressure sensor in the mass flow range of 1-8 mg/s. Hence, the contribution of the slumps to the pressure drop can be neglected. To estimate the effect of flow development in the first and last rows of pillars, a test sample (circle aligned pattern) was designed with diameter of the circle, pitch of the matrix, length and width of the channel twice that of the original one. The two samples were tested and the resulting ratio of pressure drop as a function of mass flow is shown in figure 7.6. The ratio was close to 2, showing less influence of flow development in the first and last few rows of pillars compared to the frictional losses.

7.4 Results

Rectangular microchannels were first tested to compare with theoretical predictions for macrosystems. The coefficient K in equation 7.3 is given by Blevins [13] for rectangular channels and is defined separately for the inlet K_{in} and exit K_{out}. The coefficient K is the sum of K_{in} and K_{out}. For fully developed laminar flow in rectangular channels the friction factor $f = \frac{C}{Re}$ ($m = 1$ in equation 7.5). The friction coefficient C for rectangular channels was given by [13],

$$C = \frac{64}{\frac{2}{3} + \frac{11}{24}\frac{o}{h_c}\left(2 - \frac{o}{h_c}\right)} \tag{7.7}$$

where h_c is the height of the channel and o is the width of the opening (as shown in figure 7.7). In our case the opening ratio $\frac{h_c}{o}$ is 10, so C equals 84.9. The outlet resistance coefficient K_{out} is given by [13],

$$K_{out} = \frac{2A_1}{A_2}\left(\alpha_1 - \alpha_2\frac{A_1}{A_2}\right) \tag{7.8}$$

where A_1 is the flow area of the channel and A_2 the area it expands to. The parameter α_1 and α_2 are constants, which for laminar flow are equal to 1.33 [13]. In our case $\frac{A_1}{A_2} = 0.5$ so $K_{out} = 0.665$. Data on the inlet resistance coefficient K_{in} is only available for relatively small values of opening ratio. Since the opening ratio in this study is 10 which was not available in literature, we would like to find K_{in} by fitting equation 7.3 to the experimentally measured pressure drop. In Figure 7.7, the pressure drop measurement for rectangular channels is plotted as a function of Reynolds number. The pressure drop data is fitted taking $C = 84.9$ and $K_{out} = 0.665$. The best fit is obtained when $K_{in} = 0.735$. The dependence of K_{in} on the aspect ratio is shown in the inset of figure 7.7 with data from [13] and the value from the experimental data for $\frac{h}{o} = 10$. The inlet loss coefficient, K_{in} decreases with increasing aspect ratio. The measured pressure drop through the rectangular microchannels agrees rather well to the theoretical prediction of equation 7.3. The

small dependence of K_{in} on the opening ratio between 8 and 10 allows the use of $K = 1.4$ for all other shapes of the pillar matrices.

Circle aligned and staggered patterns of pillar structures were studied in great detail for macro heat exchanger applications and several correlations were available. Zukauskas and Ulinskas [8] compiled correlations from several studies which were numerically shown to be valid for even lower Reynolds number by Ghosh Roychoudhury et al. [14]. Experiments preformed by Kosar et al. [15] on microcircular pillar structures have no good agreement with those of conventional macro correlations. However, the aspect ratio of pillars used in their study was about 2, which is quite small and the interaction of fluid with the top and bottom capping walls cannot be neglected. The aspect ratio of pillars used in this study was about 10 and the experimental results are compared with that compiled by Zukauskas and Ulinskas [8]. The friction factor f^* used by Zukauskas and Ulinkas is given by equation 7.2. The experimentally determined friction factors with Reynolds number for circle aligned and staggered patterns are shown in figure 7.8. Zukauskas and Ulinskas [8] defined relative horizontal pitch $S_L = \frac{P_L}{D}$ and a relative vertical pitch $S_T = \frac{P_T}{D}$, where D is the diameter of the circle. Both relative pitches in our study were 1.77. However, correlations from [8] were available only for relative pitch equal to 1.5 and 2.0, which are plotted in figure 7.8 for both aligned and staggered patterns. The experimentally determined friction factors lie in between the two curves proposed by Zukauskas and Ulinskas. Hence there was no significant deviation in the friction factors in the microscale.

Friction factor f and Reynolds numbers Re for all shapes in table 7.1 were determined from the experimentally measured pressure drop and mass flow and using equations 7.3 and 7.6. The coefficient K was taken to be 1.4. The correlation between friction factor and Reynolds number is given in table 7.1 and the data is plotted in figure 7.9. Circle staggered patterns which are conventionally used in macro heat exchangers have the highest friction factors among all shapes. The reason could be that circle shaped pillars have a significant variation in the cross-sectional area in the direction of the flow which results in velocity changes in flow leading to higher friction factors. Lenticular (slim) elements such as rhombus, eye, ellipse and sine shaped have relatively smaller changes in cross-sectional area compared to circle and square shaped pillars. Among the lenticular elements, sine shaped pillars have fairly uniform gap (less flow area variation) in the flow direction leading to lower velocity changes and a lower friction factor. Although, rhombus elements have uniform gaps, they have abrupt change in direction of flow at the corners of the pillar, also contributing to a higher friction factor. Elliptical shape has rounded corners and has lower friction factor compared to rhombus shape but still greater than sine shaped elements. Friction factor data from Kays and London [12] for stacked screens and rectangular channel data from Blevins [13] is also shown in figure 7.9. In the region of interest of Reynolds number between 50-250, elliptical and sine patterns have lower friction factor than screens and rectangular channels. The exponent m in equation 7.5 for sine patterns is about 0.94 and is close to 1.00

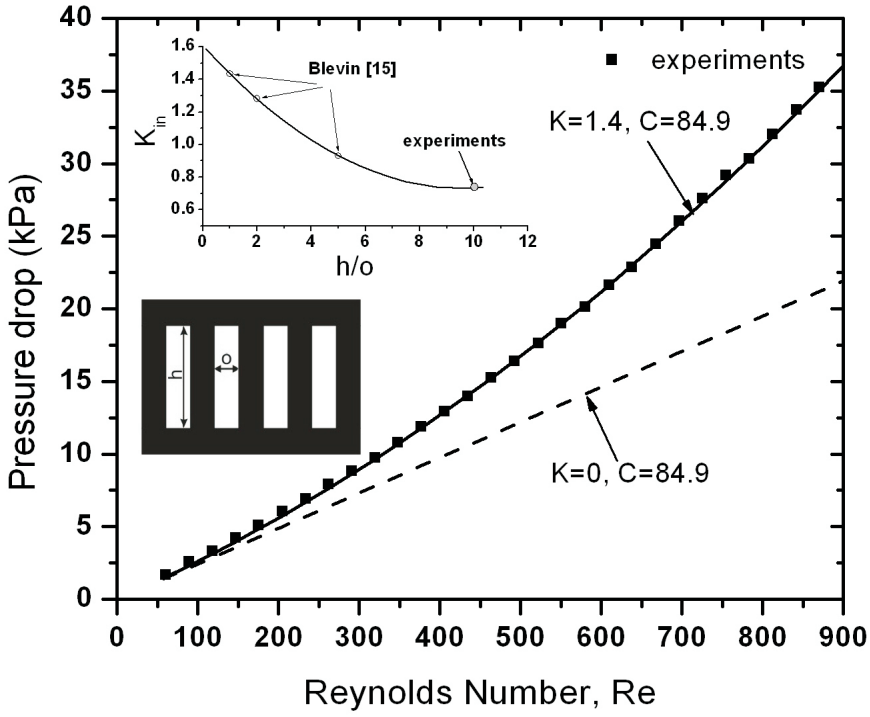

***Figure* 7.7:** *Pressure drop measurement on rectangular channels with a fit to the measurements. From this fit the inlet resistance coefficient K_{in} is determined. The theoretical pressure drop (equation 7.3) without considering the inlet and exit losses is also plotted. In the inset K_{in} is plotted for the available data [13] and from that determined from experiments for aspect ratio of 10. Cross-section of rectangular channels perpendicular to the gas flow is also shown.*

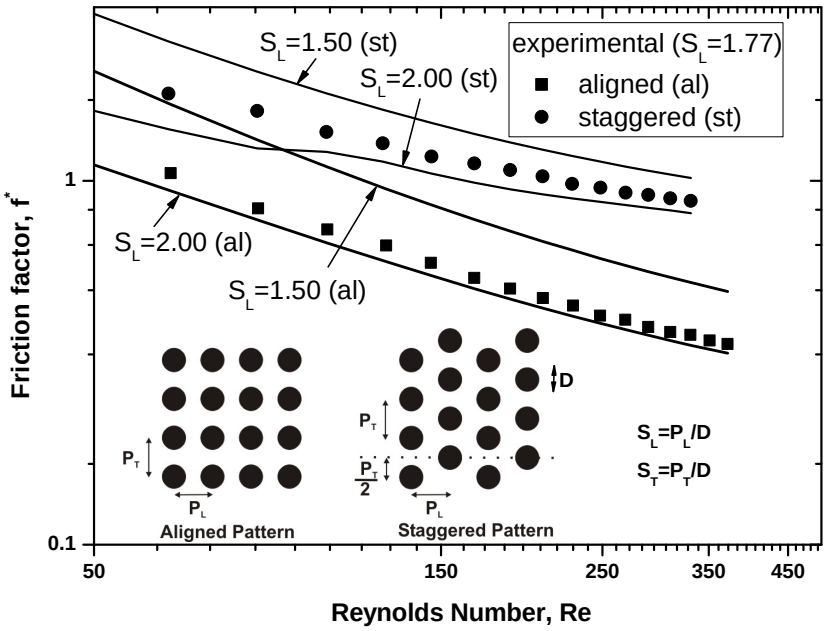

Figure 7.8: *Comparison of experimentally determined friction factors for circle aligned and staggered patterns with that compiled by Zukauskas and Ulinskas [8]. The bold line is the data from [8] for a relative pitch ratio of 1.50 and 2.00.*

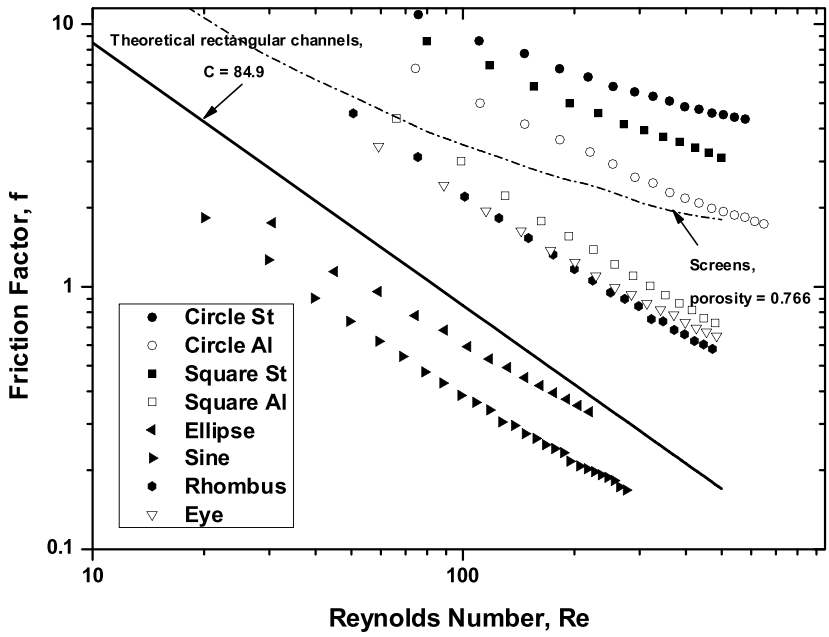

Figure 7.9: *Compiled friction factor data for all the geometrical shapes described in Table 7.1. Data for screens Kays and London [12] (Fanning friction factor used in [12] is one fourth of the friction factor f, also called Darcy-Wesisbach friction factor defined in equation 7.3) and rectangular channels [13] with porosity 0.5 is also shown. Sine and elliptical pillar cross-section has friction factors smaller than screens which was the commercially used regenerative material. The slope of friction factor data for sine cross-section is close to that of theoretical rectangular channels.*

for rectangular channels indicating a similar flow behavior.

7.5 Conclusions

We have experimentally determined the friction factors for gas flow across various pillar cross-sections in the Reynolds number between 50 and 500. The head loss coefficient K at the inlet and outlet of the rectangular channels, for an opening ratio of 10 was experimentally determined to be about 1.4. Friction factor comparison of circle shaped pillar matrices with studies in macroscale has rather good agreement, showing no significant microfluidic effects. Sine shaped pillar cross-sections have the lowest friction factor compared to all other pillar cross-sections including screens which is a conventionally used regenerator material. The low friction factor in sine shaped pillar matrices is attributed to the lower velocity changes because of almost uniform gap in the flow direction. Further study will need to be carried out to measure heat transfer coefficients of these pillar matrices to obtain an optimum geometry considering both hydraulic and thermal performance of the pillar matrix.

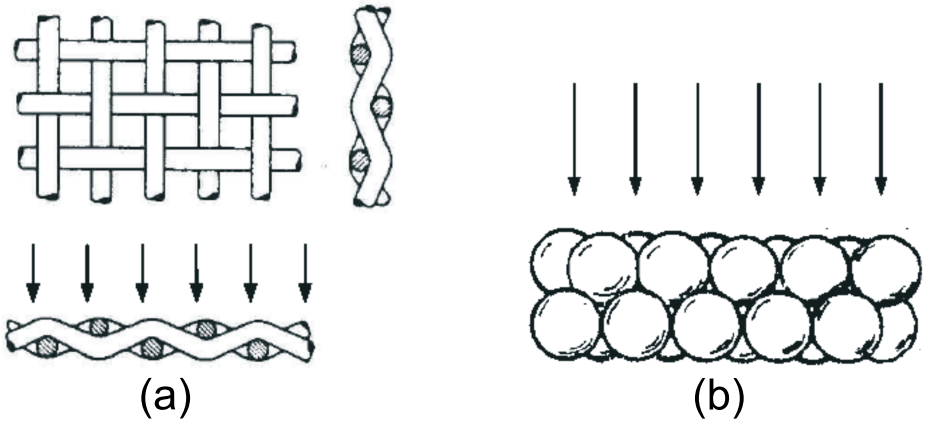

Figure* 7.10: (a) Wire mesh screen. (b) Packed sphere matrix.*

Addendum

This chapter has been adapted from the published article titled, "Pressure drop of laminar gas flow in a microchannel containing various pillar matrices". In this section more information on the regenerator materials typical used, detailed definition of hydraulic diameter and some remarks on the oscillating and steady flow correlations are given.

Regenerator materials

For optimum performance of the regenerator, the regenerator material should have high heat capacity (even at low temperatures), a lower axial heat conduction, a low dead volume, low pressure drop and good heat transfer characteristics. Some of the geometries widely used in regenerator design and new developments on regenerator materials are discussed in the following sections.

Wire screens

The woven wire mesh screen shown in figure 7.10 (a) is the most commonly used regenerator material. The screens are also used in many other applications such as filters, as insect screens, decorative mesh and for radio frequency (RF) shielding [16], leading to ready availability and low cost. The advantage of the screen is that it provides high heat transfer area with minimum pressure drop and that is available in various mesh sizes, from less than 50 mesh to 635 mesh. The mesh number indicates the number of wires per inch. Small diameter of wire (see chapter

5, section 5.2) used for weaving the screen leads to complete utilization of the thermal capacity of the material. Stainless steel and phosphor-bronze screens are typically used as regenerator material (to have low axial thermal conductivity) and copper screens are used for making heat exchangers (high thermal conductivity). The porosity n_g of the wire screen is given by,

$$n_g = 1 - \frac{\pi}{4}\left(\frac{d}{s}\right) \tag{7.9}$$

where d is the wire diameter and s is the spacing between the wires. Typical porosities of screens is about 0.60. The hydraulic diameter is given by,

$$D_h = \frac{dn_g}{1 - n_g} \tag{7.10}$$

The screen characteristics of various mesh numbers is given in section 5.2.

Sphere packing

Figure 7.10 (b) shows the schematic of sphere packing for use as regenerator material. For a perfectly packed sphere matrix of uniform particle size, the porosity is independent of the particle size and approaches a limit of 0.3 [9]. This low porosity increases the heat transfer area but also significantly increases the pressure drop. Hence, sphere packing is used only at temperature (below 50 K) where the viscosity of the helium gas is low and higher gas density. Lead spheres are typically used which has high specific heat capacity at low temperatures compared to stainless steel or phosphor bronze.

Parallel wire regenerator

Jeong et al. [17] describes a regenerator geometry which is shown in figure 7.11. It consists of wires which are wrapped in a bundle. The flow area is made up of the gap between the wires and they suggest that this particular geometry is comparable to a parallel plate geometry. The friction factor of the parallel wire regenerator was found to be about 20-30 % of that of wire mesh screen whereas the parallel plate geometry has a friction factor about a factor of 10 less than screens [7]. Also the parallel wire geometry has larger heat conduction losses compared to the wire mesh screen. Moreover, the production process described in the paper is very cumbersome.

LIGA process

The LIGA [19] micro-machining process was used by Kelly et al. [20],[21] to fabricate discs of regenerator material which were assembled to form a regenerator as shown in figure 7.12. The advantage of this process is that these discs can be made

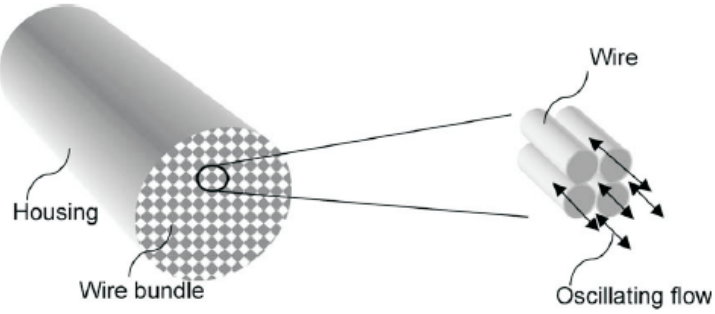

***Figure* 7.11:** *Parallel wire regenerator [17]*

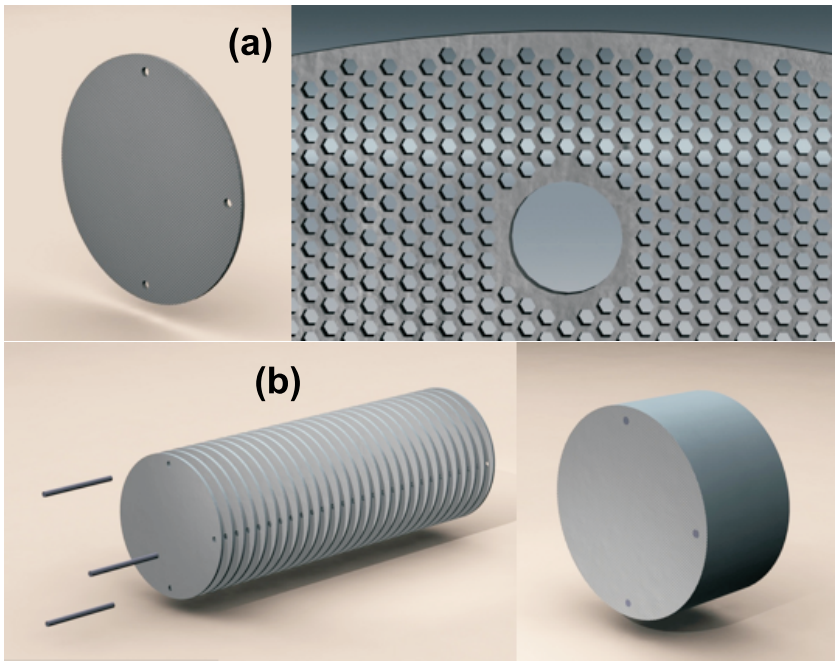

***Figure* 7.12:** *Procedure to make a regenerator with the LIGA process by Mezzo technologies [18]. (a) The required geometry is etched into a regenerator disc which serves as the building block. (b) The discs are assembled to form a regenerator.*

of a wide variety of materials such as rare-earth alloys, stainless steel, lead, copper or nickel alloys. These discs can also have a well defined porosity, channel shape and size. However, assembling these discs might be complicated. Also, similar to the parallel wire regenerator, the conduction losses along the matrix will be dominant. The authors did not present experimental results on the fabricated regenerators.

What is hydraulic diameter?

It is significant to note that the hydraulic diameter is just a definition to represent noncircular geometries with an effective diameter of the circle. The hydraulic diameter is equal to,

$$D_h = \frac{4A_g}{O} \tag{7.11}$$

where A_g is the gas cross-sectional area and O is the perimeter of the geometry. The factor 4 is introduced so that the hydraulic diameter will be equal to the diameter of the circle for a circular cross-sectional geometry. In geometries such as screens and sphere packing the definition of the hydraulic diameter is modified to include gas volume V_g and the wetted area A_w as,

$$D_h = \frac{4V_g}{A_w} \tag{7.12}$$

A particular geometry of the regenerator is completely defined once the porosity n_g and the hydraulic diameter D_h are know. Correlations of friction factor (non-dimensional representation of pressure drop) and Stanton number (non-dimensional representation of heat transfer) [12] are available for various regenerator materials which can be used to calculate the actual pressure drop and heat transfer losses.

Motivation

As mentioned above, the parallel wire regenerator and the LIGA discs are some of the efforts on the improvement of the regenerator geometry. The objective of our study is to fabricate a regenerator with the standard micromachining process steps but with better performance than wire mesh screens. A parallel wire regenerator suffers from the fact that it has high conduction loss compared to the stacked screens. The LIGA process is very complicated and it suffers also from the large conduction losses along the regenerator. To overcome these problems we propose a very simple geometry that consists of pillars etched into the material. Since the pillars are not in contact with each other the conduction heat loss decreases except along the walls. The porosity and the hydraulic diameter of the regenerator material can also be adjusted by varying the pillar dimensions and the spacing between them. Note that the samples used in pressure drop measurements were made of silicon which has a very high thermal conductivity compared to stainless steel. Regenerator made of only silicon would lead to high thermal conduction loss and hence is not

preferred. Glass is a widely used material in microsystems technology and has a low thermal conductivity, comparable to stainless steel and hence is a suitable material for regenerator fabrication.

Bibliography

[1] Im H Srinivas S, Dhingra A and Gulari E. A scalable silicon microreactor for preferential co oxidation: performance comparison with a tubular packed-bed microreactor. *Appl. Catalysis A*, 274:285–293, 2004.

[2] Y. Peles, A. Kosar, C. Mishra, C. J. Kuo, and B. Schneider. Forced convective heat transfer across a pin fin micro heat sink. *Int. J. Heat Mass Transfer*, 48:3615–3627, 2005.

[3] C. Harris, K. Kelly, Wang. Tao, A. McCandless, and S. Motakef. Fabrication, modeling, and testing of micro-cross-flow heat exchangers. *J. Microelectromech. Syst.*, 11:726–735, 2002.

[4] P. P. P. M. Lerou, G. C. F. Venhorst, C. F. Berends, T. T. Veenstra, M. Blom, J. F. Burger, H. J. M. ter Brake, and H. Rogalla. Fabrication of a micro cryogenic cold stage using MEMS-technology. *J. Micromech. Microeng.*, 10:1956–1960, 2006.

[5] R. Radebaugh and A. O´ Gallagher. Regenerator operation at very high frequencies for microcryocoolers. *Advances in cryogenic engineering*, 51:1919, 2006.

[6] S. Vanapalli, M. Lewis, Z. Gan, and R. Radebaugh. 120 Hz pulse tube cryocooler for fast cooldown to 50 K. *Applied Physics Letters*, 90(072504), 2007.

[7] I. Ruhlich and H Quack. Investigations on regenerative heat exchangers. *Cryocoolers*, 10, 1999.

[8] Zukauskas and Ulinskas. Heat transfer from tubes in cross flow. *Adv. Heat Transfer*, 8:72–160, 1989.

[9] Ackermann R A. *Cryogenic Regenerative Heat Exchangers*. New York: Plenum, 1997.

[10] J. Gary, D. E. Daney, and R. Radebaugh. A computational model for a regenerator. *Proc. 3rd cryocooler conf.:NIST special pulication*, 698:199–211, 1985.

[11] J. Gary and R. Radebaugh. An improved model for the calculation of regenerator performance (regen3.1). *Proc. 4th Interagency Meeting on Cryocooler: David Taylor Research Center Technical Report DTRC91/003*, pages 165–176, 1991.

[12] W. M Kays and A. L. London. *Compact Heat Exchangers*. New York: McGraw-Hill, 1964.

[13] R. D. Blevins. *Applied Fluid Dynamics Handbook*. Malabar, FL: Krieger, 1992.

[14] D. G. Roychoudhury, S. K. Das, and T. Sundararajan. Numerical simulation of laminar flow and heat transfer over banks of staggered cylinders. *Int. J. Numer. Methods Fluids*, 39:23–40, 2002.

[15] A. Kosar, C. Mishra, and Y. Peles. Laminar flow across a bank of low aspect ratio micro pin fins. *J. Fluids Eng.*, 127:419–430, 2005.

[16] TWP Inc. 2831 Tenth street, Berkeley, CA 94710 USA, www.twpinc.com.

[17] Nam K. and Jeong S. Development of parallel wire regenerator for cryocoolers. *Cryogenics*, 46:278–287, 2006.

[18] Mezzo Technologies, Bon Carre Business Center, 7167 Florida Blvd, Baton Rouge, LA 70806, www.mezzotech.com.

[19] H. Schift and J. Sochtig. LIGA-technology for the fabrication of positioned planar structures. *Microsystem technologies*, 4:132–134, 1998.

[20] K. Kelly, A. McCandless, and S. Motakef. LIGA-fabricated high-performance micro-channel regenerators for cryocoolers. *Cryocoolers*, 12:489–497, 2003.

[21] D. J. Guidry, J. T. Parker, A. McCandless, S. Motakef, and K. Kelly. X-ray lithography fabricated microchannel regenerators for cryocoolers. *Cryocoolers*, 13:405–409, 2004.

[22] R. Radebaugh. Microscale heat transfer at low temperatures. *Microscale Heat Transfer Fundamentals and Applications*, pages 93–124, 2005.

Chapter 8

High-frequency pressure oscillator

Micro miniature pulse-tube cryocoolers should operate at a frequency of an order higher than the conventional macro ones because the pulse-tube cryocooler operating frequency scales inversely with the square of the pulse-tube diameter. Piezoelectric actuators operate efficiently at high frequencies and have high power density making them good candidates as drivers for high frequency pressure oscillators. The pressure oscillator described in this work consists of a membrane driven by a piezoelectric actuator. A pressure ratio of about 1.11 was achieved with a filling pressure of 2.5 MPa and compression volume of about 22.6 mm^3 when operating the actuator with a peak-to-peak sinusoidal voltage of 100 V at a frequency of 1 kHz. The electrical power input was about 2.73 W. A high pressure ratio and low electrical input power at high frequencies would herald development of micro miniature cryocoolers.

8.1 Introduction

With emerging superconducting devices [1–3], infrared sensors for atmospheric studies [4, 5], terahertz imaging sensors for military applications [6] and other electronic devices in Micro-Electro-Mechanical-Systems (MEMS), the development of efficient and small cryocoolers to cool these devices is imperative. The existing cryocoolers are rather bulky and expensive. A cryocooler fabricated with microsystem technology is an ideal solution to integrate these devices directly on the cryocooler, enabling on-chip cryogenic devices. For achieving cryogenic temperatures below 100 K, gas compression cycles are the viable options as it was shown that the lowest temperature ever achieved with optical coolers was about 220 K [7]. Multiple stages are required for thermoelectric coolers and these have very low performance below 200 K [8]. Magnetic refrigerators operating from room temperature are rather in-

efficient [9]. Among the gas cycles reviewed by Radebaugh [10], the Joule-Thomson cycle which is a recuperative type and the pulse tube cryocooler which is a regenerative type are of interest to miniaturization because of no moving parts in the cold end. Figure 8.1 (a) shows the schematic of a closed cycle Joule-Thomson cycle. In this cycle there is a steady flow of refrigerant around the loop brought about by a reciprocating compressor with inlet and outlet valves. A pulse-tube cryocooler (see figure 8.1 (b)) operates with oscillating pressure and oscillating flow. A high pressure ratio of about 16:1 [11] is required in the Joule-Thomson cycle where as pressure ratios of about 1.15 to 1.3 are common in pulse-tube cryocoolers [12].

The schematic of a pulse-tube cryocooler is shown in figure 8.1 (b). The inertance tube causes the flow to oscillate with the pressure in the right phase relationship. The pulse-tube cryocooler requires adiabatic (no heat transfer between gas and the walls) compression and expansion in the pulse-tube component to produce an oscillating temperature in the gas. As heat transfer between the gas and the pulse-tube wall increases, the amplitude of the temperature oscillation decreases and the efficiency of the process decreases. For the process to be nearly adiabatic, the tube radius must be large compared to the thermal penetration depth δ_{th} in the helium gas. The thermal penetration depth varies with the frequency of operation f as $\delta_{th} \propto f^{-1/2}$ [13]. Conventional pulse-tube cryocoolers operate at about 60 Hz, leading to a lower size limit for efficient operation of such a cryocooler. Increasing the frequency to about 1 kHz, the tube radius of the pulse-tube can be made considerably smaller, allowing the miniaturization of the cryocooler. Design rules for efficient high frequency operation of a regenerator was reported by Radebaugh et al. [13] which, was experimentally verified on a macroscale by Vanapalli et al. [14]. The next step is to realize an efficient high frequency pressure oscillator to drive the micro cold stage.

We have evaluated various mechanisms for actuating such a high frequency pressure oscillator: electrostatic, thermal, electromagnetic, and piezoelectric. Electrostatic actuators provide very low force and stroke and hence was eliminated from consideration. Thermal actuators have very low thermal-to-mechanical conversion efficiency and hence are not desirable. Electromagnetic actuation is widely used in commercial refrigerators. The force exerted by the electromagnetic actuator is proportional to the current flowing in the coil. In scaling down the actuator the Joule heating of the coil could be a major concern for high power density. Piezoelectric actuators have high power density, can operate at high frequencies, have good electrical-to-mechanical efficiency and potentially have a very long operating life. However, they provide a very low stroke, but this is not a severe drawback because of the low dead volume in micro cryocoolers. Because of excellent characteristics of piezoelectric actuators, this option was selected as a driver in the pressure oscillator.

The configuration of pressure oscillators are generally of two types: one is a piston moving in a cylinder and second is deflection of a membrane. A free-piston compressor of typical pulse-tube cryocooler operates with a small diameter piston

and a long stroke [15]. The piston is suspended by springs combined with a clearance seal between the piston and the cylinder wall. The length is usually long compared to the diameter of the piston to reduce leakage loses. In contrast, membrane compressors have large diameter and a short stroke to limit the bending and tension stresses in the membrane. The membrane design was chosen for the pressure oscillator because it fits to the limited stroke capability of piezoelectric actuators.

8.2 Design

Figure 8.1 (c) shows the schematic of the trace of pressure in a pulse-tube refrigerator. The sinusoidal pressure amplitude is represented by P_1 and the average pressure by P_0. The pressure ratio P_r, which is the ratio of the maximum to the minimum pressure over one cycle and is given by

$$P_r = \frac{P_0 + P_1}{P_0 - P_1} \tag{8.1}$$

The gross refrigeration power $\dot{Q}_r$ of a pulse-tube refrigerator is equal to the acoustic or PV power at the cold end of the regenerator and is given by,

$$\dot{Q}_r = \dot{W}_{PV} = \frac{1}{2} P_1 \dot{V}_{1,c} \cos\phi \tag{8.2}$$

where $\dot{V}_{1,c}$ is the amplitude of the sinusoidal volume flow rate at the cold end of the regenerator, and ϕ is the phase by which the volume flow leads the pressure. The volume flow rate $\dot{V}_{1,c}$ is related to the volume amplitude at the cold end $V_{1,c}$ as,

$$\dot{V}_{1,c} = j2\pi f V_{1,c} \tag{8.3}$$

where j is the imaginary unit and f is the frequency of operation. The swept volume varies proportionally with temperature in the regenerator. The swept volume at the warm end of the regenerator $V_{1,w}$ is related to the swept volume at the cold end as,

$$\dot{V}_{1,w} = \frac{T_w}{T_c} \dot{V}_{1,c} \tag{8.4}$$

where T_w and T_c are the temperatures at the warm and cold ends of the regenerator, respectively. The swept volume of the compressor should be larger than $V_{1,w}$ to account for dead volume losses in the interconnects.

The pressure wave in the compression volume V_c is created by the oscillating motion of the membrane. The generated pressure is a function of the temperature T_0 and the filling pressure P_0. The variation of temperature is rather small and can be neglected. In Figure 8.2 the deflection profile of the membrane under a load F is shown; $w(r)$ is the deflection of the membrane at position r and $\tau(r)$ is the

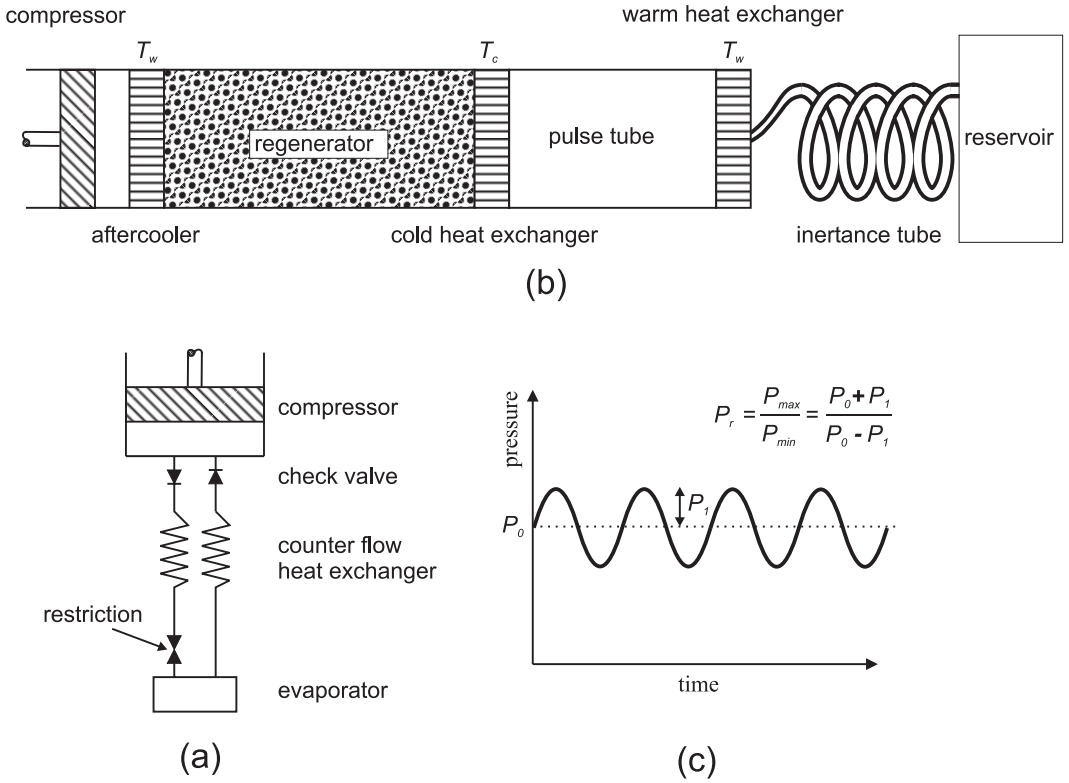

Figure* 8.1: (a) Schematic representation of Joule-Thomson refrigerator. The steady flow of refrigerant in the cooler is provided by the compressor and the check valves. (b) Schematic of the pulse-tube refrigerator with an inertance tube. This cycle operates with an oscillating pressure and flow. (c) Schematic of the sinusoidal pressure variation in the pulse-tube refrigerator showing the pressure amplitude P_1 and the average pressure P_0. The pressure ratio is calculated from P_1 and P_0*

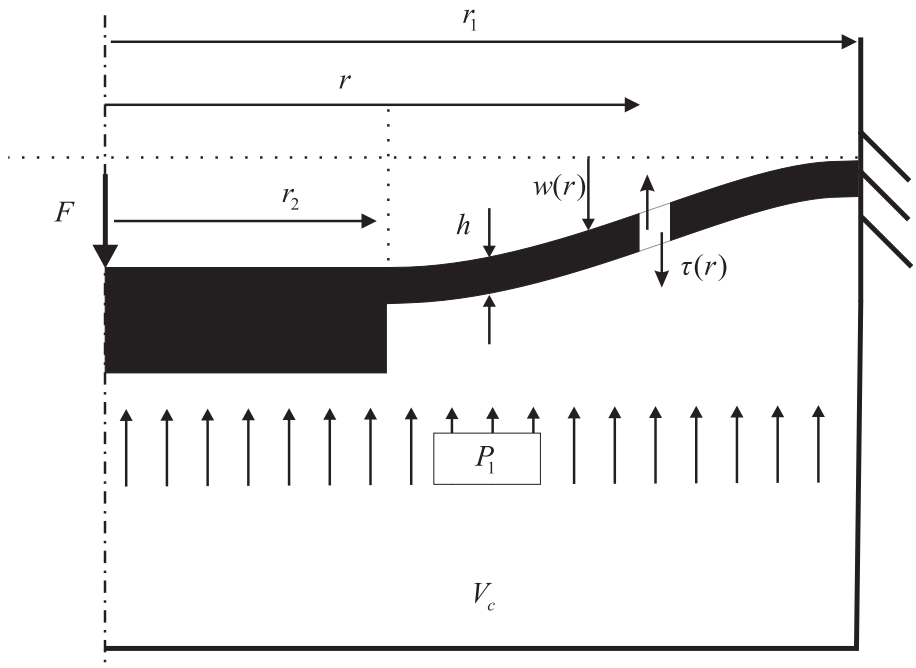

Figure* 8.2: Cross-section of the deflection profile of the membrane subjected to a force by the actuator and the subsequent generation of differential pressure in the compression volume.*

shear force per unit length at position r. The center of the membrane has a rigid part of radius r_2, which is attached to the actuator. The membrane also has two laser drilled holes (not shown in figure 8.2) for static pressure equalization across the membrane. The dynamic pressure P_1 acting on the membrane gives a force balance,

$$2\pi r\tau\left(r\right) = F - P_1 \cdot \pi r^2 \tag{8.5}$$

The differential equation for the deflection of the membrane is derived by using the linear elasticity theory for plates [16]

$$\frac{d}{dr}\left(\frac{1}{r}\frac{d}{dr}\left(r\frac{dw\left(r\right)}{dr}\right)\right) = \frac{\tau\left(r\right)}{D} \tag{8.6}$$

where D is the flexural rigidity of the membrane given by,

$$D = \frac{Eh^3}{12\left(1-\nu^2\right)} \tag{8.7}$$

In equation 8.7, E is the Young's Modulus, ν is Poisson's ratio and h is the thickness of the membrane. The general solution of equations 8.5 and 8.6 is,

$$w(r) = -\frac{r^4}{64D}P_1 + \left(\frac{r^2}{8\pi D}\ln(r)\right)F + C_1 + C_2 r^2 + C_3 \ln(r) \tag{8.8}$$

The constants C_1,C_2 and C_3 are determined by applying the following boundary conditions,

$$w(r_1) = 0; \frac{dw(r_1)}{dr} = 0; \frac{dw(r_2)}{dr} = 0 \tag{8.9}$$

The volume of the gas ΔV displaced by the membrane is given by,

$$\Delta V = \pi r_2^2 w(0) + \int_{r_2}^{r_1} 2\pi r w(r)\, dr \tag{8.10}$$

which is equal to the volume change corresponding to the dynamic pressure P_1 that can be obtained from the ideal gas law for constant temperature conditions;

$$\Delta V = -\frac{V_c}{P_0}P_1 \tag{8.11}$$

where P_0 is the average pressure in the compression volume.

The maximum force generated by the piezo actuator with stiffness k_p, on a load with stiffness k_l is given by,

$$F = k_p \cdot \Delta L_0 \frac{k_l}{k_p + k_l} \tag{8.12}$$

where ΔL_0 is the maximum no-load displacement of the actuator. The force F generated by the piezo actuator depends on the no-load displacement ΔL_0 at a certain frequency f and voltage applied V for a known load and piezo stiffness. The load stiffness k_l is given by,

$$k_l = k_m + k_g \tag{8.13}$$

where k_m is the membrane stiffness and k_g is the stiffness of the gas in the compression volume V_c. Assuming isothermal conditions in the compression volume V_c, the gas spring stiffness k_g is given by [17],

$$k_g = \frac{P_0 A_c^2}{V_c} \tag{8.14}$$

where A_c is the membrane cross-sectional area.

In the present study, we aim at cooling a high-temperature superconducting device at 80 K. Since such a device is non-dissipating, a net cooling power of 10 mW is adequate [18]. With the refrigerator operating at $f = 1$ kHz, $T_w = 300$ K,

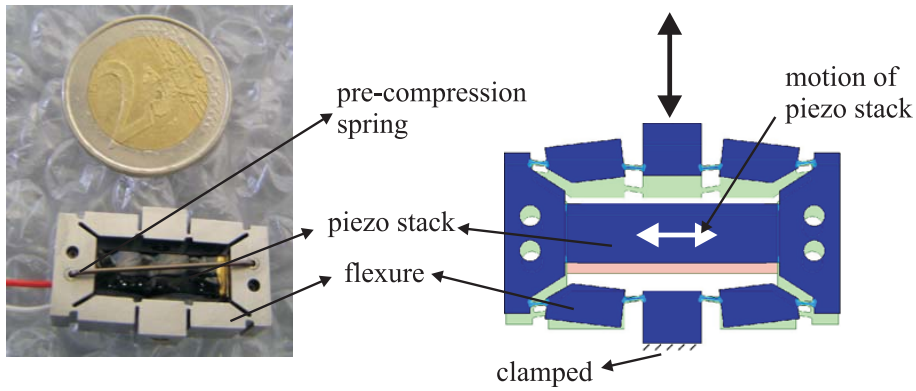

***Figure* 8.3:** *The piezoactuator used in the experiments. The motion of the piezo stack is amplified by the flexure. A two Euro coin (25.75 mm) is shown for size comparison.*

T_c = 80 K, $\phi = -30^0$, P_r = 1.3, P_0 = 2.5 MPa, the $V_{1,w}$ is equal to 0.085 mm^3 (equations 8.2, 8.3 and 8.4), for a gross refrigeration power of 20 mW (assuming losses to be about 10 mW). The compressed volume V_c is equal to 22.6 mm^3 and is larger than $V_{1,w}$ to simulate a load attached to the compressor. The dimensions of the membrane are given in table 8.1. The relationship between the force F and dynamic pressure P_1 is derived from equations 8.8 and 8.11 which, for the membrane dimensions given in table 8.1, with an average pressure P_0 = 2.5 MPa results in $P_1\,(bar) = 0.11 \cdot F\,(N)$. The piezo actuator used in the experiments is shown in figure 8.3. The piezo stack elongates in the axial direction and the stainless steel flexure attached to it amplifies the stroke into a perpendicular motion. The specifications of the actuator are given in table 8.1.

The no-load displacement of the piezo was measured with a laser vibrometer with a resolution of 0.1 μm which, works on the Mach-Zender interferometer principle. Figure 8.4 shows the amplitude of the displacement of the piezo actuator with voltage for several frequencies of operation. For a peak to peak voltage V_{pp} of 90 V the displacement was about 30 μm at a frequency of 500 Hz. With the same measuring technique, the no-load resonance frequency was determined as 1.43 kHz.

The layout drawing of the pressure oscillator is shown in figure 8.5. The piezo actuator was clamped to the cap of the oscillator. The membrane was laser cut from a stainless steel sheet of nominal thickness equal to 50 μm. Two holes of diameter less than about 10 μm were laser drilled on the membrane for filling the compression chamber with high pressure gas. The holes were small enough to be leak tight under dynamic operation. A screw was laser welded on to the membrane.

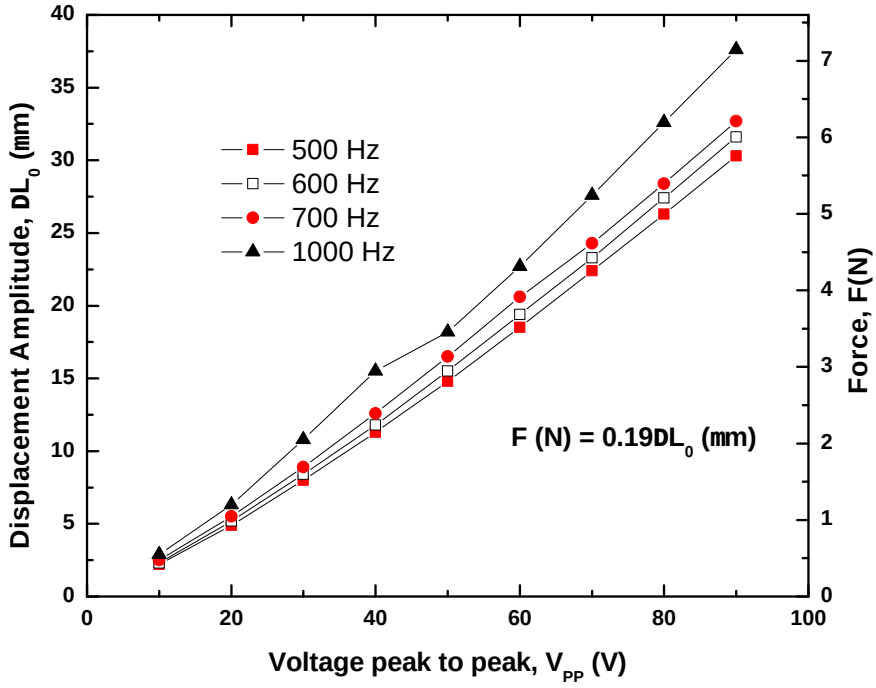

***Figure* 8.4:** *The no-load displacement amplitude of the piezo actuator with voltage for several frequencies of operation measured with a laser vibrometer.*

Table* 8.1: Specifications of the piezoelectric actuator and the dimensions of the membrane and the compression volume.*

Parameter	Value
Stroke	145 μm
Stiffness	1.0 N/μm
Unloaded Resonant Frequency	1400 Hz
Dimensions	$17 \times 28.5 \times 12$ mm
Mass	22 g
Membrane	
r_1	6.0 mm
r_2	3.0 mm
h	50 μm
Compression space	
V_c	22.6 mm^3

Fluidic and electrical feed throughs were provided on the cap of the oscillator. The bottom flange clamps the membrane to the housing of the oscillator. A pressure tap on the flange was provided to measure the oscillating pressure generated in the compression volume V_c.

The stiffness of the membrane was obtained from equation 8.8 with $P_1 = 0$. The calculated stiffness of the membrane k_m was about 0.145 N/μm. For an average pressure P_0 equal to 2.5 MPa the gas spring stiffness k_g is 0.088 N/μm. As a result, the load stiffness k_l is equal to 0.233 N/μm.

8.3 Experiments

The pressure oscillator was filled with nitrogen gas from a pressure-regulated gas bottle. The pressure sensor located on the filling line close to the pressure oscillator measures the filling pressure in the system. A PT100 temperature sensor is glued on the piezo stack to monitor its temperature. The current i_e flowing into the piezo stack was determined from the voltage across a calibrated resistor. From the voltage V_e across the piezo and the current i_e, the electrical power $\dot{W}_e$ supplied to the piezo actuator is given by,

$$\dot{W}_e = \frac{1}{2}|V_e||i_e|\cos\theta_e \tag{8.15}$$

where θ_e is the phase angle between voltage and current. The dynamic pressure P_1 generated in the compression space of the oscillator was measured by a pressure sensor with a range of 0-3.5 MPa, sensititivity of 22.0 mV/MPa and a resolution of about 1 mbar. A lock-in amplifier was used to read the oscillating pressure.

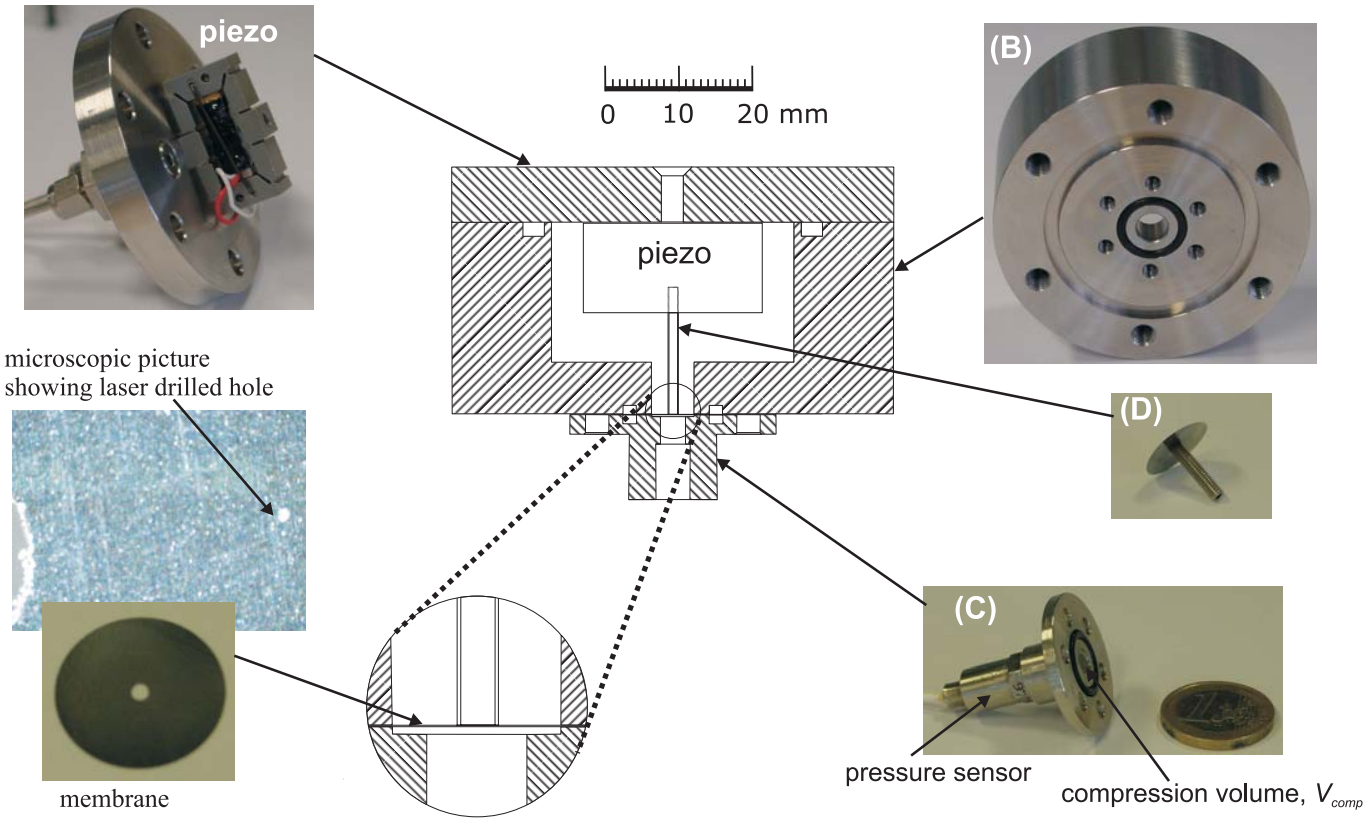

***Figure* 8.5:** *The layout of the pressure oscillator showing various components. The stainless steel membrane which was laser cut from a sheet is also shown. Two holes of diameter about 10 μm were laser drilled, one of the hole is shown in the microscopic picture of the membrane.*

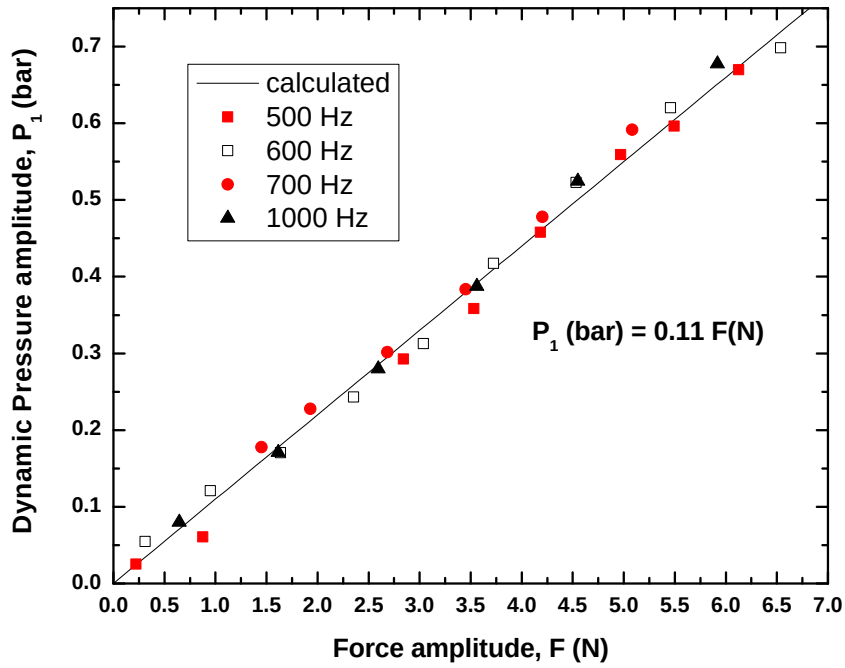

***Figure* 8.6:** *Calculated and experimentally generated oscillating pressure amplitude in the compression volume to the force exerted by the piezo actuator for several frequencies. The force is calculated from the voltage applied, the stiffness of the load and the no-load displacement in figure 8.4.*

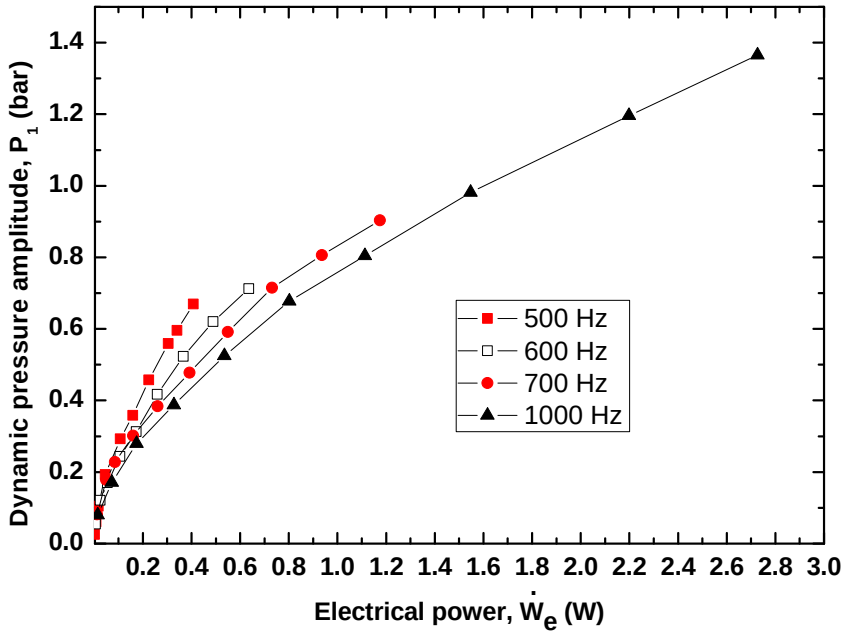

***Figure* 8.7:** *Measured pressure amplitude with electrical power supplied to the piezo actuator for several frequencies at a filling pressure of 2.5 MPa.*

Experiments were performed with a filling pressure P_0 of 2.5 MPa and varying the amplitude and frequency of the applied voltage. Fig. 8.6 shows the amplitude P_1 for several frequencies of operation. The force was calculated from equation 8.12 with the no-load displacement ΔL_0 obtained from figure 8.4 for an applied voltage on the piezo actuator. The calculated pressure with force as described in section 8.2 is also plotted in the same figure. The measured pressure data agrees rather good with the theoretical model.

Fig 8.7 shows the measured dynamic pressure amplitude P_1 as a function of the measured electrical power for several frequencies and a filling pressure P_0 of 2.5 MPa. For an applied peak-to-peak sinusoidal voltage of 100 V the measured pressure ratio P_r at a frequency of 1 kHz was about 1.11 and the measured electrical power input was about 2.73 W. Figure 8.8 shows the calculated work amplitude

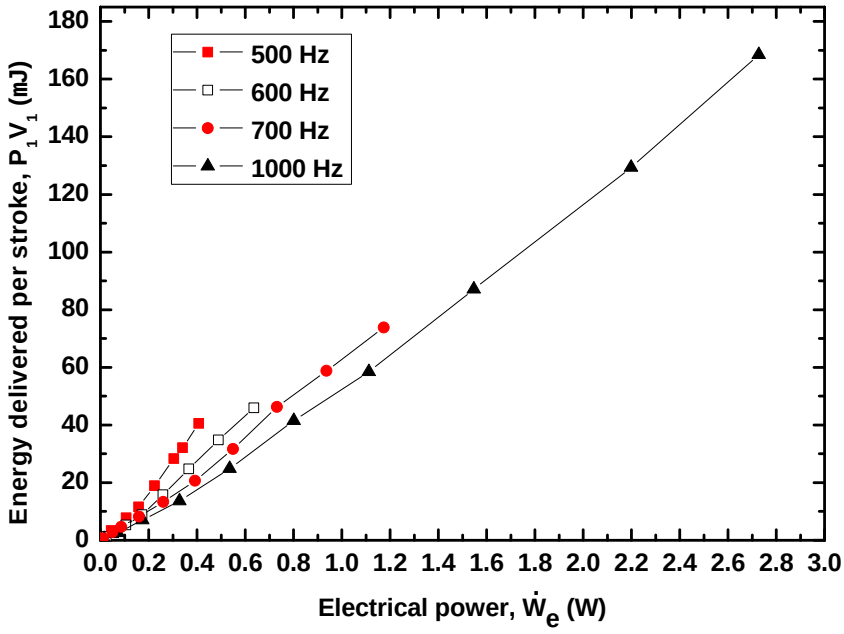

Figure* 8.8: Work done per stroke by the piezo actuator with electrical power, for several frequencies at a filling pressure of 2.5 MPa.*

P_1V_1 of the piezoactuator as a function of measured electrical power for several frequencies and a filling pressure P_0 of 2.5 MPa. The PV work amplitude (P_1V_1), produced at an operating frequency of 1 kHz was about 0.17 mJ for an electrical input of 2.73 W when operating the piezoelectric actuator at 100 V peak-to-peak sinusoidal voltage. The PV power transmitted for the above conditions is about 0.54 W (using equation 3.5 and 8.3 with $\phi = 0$) which gives an efficiency of 20 %.

8.4 Discussion and Conclusion

A pressure oscillator operating at high frequency for driving micro pulse cryocoolers was presented. Piezoelectric actuators produce large forces but low stroke and can operate over wide range of frequencies and hence are ideal drivers for low dead-volume MEMS cryocoolers. The theoretical model for deflection of membranes agrees well with experimental data. A pressure ratio of about 1.11 at a frequency of 1 kHz was achieved when operating the piezo with a peak-to-peak sinusoidal voltage of 100 V. For these conditions, the work produced by the piezo actuator was about 0.17 mJ for an electrical input power of 2.73 W which gives an efficiency of 20 %. Higher pressure ratios can be achieved by driving the actuator at higher voltages. This pressure oscillator can be directly coupled to a micro pulse-tube cold head resulting in the development of new generation of micro cryocoolers. The development of high frequency pressure oscillators would pave the way to a new generation of on-chip micro pulse-tube cryocoolers.

Increasing the load stiffness k_l, by increasing the thickness of the membrane and decreasing the compression volume V_c would result in large force exerted by the piezo. The large force, would provide high pressure ratio P_r, but low swept volume. Coupling the compression chamber with low void volume check valves as shown in figure 8.1 (a), a steady high pressure flow can be generated. Operating the actuator at higher frequencies will provide sufficient high pressure flow to power a micro Joule Thomson cold tip [11].

In a classical (ideal) Stirling refrigerator the compression, expansion and displacement of the gas is often represented by discontinuous piston and displacer motions [19]. The fast response time of piezoelectric actuators would allow exploring non-sinusoidal operation of Stirling cycle which was not possible with conventional electromagnetic pressure oscillators. Further research must be carried out to utilize piezoelectric actuators to realize new variants of regenerative gas cycles.

Bibliography

[1] C. H. Downey. *Cryogenics*, **31**,48 (1991).

[2] A. E. Mahdi and D.J. Mapps. *Sensors and Actuators A: Physical*, **81**,367 (2000).

[3] H. Nagata, J. Kobayashi, H. Matsuo, M. Akiba, and M. Fujiwara. *Nuclear instruments and methods in physics research section A- accelerators spectrometers detectors and associated equipment*, **559**,823 (2006).

[4] A. Rogalski. *Journal of Applied Physics*, **93**,4355 (2003).

[5] M. Jhabvala. *Sensors and Actuators A: Physical*, **42**,363 (2001).

[6] P. H. Siegel. *IEEE Transactions on Microwave Theory and Techniques*, **50**,910 (2002).

[7] T. R. Gosnell. *Optics Letters*, **24**,1041 (1999).

[8] MELCOR corp. 1040 Spruce Str., Trenton, NJ 08648, USA, http://www.melcor.com.

[9] R. Radebaugh. *G. Walker, Cryocoolers part 2:Applications*, pages 129–175 (Plenum Press, New York 1983).

[10] R. Radebaugh. *IEEE proceedings on electronic and large scale applications of superconductivity*, **92**,1719 (2004).

[11] P. P. P. M. Lerou, G. C. F. Venhorst, C. F. Berends, T. T. Veenstra, M. Blom, J. F. Burger, H. J. M. ter Brake, and H. Rogalla. *Journal of Micromechanics and Microengineering*, **16**,1919 (2006).

[12] R. Radebaugh. *Pulse tube cryocoolers*, pages 415–434. (edited by S. Kakac, H. Smirnov, and M.R. Avelino, Kluwer academic publishers, Dordrecht, The Netherlands. 2003)

[13] R. Radebaugh and A. O´ Gallagher. *Advances in cryogenic engineering*, **51**,1919 (2006).

[14] S. Vanapalli, M. Lewis, Z. Gan, and R. Radebaugh. *Applied Physics Letters*, **90**, (2007).

[15] E. D. Marquardt, R. Radebaugh and p. Kittel. *In: Seventh International Cryocooler Conference Proceedings, Air Force Phillips Laboratory Report PL-CP-93-1001. Kirtland Air Force Base, NM*, 783, (1993).

[16] S. P. Timoshenko and S. Woinowsky-Krieger. *Theory of Plates and Shells*, chapter 2 (McGraw Hill Book Company, 1959).

[17] G. W. Swift. *Thermoacoustics*, pages 61–63 (Acoustical Society of America, through American Institute of Physics 2002).

[18] P. P. P. M. Lerou, S. Vanapalli, H. V. Jansen, J. F. Burger, T. T. Veenstra, G. C. F. Venhorst, H. J. Holland, M. Elwenspoek, H. J. M. ter Brake, and H. Rogalla. *Advances in cryogenic engineering: Transactions of the Cryogenic Engineering Conference - CEC*, **51**,977 (2006).

[19] G. Walker. *Cryocoolers, Part 1: Fundamentals*, (Plenum Press, New York, 1983).

Chapter 9

Conclusions and recommendations

This thesis set out to investigate miniaturization aspects of regenerative thermodynamic cycles with an aim to develop micro-miniature cryocoolers for on-chip cryogenic cooling of non-dissipating high T_c superconductors. Regenerative cryocoolers operate with oscillating pressure and flow. A pulse-tube cryocooler is a particular type of regenerative cryocooler without any moving parts at the cold side, making it a good candidate for miniaturization. In chapter 2 section 2.4 we have formulated several questions concerning the miniaturization of pulse-tube cryocoolers which will be answered here:

(a) What are the limitations of scaling down of pulse-tube cryocoolers?

A pulse-tube cryocooler requires adiabatic (no heat transfer between gas and the tube walls) compression and expansion in the pulse-tube component to produce an oscillating temperature in the gas. As heat transfer between the gas and the pulse-tube wall increases, the amplitude of the temperature oscillation decreases and the efficiency of the process decreases. For the process to be nearly adiabatic, the tube radius must be large compared to the thermal penetration depth δ_{th} in the gas. The thermal penetration depth varies with the frequency of operation f as $1/\sqrt{f}$. Conventional pulse-tube cryocoolers operate at about 60 Hz, leading to a lower size limit for operation of such a cryocooler. Increasing the frequency to about 1 kHz, the tube radius of the pulse-tube can be made considerably smaller, allowing the miniaturization of the pulse-tube cryocooler. Further, the size of conventional pulse-tube cryocoolers for a fixed refrigeration power could also be reduced at high

frequencies which, is important for many applications.

However, simply increasing the operating frequency will increase the buffered mass in the void volume of the regenerator, resulting in an increase in the average mass flow in the regenerator. The losses, both pressure drop and heat transfer are proportional to mass flow and hence increases with frequency, reducing the efficiency of the cryocooler at high frequencies. The buffered flow in the regenerator at higher frequencies can be reduced by decreasing the gas volume in the regenerator. Parametric analysis performed in this thesis (see chapter 3) indicates that the gas volume can be reduced with an increase in average pressure. Decreasing the gas volume would decrease the regenerator heat transfer area for a fixed porosity. For a certain material volume, the heat transfer area can be increased by choosing a smaller hydraulic diameter regenerator material. Hence, to efficiently operate the regenerator at high frequencies, the average pressure should be increased and a smaller hydraulic diameter regenerator material should be used.

A 120 Hz pulse-tube cryocooler was designed and built. A no-load temperature of 50 K was achieved when operating with an average pressure of 3.5 MPa. This is for the first time such low temperatures could be achieved for operating frequencies above 100 Hz. REGEN3.2 numerical model was used to optimize the dimensions of the regenerator, which used #635 mesh stainless steel screen. The length and diameter of the regenerator was about 30 mm and 10 mm respectively. The net refrigeration power at 80 K was 3.37 W. The input acoustic power at the aftercooler was 66.0 W, which yields a cooler efficiency of 14.0 % of Carnot with an aftercooler temperature of 298.7 K. The background loss consisting of heat conduction and radiation, was about 0.93 W at 120 K. The successful operation of 120 Hz pulse-tube cryocooler at cryogenic temperatures gives us confidence on the design rules and the model for predicting high frequency regenerator operation.

The 120 Hz pulse-tube cryocooler cooled from 285 K to 80 K in about 5.5 minutes, even though the additional thermal mass at the cold end due to the flanges, screws, heater and thermometer was 4.2 times that of the regenerator. This fast cooldown is about two to four times faster than that of typical pulse-tube cryocoolers and is attractive to many applications. This was studied in detail by attaching various thermal masses to the cold end of the cryocooler and measuring the cooldown times to 80 K. An analytical model was developed to compare with experiments. The model predicts a zero cold-end mass cooldown time to 80 K of 31.5 s. With an optimized design of cold heat exchanger, the heat capacity ratio of the cold end mass to regenerator can be reduced to about 1 which, gives a cooldown time of about 100 s. Further reduction in cooldown time can be obtained by increasing the frequency of operation of the cryocooler.

recommendations

Besides proving the theory of efficient high frequency operation of pulse-tube cryocooler (hence the confidence gained to design a micro pulse-tube), several ad-

vantages of the 120 Hz pulse-tube cryocooler have an impact on the existing commercial cryocoolers. For a certain refrigeration power, the high frequency operation of the cryocooler reduces the size of the cooler and also allows shorter cooldown time which is advantageous for portable applications. However, existing commercial linear flexure pressure oscillators are designed for 60 Hz operation. Further research should be carried out in optimizing the linear flexure pressure oscillators to operate in resonance at 120 Hz.

As discussed in chapter 4 section 4.3.4 for micro pulse cryocoolers, the inertance tube and reservoir combination cannot produce sufficient phase shift. Hence in this case, a double inlet orifice pulse-tube [1] configuration might have to be used. Another solution is to use a mechanical oscillator (spring mass combination) to provide the phase shift between mass flow and pressure amplitude [2].

(b) Can microsystems technology be used to fabricate micro pulse-tube cryocoolers?

Microsystems technology was used to fabricate the regenerator. The geometry of the regenerator consists of several pillars in a microchannel. Previous theoretical studies indicate the importance of pillar shape for good hydraulic and thermal performance. However, no experimental verification was done. In this study, the regenerator material was chosen to be silicon because we were interested in characterizing the performance of the pillar and it is relatively easy to fabricate high-aspect ratio microstructures in silicon compared to other materials such as glass. The height of the pillar was 250 μm with an aspect ratio of 10. Pressure drops of gas flows in microchannels filled with circle, square, rhombus, elliptical, eye (formed by intersection of two circles) and sine shaped pillars cross-sections were measured and friction factors were determined in the range of Reynolds number between 50 and 500. Friction factor comparison of circle-shaped pillar matrices with studies in macroscale has rather good agreement, showing no significant microfluidic effects. Sine shaped pillar cross-sections have the lowest friction factor compared to all other pillar cross-sections including wire mesh screens.

recommendations

Heat transfer coefficient of the pillar matrices should be measured to obtain an optimum geometry considering both hydraulic and thermal performance. However, thermal experiments in the microscale is challenging because of the high effectiveness of the pillars. To measure accurately the temperature of the gas, thermometers might have to be made on chip. Hetsroni et al. [3] reviewed the thermal experiments performed by several authors in the microscale. The investigators attributed the divergence of the measured data from theory to several microscale effects which later proved to be wrong. The errors could be because of the instrumentation used

to measure various parameters, the fabrication errors and many other heat leaks which were not accounted for in the analysis.

Glass is a suitable material for fabricating the cold stage of the micro pulse-tube cryocooler. Micromachining high aspect ratio structures in glass was investigated as a part of this research. Preliminary etching experiments were performed based on the recommendations of several authors [4]. Further investigation is currently being carried out in the TST group at the University of Twente [5].

(c) Micro pulse-tube cryocooler would need an accompanying compressor, can conventional compressors be scaled down?

As noted above, the operating frequency should be increased in order to miniaturize the pulse-tube cryocooler. Conventional pulse-tube cryocoolers are powered by moving coil or moving magnet type of linear electromagnetic actuators [6]. For efficiency reasons, these actuators are operated in resonant conditions. The resonance frequency is given by $\sqrt{k/m}$ (k is the flexure stiffness and m is the moving mass). In order to operate in resonance at higher frequencies the stiffness of linear flexures k should be increased and/or the moving mass m should be reduced. There is an upper limit on increasing the stiffness of the linear flexure springs for a given moving mass (the flexures also contribute to moving mass) and the resonance frequency could be limited to about 150 Hz [7]. Another limitation of electromagnetic actuators is their limited power density compared to piezoelectric actuators.

Piezoelectric actuators produce large forces but low stroke and can operate over wide range of frequencies and hence were chosen as a driver for micro pulse-tube cryocooler. A pressure ratio of about 1.11 at a frequency of 1 kHz was achieved when operating the piezoelectric actuator with a peak-to-peak sinusoidal voltage of 100 V. For these conditions, the work amplitude produced by the piezoelectric actuator was about 0.17 mJ for an electrical input power of 2.73 W which gives an efficiency of 20 %. Higher pressure ratios can be achieved by driving the actuator at higher voltages. This is for the first time successful demonstration of piezoelectric actuators for pressure oscillators was demonstrated.

recommendations

The pressure oscillator size is dominated by the size of the piezoelectric actuator. Piezoelectric actuators of even smaller size than that used in this investigation are now commercially available [8]. Further investigation has to be carried out in interconnecting the micro cold stage to the pressure oscillator.

Bibliography

[1] R. Radebaugh. *Pulse tube cryocoolers*, pages 415–434. 2003. edited by S. Kakac, H. Smirnov, and M.R. Avelino, Kluwer academic publishers, Dordrecht, The Netherlands.

[2] R. Radebaugh *private communication.*

[3] G. Hetsroni, A. Mosyak, E. Pogrebnyak, and L. P. Yarin *International journal of heat and mass transfer*, **48** (2005).

[4] X. Li, T. Abe and M. Esashi *Sensors and Actuators A:Physical*, **87**:3 (2001).

[5] H. V. Jansen and M. deBoer. *Private communication, TST group, University of Twente*, (2006).

[6] E. D. Marquardt, R. Radebaugh and p. Kittel. *In: Seventh International Cryocooler Conference Proceedings, Air Force Phillips Laboratory Report PL-CP-93-1001. Kirtland Air Force Base, NM*, 783, (1993).

[7] R. Radebaugh. *Private communication*, (2006).

[8] Dynamic Structures and Materials, LLC. 205 Williamson Square, Franklin, TN 37064, USA. (www.dynamic-structures.com)

Summary

Cryocoolers are small refrigerators capable of achieving useful refrigeration below 120 K. Recent developments in the field of high T_c superconductors spawned a wide range of applications such as terahertz sensors, SQUIDS, low noise amplifiers, filters for microwave applications and many more. These devices are typically, non-dissipating and require a cryocooler delivering refrigeration power of about 10 mW operating at 80 K. The existing commercial closed loop cryocoolers are huge, less reliable and expensive. Several research groups have been investigating development of cryocoolers using microsystems technologies for on-chip cryocooling. Gas cycles which, can be broadly divided into recuperative (steady flow) and regenerative (oscillating flow) cycles are the only current means of reaching cryogenic temperature in a single stage. The aim of this thesis is to investigate miniaturization of regenerative cycles. Pulse-tube cryocoolers, a variation of the Stirling cycle (regenerative type), are a fairly recent development in cryocooler technology. The principal advantage of a pulse-tube refrigerator is that it has no cold moving parts in the refrigerator.

Processes in the pulse-tube must be nearly adiabatic for efficient operation, which occurs when the tube radius is large compared with the thermal penetration depth δ_{th} in the working fluid, usually helium gas. At a temperature of 300 K and a pressure of 3.5 MPa, δ_{th} is 0.12 mm for helium at a frequency of 120 Hz, and it varies with the frequency f as $\delta_{th} \propto 1/\sqrt{f}$. Thus, higher frequency operation can enable miniature pulse-tube cryocoolers fabricated with MEMS technologies. High frequency operation of the pulse-tube refrigerator has several other advantages. For a certain acoustic power the swept volume would decrease with higher frequency. The size of the compressor is usually a function of the swept volume and hence increasing the frequency of operation would reduce the size of the compressor. The size of the pulse-tube and regenerator would also be reduced at higher frequencies for a given cooling power. Reduction in size and mass is a huge advantage for portable and space applications. Simply increasing the frequency of a pulse-tube refrigerator designed for 60 Hz would lead to higher losses in the regenerator. For efficient high frequency regenerator operation the parametric analysis performed in the thesis indicate that the average pressure should be increased and a smaller hydraulic diameter regenerator material should be used.

A 120 Hz pulse-tube refrigerator was designed and built. A no-load temperature of 49.9 K was achieved. This was for the first time such a low temperature was achieved for a pulse-tube refrigerator operating above 100 Hz. The net refrigeration power at 80 K was 3.37 W. The input acoustic power at the aftercooler was 66.0 W, which yields a cooler efficiency of 14.0 % of Carnot with an aftercooler temperature of 298.7 K. The cooldown time from 285 to 80 K was about 5.5 minutes, even though the additional thermal mass at the cold end due to flanges, screws, heater and thermometer was 4.2 times that of the regenerator. This fast cooldown is about two to four times faster than that of typical pulse-tube refrigerators and is very attractive to many applications. This fast cooldown was studied by measuring the cooldown time to 80 K for different cold-end masses and extrapolate to zero cold-end mass. An analytical model was developed and was compared with the experimental results. The model and the extrapolated experimental results indicate that with zero cold-end mass the cooldown time to 80 K with the 120 Hz pulse-tube refrigerator would be about 32 s.

As a step towards investigating fabrication methods for micro regenerators, a matrix of pillars were etched in silicon using a customized Bosch dry etching process. Several pillar cross-sections such as circle, square, rhombus, elliptical, eye (formed by intersection of two circles) and sine shapes were investigated. The height of the pillars was 250 μm and the aspect ratio was about 10. Pressure drop measurements performed on these pillar matrices show that the sine shaped pillar matrices have friction factors which are an order lower than the wire mesh screens typically used in commercial regenerators.

A miniature pulse-tube cryocooler would need an accompanying pressure oscillator operating at high frequency of about 1 kHz. Electromagnetic actuators such as moving coil or moving magnet type used in conventional cryocoolers have scaling down problems because of the issues relating to cooling the coil. Piezoelectric actuators have high power density, can operate at high frequencies, have good electrical-to-mechanical efficiency and potentially have a very long operating life. A pressure oscillator consisting of a stainless-steel membrane driven by a piezoelectric actuator was designed and experiments were performed. A pressure ratio of about 1.11 at a frequency of 1 kHz was achieved with a filling pressure of 2.5 MPa and a compression volume of about 23 mm^3 when operating the piezoelectric actuator with a sinusoidal peak to peak voltage of 100 V. For these conditions, the work produced per cycle was about 0.17 mJ for an electrical input power of 2.73 W which gives an efficiency of 20 %. Higher pressure ratios can be achieved by further optimizing the membrane.

This thesis has covered various subjects relating to the miniaturization of pulse-tube refrigerators. With further development in the fabrication technologies, a micro miniature pulse tube refrigerator should be possible.

Samenvatting

Cryogene koelers zijn koelers die een temperatuur lager dan 120 K kunnen bereiken. Recente ontwikkelingen op het gebied van hoge-T_c supergeleiders hebben gezorgd voor een breed spectrum aan toepassingen, zoals terahertz sensoren, SQUIDs, ruisarme versterkers, filters voor microgolf toepassingen en nog veel meer. In veel van deze toepassingen wordt een zeer gering vermogen gedissipeerd en daarom is een koeler met een koelvermogen van slechts 10 mW afdoende bij een temperatuur van typisch 80 K. De huidige commerciële cryogene koelers met een gesloten cyclus zijn in dit verband te groot, hebben een te beperkte levensduur en een te hoge aanschafprijs. Verschillende onderzoeksgroepen hebben onderzoek gedaan naar de ontwikkeling van cryogene koelers met behulp van microsysteemtechnologie voor geïntegreerde ('on-chip') cryogene koeling. Deze koelers maken gebruik van gascycli, die onderverdeeld kunnen worden in recuperatieve (continue) en regeneratieve (oscillerende) cycli. Momenteel is het bereiken van cryogene temperaturen middels een enkele koelertrap uitsluitend mogelijk met dit soort koelers. Het doel van dit proefschrift is om de miniaturisatie van regeneratieve cycli te onderzoeken. De cryogene pulsbuiskoeler, een variant op de Stirling koeler (regeneratieve soort), is een vrij recente ontwikkeling op het gebied van cryokoelertechnologie. Het voordeel van een pulsbuiskoeler is dat het geen bewegende delen heeft in het koude deel van de koeler.

Voor een efficiënte werking moeten processen in de pulsbuis zo goed mogelijk adiabatisch zijn. Dit is het geval wanneer de buisdiameter groot is vergeleken met de thermische indringdiepte δ_{th} van het werkgas, meestal helium. Bij een temperatuur van 300 K en een druk van 3.5 MPa is δ_{th} 0.12 mm voor helium bij een frequentie van 120 Hz, en varieert δ_{th} met de frequentie f als $1/\sqrt{f}$. Dit betekent dat een hoge werkfrequentie miniaturisatie van cryogene pulsbuiskoelers mogelijk kan maken, die vervolgens gefabriceerd kunnen worden met MEMS technologie. Een hoge werkfrequentie van de pulsbuis koeler heeft ook verschillende andere voordelen. Bij een bepaald akoestisch vermogen neemt het slagvolume af voor een hogere frequentie. De grootte van de compressor is een functie van het slagvolume en dus zorgt het verhogen van de werkfrequentie ervoor dat de compressor verkleind kan worden. Bij een gelijkblijvend koelvermogen zullen ook de afmetingen van de pulsbuis en de regenerator afnemen voor een hogere frequentie. Een afname van de grootte en de

massa van een cryogene koeler is van groot belang voor draagbare- en ruimtevaarttoepassingen. Het verhogen van alleen de werkfrequentie is echter niet afdoende. Het verhogen van de frequentie van een pulsbuiskoeler die ontworpen is voor 60 Hz leidt tot hogere verliezen in de regenerator. Voor een efficiënte hoogfrequente werking van de regenerator geeft de parametrische analyse, uitgevoerd in dit proefschrift, aan dat de vuldruk verhoogd moet worden en een kleinere hydraulische diameter gebruikt moet worden in de regenerator.

Een 120 Hz pulsbuis koeler is ontworpen en gebouwd. De koeler bereikt een temperatuur van 49.9 K, wanneer deze niet thermisch belast wordt. Het was voor het eerst dat zulke lage temperaturen bereikt waren met een pulsbuis die werkt op een frequentie boven 100 Hz. Het netto koelvermogen op 80 K is 3.37 W. Het akoestisch inputvermogen is 66.0 W. Dit betekent dat de efficiëntie van de koeler 14.0 % van de Carnot efficiëntie is bij een afvoertemperatuur van 298.7 K. De afkoeltijd van 285 K naar 80 K is ongeveer 5.5 minuut, met aan de koeltip een thermische massa, die door flensen, schroeven, het verwarmingselement en de temperatuursensor, 4.2 keer zo groot is als die van de regenerator. Deze afkoeling is ongeveer twee tot vier keer sneller dan die van de huidige pulsbuiskoelers en is erg aantrekkelijk voor veel toepassingen. De snelle afkoeling is bestudeerd door de afkoeltijd naar 80 K te meten voor verschillende thermische massa's aan de koude zijde. Een analytisch model is ontworpen en vergeleken met de experimentele resultaten. Het model en de geëxtrapoleerde experimentele resulaten geven aan dat, zonder extra thermische massa aan de koude zijde, de afkoeltijd van de 120 Hz pulsbuiskoeler naar 80 K ongeveer 32 s is.

Als een belangrijke stap in het onderzoek naar fabricatiemethodes voor miniatuur pulsbuiskoelers zijn matrices van paaltjes ge-etst in silicium met behulp van een aangepast Bosch etsproces. Verschillende doorsnedevormen van deze paaltjes zijn onderzocht, zoals een cirkel, een vierkant, een ruit, een ellips, een oogvorm (de intersectie van twee cirkels) en een sinusvormige doorsnede. De hoogte van de paaltjes is 250 μm en de aspect ratio is ongeveer 10. Drukvalmetingen, uitgevoerd op de matrices, tonen aan dat de sinusvormige paaltjesmatrix een frictiefactor heeft die een orde kleiner is dan de gestapelde gaasjes die normaal gebruikt worden in commerciële regeneratoren.

Een cryogene minipulsbuiskoeler heeft een bijbehorende drukoscillator nodig die werkt met een hoge frequentie van ongeveer 1 kHz. Electromagnetische aandrijving, bijvoorbeeld met een bewegende spoel of een bewegende magneet, zoals gebruikt in conventionele cryogene koelers, zelfs bij verkleining problemen met het koelen van de spoel. Piëzo-electrische actuators hebben een hoge vermogensdichtheid, kunnen werken op hoge frequenties, hebben een efficiënte omzetting van electrische naar mechanische energie, en hebben in potentie een erg lange levensduur. Een drukoscillator, die bestaat uit een roestvaststalen membraan, aangedreven door een piëzo-electrische actuator, is ontworpen en er zijn experimenten met deze drukoscillator uitgevoerd. Wanneer de piëzo-electrische actuator wordt aangedreven met een sinusvormige piek-piek spanning van 100 V kan een drukverhouding van onge-

veer 1.11 bij een frequentie van 1 kHz bereikt worden bij een vuldruk van 2.5 MPa en een compressievolume van ongeveer 23 mm^3. Voor deze condities is de geproduceerde arbeid per cyclus ongeveer 0.17 mJ voor een elektrische inputvermogen van 2.73 W, wat leidt tot een efficiëntie van 20 %. Grotere drukverhoudingen kunnen bereikt worden door het verder optimaliseren van het membraan.

Dit proefschrift behandelt verschillende onderwerpen die gerelateerd zijn aan de miniatuarisatie van pulsbuiskoelers. Met verdere ontwikkelingen in de fabricatietechnologieën, moet het mogelijk zijn om een miniatuur pulsbuiskoeler te fabriceren.

Appendix A

Solution to heat diffusion equation for chapter 6

Problem definition

The regenerator is considered as a uniform rod of cross-sectional area A having an effective thermal conductivity λ, specific heat capacity c_p and density ρ. The rod is initially at temperature T_0 (in our case ambient temperature). At time, $t = 0$, cooling power $\dot{Q}$ is introduced at length $x = 0$. We assume the properties of the rod to be independent of temperature. The aim is to obtain a temperature profile of the rod as a function of position x and time t.

Mathematically, the problem can be written as,

$$u_t = ku_{xx}, for 0 < x < L, t > 0 \tag{1}$$

where $u_t = \frac{du}{dt}$, $u_{xx} = \frac{d^2u}{dx^2}$, with boundary conditions

$$u_t(0,t) = -\frac{\dot{Q}}{\lambda A} = C_1 \tag{2}$$

$$u(L,t) = T_0 \tag{3}$$

initial condition

$$u(x,0) = T_0 \tag{4}$$

Approach

The heat diffusion problem described above has non-homogeneous boundary conditions. Hence, separation of variables cannot be applied directly. However, by perturbing the temperature function $u(x,t)$ in such a way the problem is transformed to a standard initial-boundary value problem having homogeneous boundary

conditions, which we know how to solve (see section below). To do this, begin putting,

$$u(x,t) = U(x,t) + \psi(x) \tag{5}$$

substitute u into the heat diffusion equation 1 to obtain,

$$U_t = k(U_{xx} + \psi''(x)) \tag{6}$$

and this is a standard heat equation for U if $\psi''(x) = 0$. Thus choose $\psi(x) = Ax+B$ to satisfy the boundary conditions.

applying boundary condition 2,

$$u_t(0,t) = U_t(0,t) + \psi\prime(0) = C_1 \tag{7}$$

$U_t(0,t)$ should be equal to zero for homogeneous case, so

$$\psi\prime(0) = C_1 \tag{8}$$

hence,

$$A = C_1 \tag{9}$$

applying boundary condition 3,

$$u(L,t) = U(L,t) + \psi(L) = T_0 \tag{10}$$

for homogenous case $U(L,t) = 0$, so

$$B = T_0 - C_1 L \tag{11}$$

The non-homogenous problem reduces to a new homogeneous problem as follows,

$$U_t = kU_{xx}, for 0 < x < L, t > 0 \tag{12}$$

boundary conditions

$$U_t(0,t) = 0 \tag{13}$$

$$U(L,t) = 0 \tag{14}$$

initial condition

$$U(x,0) = C_1(L - x) \tag{15}$$

Homogeneous solution

The homogeneous problem,

$$u_t = ku_{xx}, for 0 < x < L, t > 0 \tag{16}$$

with boundary conditions

$$u_t(0,t) = 0 \tag{17}$$

$$u(L,t) = 0 \tag{18}$$

and initial condition

$$u(x,0) = f(x) \tag{19}$$

can be solved by using separation of variables or the Fourier method and is a standard textbook problem. The solution is,

$$u(x,t) = \sum_{n=1}^{\infty} b_n sin\left(\frac{(2n-1)\pi x}{2L}\right) e^{-\frac{(2n-1)^2\pi^2 kt}{4L^2}} \tag{20}$$

with

$$b_n = \frac{2}{L}\int_0^L f(\xi) sin\left(\frac{(2n-1)\pi\xi}{2L}\right) d\xi \tag{21}$$

Solution

The solution to problem defined by 12, 13, 14, 15 is the same as equation 20 with,

$$b_n = \frac{8C_1 L}{(2n-1)^2\pi^2} \tag{22}$$

so the final solution is,

$$u(x,t) = T_0 + C_1(x-L) + \sum_{n=1}^{\infty} \frac{8C_1 L}{(2n-1)^2\pi^2} sin\left(\frac{(2n-1)\pi x}{2L}\right) e^{-\frac{(2n-1)^2\pi^2 kt}{4L^2}} \tag{23}$$

This equation satisfies both the boundary conditions described by 2, 3.

Acknowledgements

My graduation work has been a mixture of pleasure of learning new things, harnessing the knowledge and many accomplishments which are sweet victories given the constraints of time. This success was possible because of many individuals who have groomed me and selflessly devoted their valuable time.

I like to thank Miko for being my promotor. He was like a baron who gave the canvas and the colors and wanted a masterpiece in return.

I am indebted to Marcel (Low temperature group, TNW) for all the care he had taken. His professional approach, meticulous attitude and his hungry for modeling has impressed me a lot. I am thankful for all your help and time in correcting draft versions of manuscripts, presentations and reports.

I consider myself very fortunate to be associated with Ray (NIST). I remember those school days when I was told by my teacher to have a role model in life giving examples of inventors, philosophers and sports achievers. I was in particular impressed by Richard Feynman because of the passion with which he explains difficult subjects. After meeting Ray and all the good experiences I had (both personal and professional terms), I consider him as my role model. Thank you much Ray and it was a great privilege working with you.

I would like to thank Mike Lewis, Peter Bradley, Gan Zhihua, Huang, Ryan, Peng, Jacki, Beverly for all the good time I had at NIST. Thank you Mike for taking me to the Rockies baseball games and the many trips you made, riding me to the supermarket and home. Gan and Peng, it was wonderful to go on a drive, on the rockies, in the weekends. Mike and Gan's help in the lab is very much appreciated. Rich McLaughlin, for the time he dedicated, to braze the flanges together.

I would like to thank my colleagues at the cooling and instrumentation group where I spent most of my time. Harry for teaching a novice what it means to handle high pressure, many useful tips on instrumentation and help in assembling my creations together. Johannes for reminding me, microcooling is no childs play. Pieter Lerou for the wonderful time. Erwin for giving me useful tips on Labview programs and the evening hangouts which I am sure Gunter should thank us. Hendrie for being my translator to dutch and also the time we spent, mostly partying in France. Theo, Robert-Jan, Bert and Gideon for some nice chit-chat's. I enjoyed very much the group outings to Geneva and Noordwijk. The poker evenings are

very memorable and Bert was my nemesis because he always knew when I bluffed. I will definitely miss the 'gezellig' environment.

I would like to express my sincere gratitude to Fons de Waele (TU Eindhoven) for reading my thesis and suggesting me very useful corrections.

I would like to appreciate the help of Henri Jansen in the cleanroom, explaining me the intricacies of dry-etching and many more discussions. Meint, Erwin and the cleanroom staff for their support.

My house-mate and colleague Marcel Dijkstra was extremely resourceful in both science and social activities. Thank you much for making the cover of this thesis. I enjoyed very much the discussions on various subjects and have learnt a lot about Netherlands and Europe. The vacation trips to London, Italy and Switzerland were memorable. I like to thank Tom and Fenny (Marcel's parents) for sending me those lovely wishes for my birthday and new year.

I would like to express my gratitude and special thanks to Evelin for making sure all the forms are sent out to the doctoral board, for being extremely prompt and the light moments we shared about life in North-Holland. Sofia Boekholt for expediting the formal procedures and for pulling a rabbit out of her hat in meeting the deadlines. Also thanks to Judith, Ingrid and Susan for doing the paper work.

It was nice to have Berker and Yiping do their final master thesis project with me. It helped me reflect upon many aspects of the project. I love to see both of them pursuing graduate studies in TST group.

Kees was very resourceful and helpful in many things and in particular to fix my car and the useful tips to avoid tax authorities. Doekle was always a very happy guy who walks in at 8:30 and leaves at 5:00. I am amazed at his time planning and of-course thank him for the authentic dutch coffee. I like to thank Dennis, Duy, Jeroen, Marcos, Nima, Ram, Remco, Shahina, Theo, Vitaly and the other TST members for the wonderful time. Dhirendra was a night-watchman for the hogekamp and I liked to sometimes work also in the evenings when the world is asleep. It was good to discuss about atoms, shells and the quantum stuff with him which is a whole different world for me.

Unfortunately, I cannot name all the people from different faculties, countries who kept me in supply of good humor. I would like to thank them all for their good wishes.

"जीवन के इस मत्वापूर्ण मोड पर मैं उन लोगों के प्रति आभार अभिव्यक्त करना चाहूँगा जिन्होंने इस कठिन यात्रा को आनंद और प्रेम से परिपूर्ण बनाये रखा| सर्व प्रथम मैं आभारी हूँ, माता कृष्णा एवं पिता मूर्थी के प्रोत्साहन और निस्वार्थ प्रेम का जिसने इस जीवन को सार्थक बनाया| मेरी पत्नी दीप्थी जिन्होंने मेरे चुनौतियों से भरे पलों में साथ दिया और जीवन को कुशियों से भर दिया| आभारी हूँ नन्हें मित्रों ऐश्वर्या, अनिरुद्ध, प्रफुल्ल, प्रियंका, सौम्या और वैभव का जिन्होंने मेरे साथ अत्यंत मनोरंजक एवं यादगार पल बिताये| ये अनदेखे रिश्ते हमारे जीवन का ताना बाना बुनते हैं और अनजाने में जीवन को शांती, आत्मज्ञान, परीपूर्णता, और सदभावना से भर देते हैं|"

--- श्रीनिवास वानापल्ली